NTNU
Innovation and Creativity

Vertical Stratification in a Ventilated Space

Comparison of Theoretical Predictions to Experimental Results from a Water Scale Model

Ole-Jørgen Feiring Myrtrøen

Master of Science in Energy and Environment
Submission date: September 2007
Supervisor: Per Olaf Tjelflaat, EPT
Co-supervisor: Paul Cooper, University of Wollongong

Norwegian University of Science and Technology
Department of Energy and Process Engineering

Problem Description

A fundamental issue in the ventilation of buildings is the prediction of the thermal stratification that would arise in a ventilated space containing vertically distributed sources of buoyancy, e.g. walls heated by solar radiation and poorly thermally insulated building envelope cooled by outdoor conditions.

The aim of this thesis is to determine the stratification in a mechanically or naturally ventilated room containing a vertically distributed source of buoyancy.

The following research questions should be addressed and objectives accomplished:

1. Commission the salt water scale model experimental apparatus. This includes traversing mechanism for measurement of conductivity/stratification.

2. Further enhance the Germeles code, Distran, developed by Professor Cooper, for prediction of transient and steady state stratification in this system and a finite thickness intrusion.

3. Test the Distran against a linearly stratified environment.

4. Compare theoretical predictions to experimental results.

Assignment given: 26. February 2007
Supervisor: Per Olaf Tjelflaat, EPT

Abstract

This study investigates the behaviour of a vertically distributed source of buoyancy on the vertical stratification in a ventilated space, an important factor for determining indoor comfort when using displacement ventilation. A new theory describing the behaviour of this buoyancy source in a ventilated space was presented previous to this work, but experimental results were required in order to validate the theoretical and numerical modelling.

The behaviour of this source of buoyancy on the stratification in a ventilated space is studied for a mechanically ventilated at steady-state and for a linearly stratified environment using salt water in a water scale model. The stratifications were measured using a traversing conductivity probe and then compared to theoretical predictions by numerically solving the plume equations for the new theory in Fortran.

High quality measurements were produced, showing excellent repeatability for stratification measurements at steady-state with deviations of less than 1 %. Moreover, the linear stratifications had linear best fits up to $R^2 = 0.999$ by using the double-bucket method.

The theoretical predictions of the influence of the vertically distributed source correlate quantitatively with the mechanically ventilated experiments, showing good agreement to the strength of the ambient stratification, the position of the first front and the ventilation flow rate. The experimental results for the determination of the height of a horizontal intrusion of fluid into the linearly stratified environment were severely affected by the occurrence of gravity current at the ceiling of the ventilated space and comparisons to the new theory was not successful because of this.

A two-layer stratification is observed where the upper layer had a weakly stratified density profile, instead of the multi-layer stratification predicted by previous researchers in their theoretical model. This discrepancy is due to smoothing and vertical turbulent mixing in the water scale model. It is recommended that the characteristic of the membrane that is used in the water scale model is investigated in relation to the gravity currents for future research.

Sammendrag

Dette arbeidet undersøker hvordan en vertikalt distribuert oppdriftskilde påvirker den vertikale stratifikasjonen i et ventilert rom, en viktig faktor for å avgjøre innendørs komfort ved bruk av fortrengningsventilasjon. En ny teori som beskriver oppførselen til en slik oppdriftskilde er tidligere presentert, men eksperimentelle resultater er nødvendig for å bekrefte de teoretiske og numeriske modelleringene av oppdriftskildens innvirkning på stratifikasjonene.

Stratifikasjonene er undersøkt ved å benytte saltvann av varierende konsentrasjon i en vannskalamodell for mekanisk ventilerte omgivelser i stasjonær tilstand, samt for lineært stratifiserte omgivelser for å studere plumens effekter på denne type stratifikasjon. Stratifikasjonene er målt ved å benytte en traverserende konduktivitetsprobe, for videre å sammenlignes med numeriske løsninger av den nye teorien i Fortran.

Målingene er av god kvalitet med 1 % avvik i repeterbarhet for stratifikasjonsmålingene i stasjonær tilstand og de lineære stratifikasjonene har lineære trendlinjer med $R^2 = 0{,}999$. De teoretiske resultatene korrelerer kvantitativt med de eksperimentelle, og de viser god overensstemmelse når det kommer til omgivelsenes oppdriftsstyrke, posisjonen til første front samt den totale ventilasjonsraten. For de lineært stratifiserte eksperimentene ble resultatene svært influert av gravitasjonsstrømninger i nedre seksjon av vannskalamodellen, og direkte sammenligning med teori var av denne grunn ikke vellykket.

For stratifikasjonene er det observert en tolagsmodell hvor det øvre sjiktet har en svak stratifikasjon i stedet for flerlagsmodellen som tidligere forskere har forutsagt. Noe av dette avviket er grunnet turbulent strømning som forårsaker utsmøring av skilleflatene, samt komplekse strømningsmønstre som ikke var en del av den teoretiske modellen. Forøvrig så økte de eksperimentelle resultatene forståelsen for gravitasjonsstrømninger i vannskalamodellen, og det er anbefalt å undersøke hvordan egenskapene til membranen er relatert til dette i fremtidige undersøkelser.

Acknowledgements

Writing this thesis has been a journey for me, starting out with planning and preparations in Norway and ending up in Wollongong, Australia. It has also been a good six months in terms of trying to understand the very fundamentals of fluid mechanics. I am glad to say that the change of environment from my student office at Department of Energy and Process Engineering at NTNU to the Fluid Mechanics Laboratory at the University of Wollongong has been less of a challenge due to the help of several people.

I am particularly grateful to my research advisor, Associate Professor Paul Cooper, Faculty of Engineering, University of Wollongong, for making my stay here in Wollongong possible, for his patience and most importantly for his unfailing interest and knowledge.

I would also like to thank my supervisor, Professor Per Olaf Tjelflaat at the Department of Energy and Process Engineering, NTNU, for his support and for getting me in contact with Paul.

Thanks to Dr Gary R. Hunt, Department of Civil and Environmental Engineering, Imperial College London, for helpful comments and for motivating me with his enthusiasm during his short stay in Wollongong.

Lastly, I would like to thank Mr Stuart Rodd and Mr Keith Maywald at the Faculty of Mechanical Engineering Workshop at the University of Wollongong for helping me with some of the experimental setup.

Table of Contents

List of Figures

List of Tables

List of Symbols

S.I (Système International d'Unités) abbreviations for units and standard notations formulae are used in this work. Other abbreviations are listed below.

A^*	Effective vent area	$\left[m^2\right]$
a^*	Non-dimensional effective vent area	$\left[-\right]$
b	Horizontal width of plume	$\left[m\right]$
c	Membrane coefficient	$[m^3 s k g^{-1}]$
C_{ps}	Specific salt at constant pressure	$\left[-\right]$
D_{AB}	Binary diffusivity	$\left[m^2 s^{-1}\right]$
F	Buoyancy flux	$\left[m^4 s^{-3}\right]$
F''	Buoyancy flux per unit area	$\left[m^2 s^{-3}\right]$
f	Non-dimensional buoyancy flux	$\left[-\right]$
G''	Salt flux per unit area	$\left[kg_{salt} \cdot m^{-2} s^{-1}\right]$
h	Convection heat transfer coefficient	$\left[W m^{-2} K^{-1}\right]$
Δh	Change in height	$\left[m\right]$
L	Characteristic length scale	$\left[m\right]$
M	Momentum flux per unit length of plume	$\left[m^3 s^{-2}\right]$
m	Non-dimensional momentum flux	$\left[-\right]$
N	Buoyancy frequency	$\left[s^{-1}\right]$
Q	Volume flow	$\left[m^3 s^{-1}\right]$
q	Non-dimensional volume flux	$\left[-\right]$
w	Vertical velocity of plume	$\left[m s^{-1}\right]$
$\forall$	Volume	$\left[m^3\right]$

Greek Symbols

α	Entrainment coefficient	$\left[-\right]$
α	Thermal diffusivity	$\left[m^2 s^{-1}\right]$
β	Volumetric expansion coefficient	$\left[K^{-1}\right]$
Δ	Reduced gravity	$\left[m s^{-2}\right]$

δ	Non-dimensional density	$[-]$
ζ	Non-dimensional height	$[-]$
κ	Thermal conductivity	$\left[Wm^{-1}K^{-1}\right]$
ν	Kinematic viscosity	$\left[m^2s^{-1}\right]$
ξ	Expansion coefficient of salt	$[-]$
τ	Non-dimensional time	$[-]$

Subscripts

0	Initial, property at free surface
b	Bottom
cond	Conductive
e	Environment, ambient conditions
nb	Point of neutral buoyancy
new	New value
out	Outflow
ref	Reference
s	Source condition
t	Top
vent	Ventilation
x	In x-direction
∞	Reference condition

(This page intentionally left blank)

1 Introduction

In a displacement ventilated space, modern architectural features such as glass atriums or large glass surfaces can be used to increase the amount of daylight experienced by it inhabitants. In addition, for the inhabitants to experience the required level of comfort, the ambient air inside has to be fresh and within a certain temperature range. Both of these requirements could be met by maintaining an appropriate temperature stratification.

An increase in daylight could mean higher internal solar heat gains. If one of the vertical walls in the ventilated space is heated as a consequence of this increase, the wall could act as a distributed source of buoyancy, producing a plume which is continuously added buoyancy while it rises next to the surface of the wall. This plume will then interact with the temperature stratification in the space as it adds buoyancy to the ambient stratification.

Predicting this interaction is necessary for maintaining the appropriate temperature stratification. Therefore, having knowledge of the behaviour of this plume on the ambient can help architects and engineers in building design, providing installations of correct dimensions, effectively reducing the needs for electricity in while providing the required comfort levels.

A newly developed theory by Cooper et al. [1] describes the behaviour of a plume from a plane distributed source of buoyancy. This theory needs to be supported by experimental results when it comes to the steady-state of a ventilated space and the behaviour of a plume in a linearly stratified environment. Moreover, the program developed in Fortran to provide a numerical solution to this theory needs certain modifications in order to produce results comparable to the experimental results.

As a result, this work aims to experimentally investigate a ventilated space in steady-state containing a vertically distributed source of buoyancy and the behaviour of a plume in a linearly stratified environment. Additionally, any modifications necessary for comparing numerical results to experimental, including a simple model for an intrusion of a finite thickness will be modelled.

Firstly, the background and theory on the fluid mechanics of plume behaviour is presented, including a detailed look at the theory describing a plume from a plane vertical distributed source of buoyancy.

This is followed by the materials and methods where two experiments on the water scale model is described. These experiments are the mechanically ventilated filling box and the behaviour of membrane flow from a plane vertical distributed source of buoyancy on a linearly stratified environment.

The next chapter is on the numerical procedures which form the basis of solving the plume equations. Modifications on the program *Distran* developed by Cooper et al. [1] and the results for the numerical simulations are presented, followed by the results for the mechanically ventilated filling box and the linearly stratified environment.

The discussion then looks at the results and draws conclusions related to the correlation between numerical and experimental results. If successful, the comparison will show a relationship between the actual and theoretical ventilation flow rates, the position of the first front in addition to similar strength of the ambient stratification. Moreover, any discrepancies between the numerical and experimental stratifications due to the analytical approach in the theory will be discussed.

Lastly, the conclusions are summarised and suggestions for future research is presented. Accordingly, the next chapter presents the background and theory of plume behaviour.

2 Background and Theory

This chapter is divided into three sections: A short introduction to a ventilated space and stratification is presented first, followed by a review on the development of theories describing plume behaviour, and lastly the theory developed by Cooper et al. for plumes from a vertically distributed source are presented.

2.1 Ventilation

Ventilation is in simple terms a method of transporting pollutants and heat away from an enclosure. The fluid mechanics involved in this process is largely dependant on which method of ventilation is used. Two commonly used methods are mixing ventilation and displacement ventilation.

2.1.1 Mixing ventilation

In mixing ventilation, the air inside an enclosure is of an approximately uniform temperature. This is often achieved by ventilating using high momentum jets, allowing them to entrain local ambient air as they slow down and spread out into the enclosure. The effect is a constant mixing of fresh air into the room. When using this method of ventilation, the volume flow has to provide the necessary heat removal or keep the required level of maximum contamination. A different method is used to achieve displacement ventilation.

2.1.2 Displacement ventilation

Instead of using momentum jets, displacement ventilation involves the supply of cool air at low velocity at floor level. This can be achieved either by mechanical ventilation or by natural ventilation where the driving pressure is generated by mechanical equipment or by pressure differences to the external environment, respectively. This fresh incoming air could then be heated by any nearby heat sources, transporting the source's contaminants to the ceiling in a plume of warm air. The contaminated air at the top of the enclosure can then be

exhausted [2,3]. The air rises as it is positively buoyant to the ambient stratification and to the environment outside the ventilated space, as illustrated in figure 2.1.

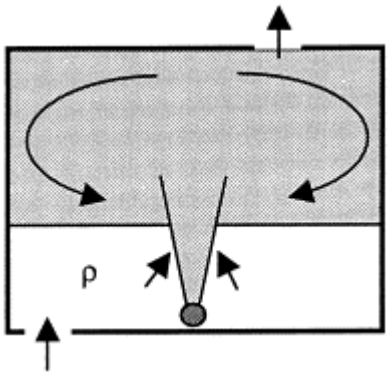

Figure 2.1. Schematic view of displacement natural ventilation in a single-zone building. The lower section consist of an ambient of uniform temperature and the upper section consist of a stratified temperature. Reproduced from Chen et al.[4].

When correctly designed, a displacement ventilated room would form an interface where the lower section consists of a uniform temperature area of fresh air, followed by a section of polluted air which has a stratification of increasing temperature. This non-mixing characteristic of displacement ventilation causes the ventilated space to have a stratified temperature. Because of this stratification, displacement ventilation has the advantage of removing more contaminants and internal heat gains in the occupied space compared to the same ventilation flow rate for mixing ventilation, taking advantage of the vertical stratification [3].

2.1.3 Vertical stratification

The stratification in a ventilated space is determined by the variation of local density with height. The strength of a stratification can be conveniently classified by the Brunt-Väisäla buoyancy frequency N, defined as

$$N^2 = -\frac{g}{\rho_\infty}\frac{d\rho_e}{dz}\left[\frac{1}{s^2}\right] \tag{2.1}$$

where ρ_e is the density in the ambient and ρ_∞ is a reference density [3]. For air, equation (2.1) can be rewritten so that it relates to temperature as

$$N^2 = \frac{g}{T}\frac{dT_\infty}{dx} \tag{2.2}$$

The buoyancy frequency relates the change in density to the change in height of the enclosure. The physical interpretation of the frequency is the oscillation of an element of air that is displaced vertically from its original position in a stably stratified environment [3]. This stability depends largely on the respective density distribution. For instance, a room with a hot section below a cool layer would be unstable and cause convective currents caused by heat sources.

If a heat source is present in a ventilated space, it heats up the local ambient air making it buoyant, thus causing it to rise. This buoyant plume will rise through the space, entraining surrounding air until it ceases to be buoyant and loses momentum. The buoyancy of a plume is related to its density difference to the ambient, commonly expressed by the reduced gravity as

$$\Delta_s = g \times \frac{\rho_e(z) - \rho_s(z)}{\rho_\infty} \tag{2.3}$$

where ρ_e, ρ_s and ρ_∞ is the density of the local ambient, the plume and a reference, respectively [1]. The ambient buoyancy can be similarly expressed as

$$\Delta_e = g \times \frac{\rho_e(z) - \rho_\infty}{\rho_\infty} \tag{2.4}$$

Moreover, for the scenario when a flow is driven by a source of heat flux q, the buoyancy flux can be expressed as [5]:

$$F_0 = \frac{g\beta q}{\rho c_p} \tag{2.5}$$

where β is the thermal expansion coefficient and c_p the specific heat capacity.

In order to look at the behaviour of plumes produced by vertically distributed sources of buoyancy in a ventilated space, it is useful to review the theoretical principles behind plumes. The next chapter reviews the development of the theories describing the behaviour of a simple plume in different environments.

2.2 Plumes

2.2.1 Plume assumptions

In Morton et al. [6] the main assumptions for plume theory were developed, forming the fundamentals of plume theory. The following assumptions were derived, valid for any height of the plume:

- *The rate of entrainment is proportional to a characteristic velocity.*
- *The mean vertical velocity and the mean buoyancy force have similar profiles.*
- *The local density variations are small compared to those of the ambient.*

In addition, the ambient fluid entrained into a plume is regarded proportional to the vertical velocity on the axis of the plume. The simplest plume that satisfies these assumptions is the maintained plume in a uniform ambient fluid.

Morton et al. [6] assumed constant velocity and buoyancy forces across the plume, and zero outside the plume, referring to this as a 'top-hat' profile due to the shape of the plume in such a case, and is in later literature referred to as the top-hat assumption [7]. They also applied the Boussinesq assumption, implying that the density variations within the plume were sufficiently small not to affects its inertia. This applies for all theories mentioned in this work.

Firstly, the point source in a stratified fluid is considered followed by the filling box and lastly the ventilated filling box.

2.2.2 Point source in a stratified fluid

In a stratified fluid the plume density increases with height due to entrainment. At the point where the density difference between the ambient and the plume is zero, the plume's buoyancy becomes zero and consequently the momentum and velocity will decrease [6]. Moreover, for the point source in a stratified fluid, the velocity and buoyancy profiles are expected to be of Gaussian shape [6]:

$$u(x,r) = u(x)e^{-\frac{r^2}{b^2}} \tag{1.6}$$

$$g\frac{\rho_0 - \rho}{\rho_1}(x,r) = g\frac{\rho_0 - \rho}{\rho_1}(x)e^{-\frac{r^2}{b^2}} \tag{1.7}$$

To solve these equations, it is necessary with three boundary conditions; Morton et al. [6] assumed the plume width and momentum to be zero at the source, and used the release of total buoyancy to satisfy the last boundary condition.

2.2.3 Filling box

For a confined region, Baines and Turner [7] considered the effects of time-dependent stratification from a turbulent plume in a confined region. Their main focus was on a steady axisymmetric plume in a box and they assumed that the plume fluid spreads out instantaneously into a thin horizontal layer as it reaches the top of the box. Moreover, they assumed that turbulence and mixing would be prevented due to the stable stratification.

When the plume is in a region of uniform ambient, it is possible to get an exact solution for the first front. This is because its dependence is only of the plume in the uniform environment. Similar to Morton et al. [6], Baines and Turner [7] assumed the mean vertical velocity and mean buoyancy profile to be similar at all heights and of Gaussian shapes. This developed into what Turner later referred to as the "filling-box" model, however, it did not include mass addition.

Mass addition was included in the model developed by Germeles [8]. His underlying motivation was to prevent the problem of roll-over during the filling of LNG tanks,

phenomenon related to stratification changes. The governing partial differential equations for the plume were solved using numerical methods, and from this he found a normalized solution in which he emphasized the applicability of.

Similar to Morton et al. [6], Germeles [8] assumed the plume liquid and density profiles to be of Gaussian shapes. To find unique solutions for these governing equations, initial and boundary conditions are required and for the stratified case, he used that

- *The initial stratification of the tank ambient must be known.*
- *The plume fluxes of volume, momentum and buoyancy must be specified at a fixed station for all times.*

Moreover, the density of the tank liquid must be equal to the average density of the liquid discharged by the plume at the free surface. Owing to the difference in density between the plume and the ambient, this condition introduces at the free surface a step discontinuity in density at $\tau = 0$, when the last plume is 'turned on' and the discontinuity moves downward with time.

Worster and Huppert [9] used a numerical approach similar to that of Germeles [8] to extend the Baines and Turner's [7] filling box model. They developed an approximate analytical method for the transient density profile using series, and their basis was the assumption that the density changes of the fluid behind the first front are independent of position.

2.2.4 Ventilated filling box

Linden, Lane-Serff and Smeed [10] investigated buoyancy driven ventilation flow in buildings in the fluid mechanics of natural ventilation. One of their major results was that only the strength of the stratification in a space is dependent on the strength of the source: The stratification itself is determined by the entrainment caused by the plume.

Furthermore, they determined a criterion for creating an arbitrary stable stratification based upon the relationship of the effective vent area. This relationship is based upon the level where the hydrostatic pressure inside and outside of a building is the same. By applying

Bernoulli's equation with losses, they found an effective vent area that can be related to the volume flux as

$$Q = A^* \left[g' \left(H - z_0 \right) \right]^{\frac{1}{2}} \tag{2.8}$$

where the effective vent area, A^*, is defined as

$$A^* = \frac{a_t a_b}{\left[\frac{1}{2} \left(\frac{a_t^2}{c} + a_b^2 \right) \right]^{\frac{1}{2}}} \tag{2.9}$$

This relationship is extensively used in natural ventilation theory and it can be related to the non-dimensional height of the interface in the box, ζ, by using the equations presented by Morton et al. [6], modified here for the current nomenclature using the same approach as Linden et al. [10].

$$\frac{A^*}{\alpha^2 H^2} = \left(\frac{6}{5} \right)^{\frac{3}{2}} \left(\frac{9}{10} \right)^{\frac{3}{6}} \pi \left[\frac{\zeta^5}{\left(1 - \zeta \right)} \right]^{\frac{1}{2}} \tag{2.10}$$

Depending on the value of A^*, Linden et al. [10] predicted that several interfaces of equal height would form in a ventilated filling box with a vertical line source, forming a multi-layer stratification where each individual layer would be fully mixed. A consequence of the modelling using interfaces is that any vertical movement has to occur through the plume, thus any interlayer communication must happen through entrainment and detrainment. The plume was assumed to completely detrain within each interface before a new plume actuated. This theory was extended by Linden and Cooper's study on two point sources [11] and multiple point sources [12].

A theory for multi-layer stratification was also presented by Chen, Li, and Mahoney [4] in experiments where hydrogen bubbles were utilized to produce point and line sources. They found that the source strength had little influence on the stratification, as predicted theoretically by Linden et al. [10].

Additionally, Chen et al.'s [4] experimental results coincided well with the theoretical predictions for the height of the first front compared to that of Linden et al. [10]. In a second study by Chen, Li and Mahoney [13], they presented a simple multilayer stratification model as an extension to that of Linden et al. [10]. They reported differences in flow direction within the theoretical layers 2 and 3 in figure 2.2 (b) compared to Linden et al.'s predictions in figure 2.2 (a). Additionally, their model suggested layers of different heights.

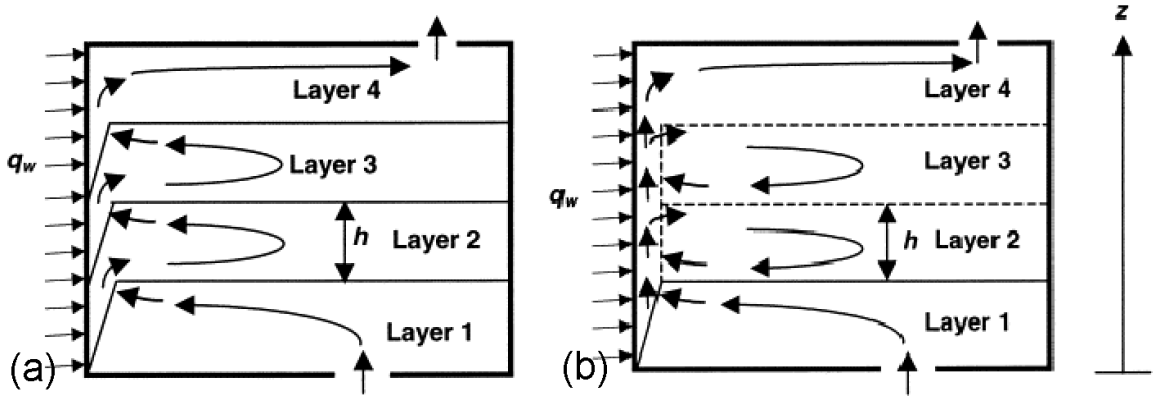

Figure 2.2. (a) Multi-layer stratification model as suggested by Linden et al. [10] (b) Multi-layer stratification model for displacement ventilation as presented by Chen et al. [13]. Reproduced from Chen et al. [13].

The change in flow direction led Chen et al. [13] to suggest that the detrained plume fluid would be re-entrained into the plume, as can be seen in figure 2.2 (b), in contrast to Linden et al.'s prediction, as demonstrated in figure 2.2 (a).

Neither Linden et al. [10] nor Chen et al. [4,13] observed signs of multiple interfaces in their experimental works. Linden et al. [10] suggested that vertical mixing during experiments can prevent the formation of the distinct multiple stratification interfaces. This vertical mixing was also reported by Chen et al. [13], observing smearing in the interface regions.

The case of a vertical source in a ventilated space is further investigated by Cooper et al. [1], extending the previous theories for a vertical line source by describing a plane vertically distributed source of buoyancy. Their theory seeks to provide a solution for a vertically plane distributed source of buoyancy in different environments.

2.3 Plume from plane distributed source of buoyancy

A theory developed by Cooper et al. [1] attempts to describe the behaviour of a plane distributed source of buoyancy, an extension of Linden et al's theory for a line source in terms of multi-layer stratification. At present, it is the first theory attempting to solve for both confined and open regions, covering both stratified and uniform ambient. Using the same plume assumptions as Morton et al. [6], Cooper et al. [1] derived the governing equations for the plane distributed source of buoyancy to

$$\frac{d(bw)}{dz} = \alpha w \tag{2.11}$$

$$\frac{d(bw^2)}{dz} = b\Delta \tag{2.12}$$

$$\frac{d(bw\Delta)}{dz} = (bw)\frac{\partial \Delta_e}{\partial z} + F_0 \tag{2.13}$$

for volume, momentum and buoyancy fluxes of the plume, respectively, where b is the width of the plume and w is its vertical velocity. Hence, the volume flux, momentum flux and buoyancy flux can be expressed as

$$Q = (bw)$$

$$M = (bw^2)$$

$$F = (bw\Delta)$$

Inserting this notation into the equations (2.11)-(2.13) returns per unit length of the plume as follows:

$$\frac{dQ}{dz} = \frac{\alpha M}{Q} \tag{2.14}$$

$$\frac{dM}{dz} = \frac{QF}{M} \tag{2.15}$$

$$\frac{dF}{dz} = Q\frac{\partial \Delta_e}{\partial z} + F_0 = -QN^2 + F_0 \tag{2.16}$$

where N is the buoyancy frequency of the ambient fluid [1]. A simplification of this exists for the special scenario of a uniform ambient.

2.3.1 Plane plume in a uniform ambient

For a plane plume in a uniform ambient where there is no change of ambient buoyancy with height ($\frac{\partial \Delta_e}{\partial z} = 0$), a similarity solution exists where $F = zF_0$ [1]. Using an approach similar to Morton et al. [6], the solution is given by Cooper et al. [1] as

$$Q = \frac{3}{4}\left(\frac{4}{5}\right)^{1/3} \alpha^{2/3} F_0^{1/3} z^{4/3} \tag{2.17}$$

$$M = \frac{3}{4}\left(\frac{4}{5}\right)^{2/3} \alpha^{1/3} F_0^{2/3} z^{5/3} \tag{2.18}$$

$$\Delta = \frac{4}{3}\left(\frac{5}{4}\right)^{1/3} \alpha^{-2/3} F_0^{2/3} z^{-1/3} \tag{2.19}$$

$$w = \left(\frac{4}{5}\right)^{1/3} \alpha^{-1/3} F_0^{1/3} z^{1/3} \tag{2.20}$$

where all properties are per unit length of the source. A simplified solution also exists for when the ambient is linearly stratified.

2.3.2 Plane plume in a linearly stratified ambient

For a plane plume in a linearly stratified ambient [1], the variables can be non-dimensionalized, returning

$$\zeta = \alpha^{1/2} F_0^{-1/2} N^{3/2} z \tag{2.21}$$

$$f = \alpha^{1/2} F_0^{-3/2} N^{3/2} F \tag{2.22}$$

$$q = F_0^{-1} N^2 Q \tag{2.23}$$

$$m = \alpha^{1/2} F_0^{-3/2} N^{5/2} M \tag{2.24}$$

representing non-dimensional height, buoyancy flux, volume flux and momentum flux for the plume, respectively. The governing equations expressed in terms of normalized variables are then

$$\frac{dq}{d\zeta} = \frac{m}{q} \tag{2.25}$$

$$\frac{dm}{d\zeta} = \frac{qf}{m} \tag{2.26}$$

$$\frac{df}{d\zeta} = -q + 1 \tag{2.27}$$

In a linearly stratified environment the buoyancy frequency is constant. Cooper et al. [1] solved equations (2.25), (2.26) and (2.27) numerically by imposing the boundary conditions $f(0) = q(0) = m(0) = 0$, i.e. no volume flux at the leading edge of the source. The result is presented in figure 2.3, predicting the behaviour of a plume in a linearly stratified environment.

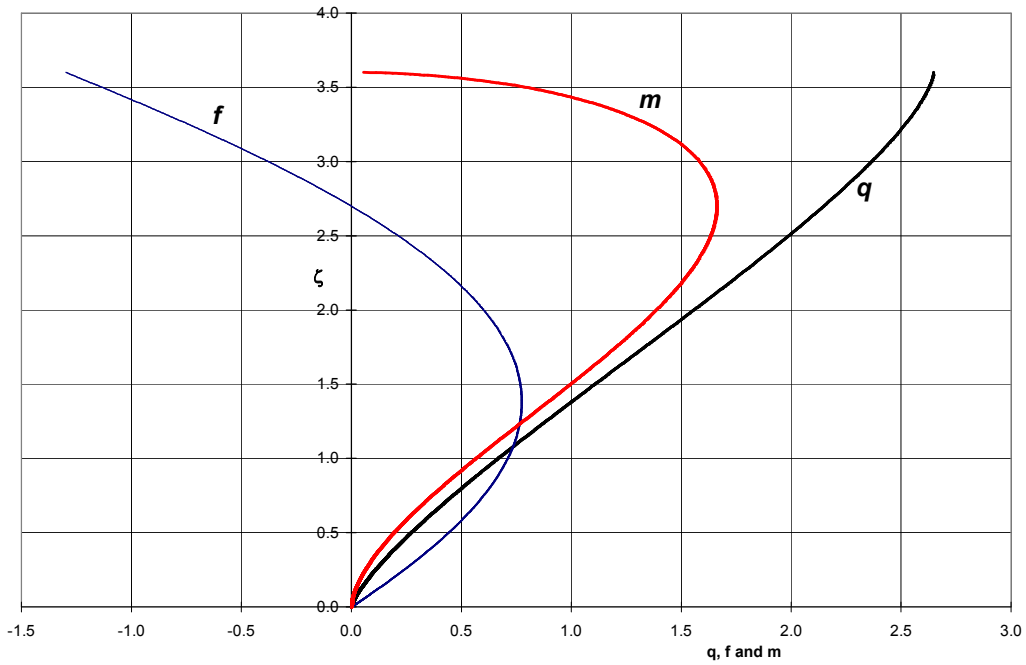

Figure 2.3. Variation in the non-dimensional volume flux, *q*, buoyancy flux, *f*, and momentum flux, *m*, of a plume due to a plane, vertically distributed source of buoyancy in a linearly and stably stratified environment of buoyancy frequency *N*. Reproduced from Cooper et al. [1].

In figure 2.3, the plume has negative buoyancy for $\zeta > 2.7$ and negative momentum for $\zeta > 3.6$. Consequently, the plume is expected to flatten out and form a horizontal intrusion into the ambient in the region $2.7 < \zeta < 3.6$.

By solving the plume equations for a linearly stratified environment numerically, Cooper et al. [1] found an expression for the volume flux in the plume as a function of height:

$$q = \frac{3}{4}\left(\frac{4}{5}\right)^{1/3} \zeta^{4/3}\left(1 - 0.0242\zeta - 0.0161\zeta^2\right) \qquad (2.28)$$

2.3.3 Sealed filling box

A sealed filling box behaves differently compared to an open region. Confining the plume and the environment creates the “filling box” behaviour, where the position of the first front is time dependent. This development of environment in the sealed filling box is presented in figure 2.4.

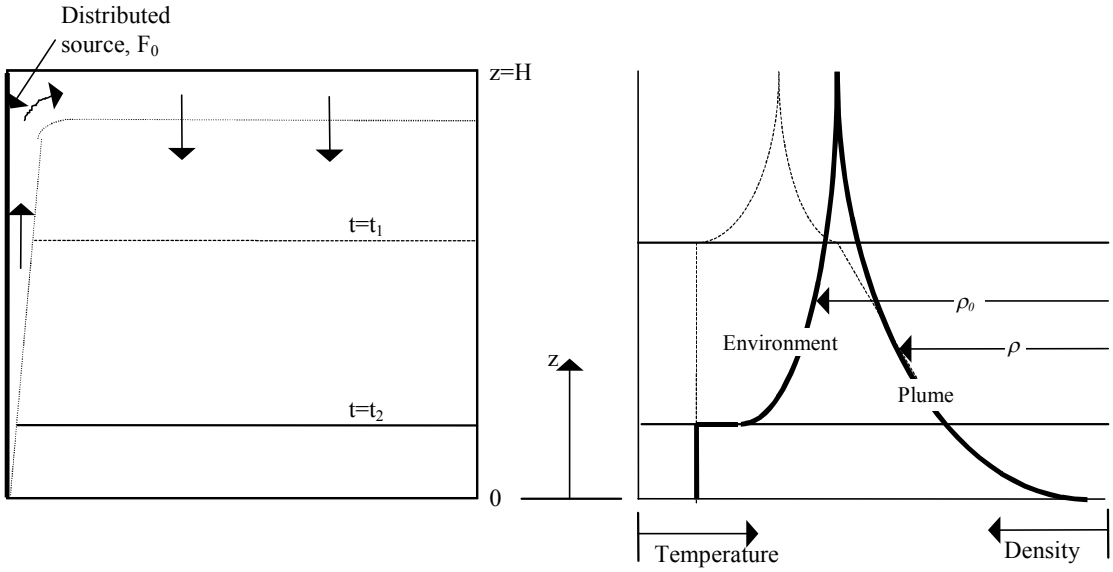

Figure 2.4. Left: the development of a plume from a plane, vertical, distributed source of buoyancy on one wall of a sealed box of height *H* showing position of the first density front at times t_1 and t_2 ($t_2 > t_1$) ; Right: the corresponding density profiles in the plume and the ambient fluid (not to scale). F_0 is the buoyancy flux per unit area of the source. ρ and ρ_0 denote the density of the plume fluid and the ambient, respectively. Reproduced from Cooper et al. [1].

For the case of the sealed filling box, variables can be made non-dimensional as follows [1].

$$\zeta = zH^{-1} \tag{2.29}$$

$$\tau = \alpha^{2/3} H^{1/3} \left(\frac{L}{A} \right) F_0^{1/3} t \tag{2.30}$$

$$\delta = \alpha^{2/3} H^{1/3} F_0^{-2/3} \Delta_e \tag{2.31}$$

$$f = H^{-1} F_0^{-1} F \tag{2.32}$$

$$q = \alpha^{-2/3} H^{-4/3} F_0^{-1/3} Q \tag{2.33}$$

$$m = \alpha^{-1/3} H^{-5/3} F_0^{-2/3} M \tag{2.34}$$

The governing equations for the filling box are then:

$$\frac{\partial \delta}{\partial \tau} = q \frac{\partial \delta}{\partial \zeta} \tag{2.35}$$

where equation (2.35) can be modified to describe a ventilated filling box.

2.3.4 Ventilated filling box

The effective vent area, as defined by Cooper et al. [1] is

$$A^* = \frac{c_d a_t a_b}{\left[\frac{1}{2}\left(\frac{c_d^2}{c} a_t^2 + a_b^2\right)\right]^{\frac{1}{2}}} \tag{2.36}$$

where c is a loss coefficient for sharp-edged opening and c_d is a discharge vena contracta coefficient accounting for the relationship between the areas of the vena contracta and the vent opening. The equation is similar to the one presented by Linden in §2.2.4, except for the introduction of this coefficient. The details are described in figure 2.5.

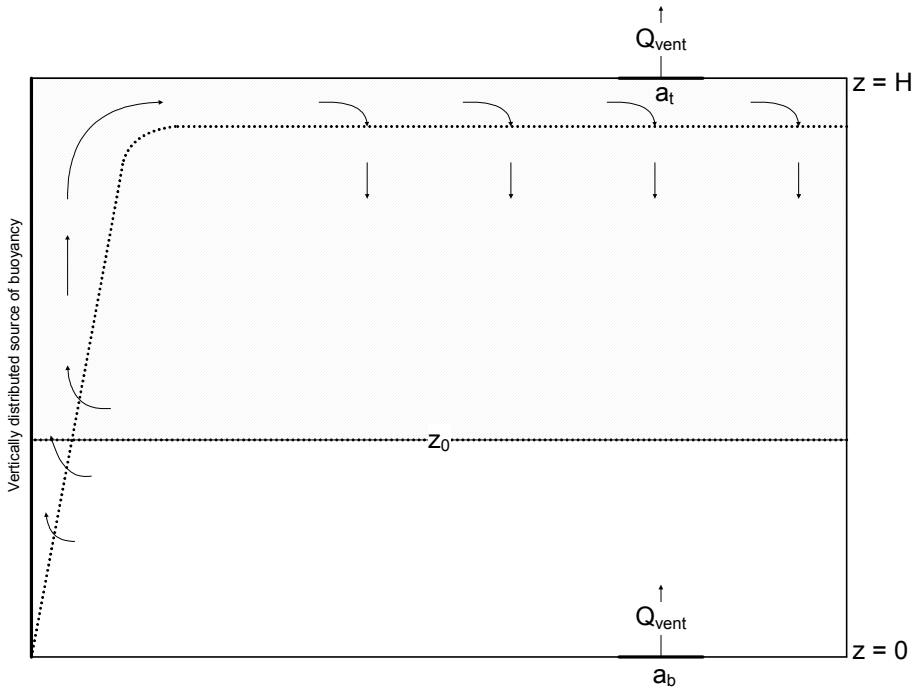

Figure 2.5. A vertically distributed source of buoyancy in a ventilated filling box. The filling process is indicated and the first front z_0 moves downwards until steady-state position is reached.

Additionally, equation (2.10) relating the effective vent area to the position of the first front by Linden et al. may be rewritten for a vertically distributed source of buoyancy to [11]

$$\frac{A^*}{\alpha HL} = C^{\frac{2}{3}}\left[\frac{\zeta^5}{(1-\zeta)}\right]^{\frac{1}{2}} \tag{2.37}$$

and the volume flux through the vent can be found as

$$Q_{vent} = A^*\left(\int_0^H \Delta_e dz\right)^{1/2} = A^*\left(\int_{z_0}^H \Delta_e dz\right)^{1/2} \tag{2.38}$$

By applying equations (2.33), (2.33) and (2.31), equation (2.38), the volume flow per unit length can be expressed in terms of dimensionless variables as

$$q_{vent} = \frac{A^*}{\alpha HL}\left(\int_0^1 \delta\, d\zeta\right)^{1/2} \tag{2.39}$$

where the non-dimensional effective vent area can be written as $\frac{A^*}{\alpha HL} = a^*$. A simple modifications similar to that of Germeles [8] can then be implemented to the governing equations: Inserting equation (2.39) into equation (2.35) produces the governing equation for the ventilated filling box,

$$\frac{\partial \delta}{\partial \tau} = \left(q - q_{vent}\right)\frac{\partial \delta}{\partial \zeta} \tag{2.40}$$

by subtracting the ventilated flow from the incoming [8].

In a ventilated filling box, steady-state can be achieved since there can be a buoyancy balance in the box when added buoyancy equals buoyancy leaving through the vent opening. Figure 2.6 shows the steady-state non-dimensional solution for the ambient stratification, as presented by Cooper et al. [1].

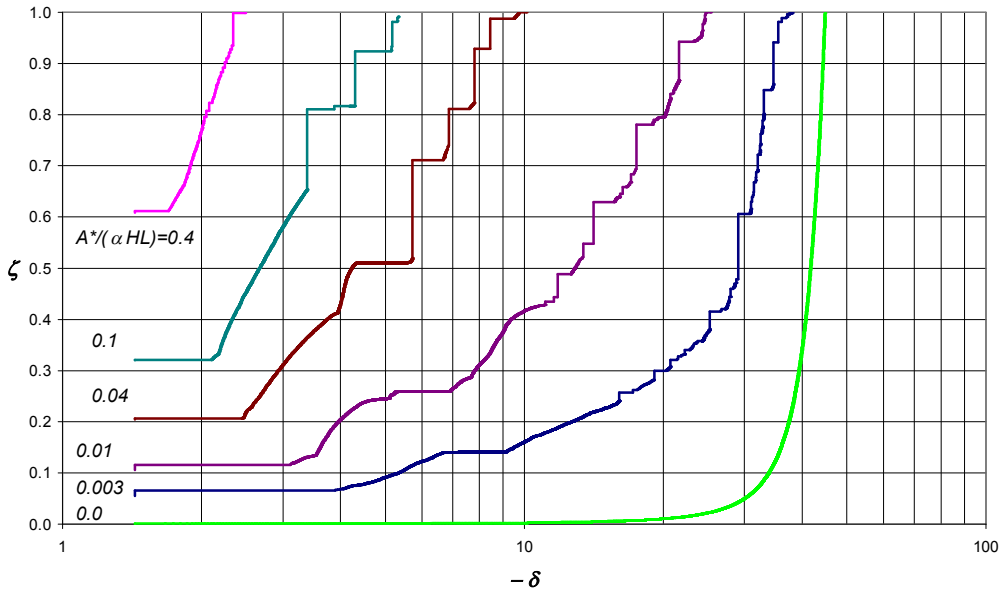

Figure 2.6. The ambient stratification generated within a filling box at $\tau = 40$ by a plane, vertically distributed source of buoyancy as a function of the non-dimensional vent area of $A^*/(\alpha HL)$. Reproduced from Cooper et al.

The steady-state solution predicts a multi-layer stratification similar to that of Linden et al. [10], related to the size of the non-dimensional vent area [1]. This relationship is displayed in figure 2.7 where the trend is that a decreasing value of the effective vent area increases the number of interfaces in the box.

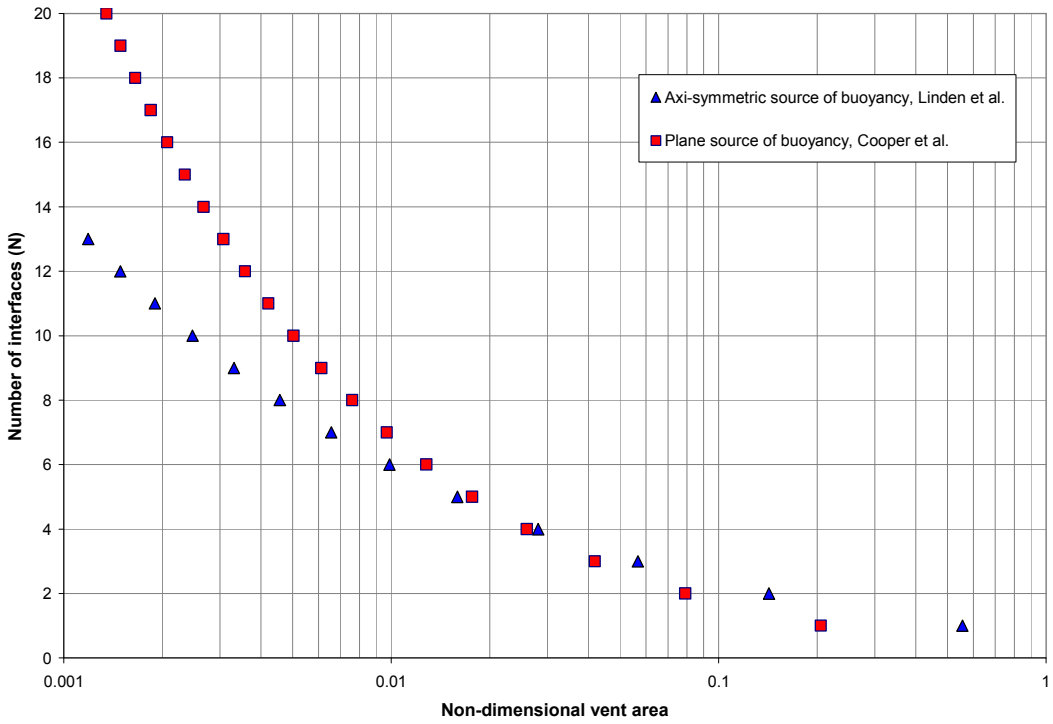

Figure 2.7. Prediction of the number of interfaces for steady-state in a ventilated filling box containing a plane, vertically distributed source of buoyancy or an axisymmetric vertical line source of buoyancy. It is assumed that all layers in the box are of equal height for a given vent area. Redrawn from Cooper et al. [1].

Some aspects of the theory presented in this chapter have been investigated experimentally by previous students at University of Wollongong, such as the position of the first front and qualitative measurements of an intrusion [14,15]. However, accurate measurements of the stratification in a ventilated filling box were yet to be done, such as observing the interfaces presented in figure 2.7. The effects of the plume in a linearly stratified environment were also still to be investigated. Hence, the ventilated filling box and the plane plume in a linearly stratified environment were the scenarios selected for experimental procedures in a water scale model. The materials and methods used for this are described in the next chapter.

3 Materials and Methods

This chapter considers the experimental equipment and methodology used throughout the experimental work, describing modifications and additions to the water scale model and its auxiliary components.

For the purpose of investigating the theory developed by Cooper et al. [1], two categories of experiments were carried out using a water scale model: one for a steady-state mechanically ventilated case and the other for a transient linearly stratified scenario, observing the behaviour of intrusions leaving the boundary layer adjacent to the source and entering the ambient fluid. The equipment used for these experiments was largely based upon various works done by previous undergraduates [14,15], but some modifications and additions were developed during the course of this thesis.

Previously, the experiments were carried out by submerging a Perspex scale model in a large water tank, which allowed for a naturally ventilated environment to be modelled. However, as a consequence of the drought and following water shortage in Australia, the use of such a model did not represent a sustainable approach to experimental research as it used a considerable amount of water. This led to the construction of a standalone water scale model designed by P. Cooper (P. Cooper, *pers. comm.*), which utilised mechanical ventilation regulated by a diffuser and a drain valve instead of natural ventilation where the flow was regulated by an effective vent area. Similarity considerations of this water scale model are presented in appendix B.2.

Figure 3.1 depicts the setup used for the mechanically ventilated water scale model and the electronics used for all experiments.

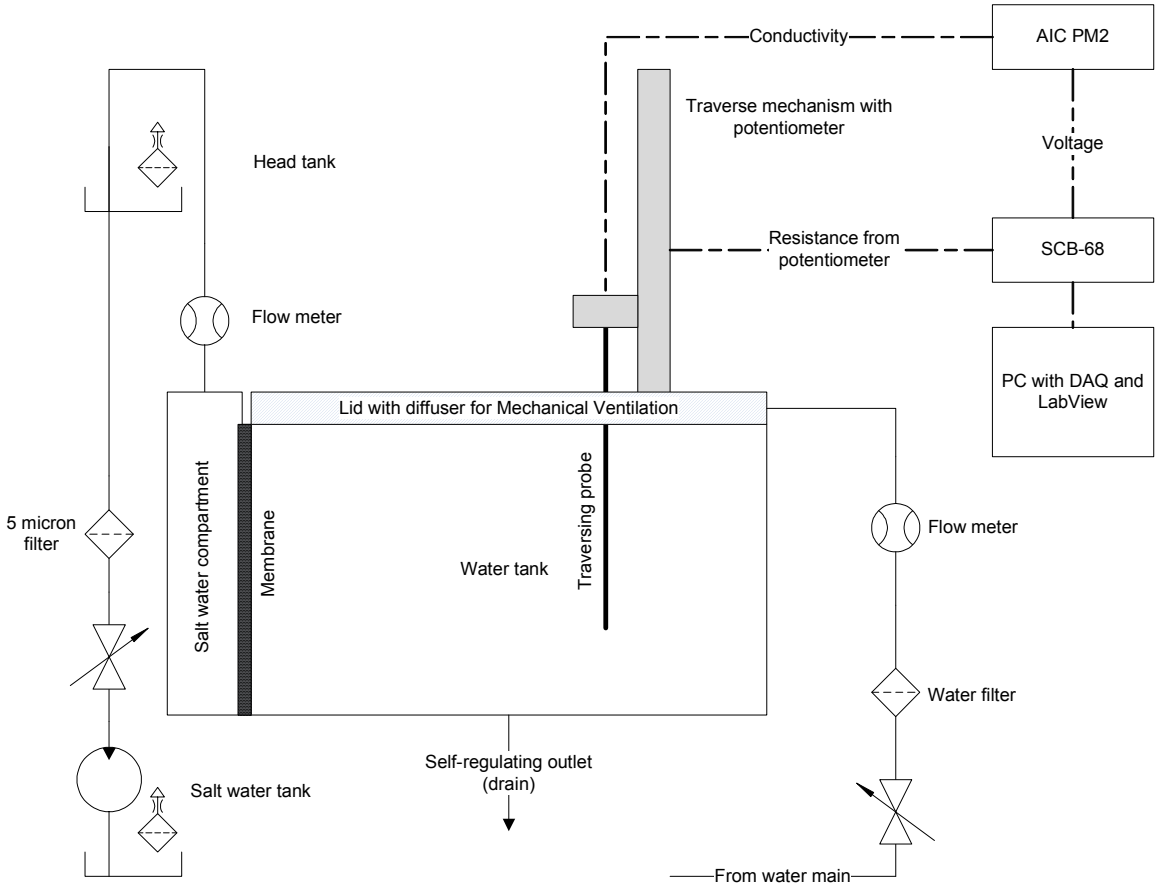

Figure 3.1. Setup used for mechanical ventilation, showing both water flow and measurement related equipment. Thin lines represent water flow and dotted lines represent electronic wiring. AIC PM2 is an electrical conductivity meter for liquids, SCB-68 is the external data acquisition box used for input from the PM2 and the potentiometer.

The conductivity probe was attached to AIC PM2, a microprocessor based conductivity monitor manufactured by Amalgamated Instrument Co. The meter uses alternating current to power the electrodes in the liquid under test to avoid any of the electrodes on the conductivity probe to become contaminated due to electrolysis. It performs one reading every other second, and returns a voltage between 0 and 1 relative to the conductivity reading. This voltage output was connected to a SCB-68 and a DAQ card from National Instruments which was connected to a PC where values were recorded using LabVIEW[1]. The height of the conductivity probe was monitored by applying a voltage to a potentiometer connected to the drive shaft of the traverse mechanism and measuring the resulting change in resistance. The potentiometer readings were then recorded in LabVIEW. Measurements of the water scale model are displayed in figure 3.2.

[1] Please see appendix A.2 for the program written in LabVIEW.

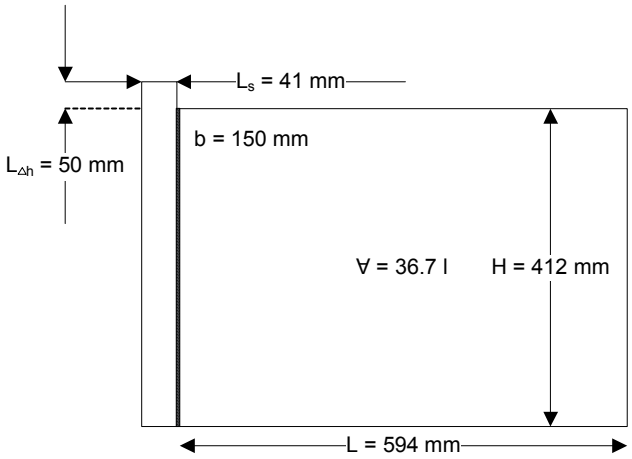

Figure 3.2. The water scale model with the following measurements indicated: Volume ∀ [litres], height *H* [mm], length $L_{\Delta h}$ [mm] of the supply chamber liquid column for initial pressure, length *L* [mm], breadth *b* [mm] and length of the supply chamber L_s [mm].

The tank itself consisted of two chambers separated by a Teflon membrane having a membrane coefficient of c = 1.134×10^{-6} [m^3s/kg] (P. Cooper, *pers. comm.*). The rig with the traversing probe was previously constructed by Logan [16], but for another water scale model and it was modified to fit the one used during the experiments of this work.

Some modifications were also required for the setup to operate in a perspicuous manner, as the previous system had water leakages, rust and components were not organized.

3.1 Modifications

The first change to the original system was to place all the auxiliary parts involving fluids on a single board using a modular approach to the design[2]. This setup stopped leaks and the organized layout made it easier to control valves. Moreover, new parts could be added if necessary. Another modification involved the diffuser used during mechanical ventilation.

3.1.1 Diffuser

A lid with a diffuser for providing mechanical ventilation was previously added to the model by Hough [15]. Ideally, this diffuser would not disturb the stratification in the water scale

[2] Photographs of the setup are in appendix A.1

model, but it had ceased to be water-tight and did not distribute water evenly. The original design was modified by the present author with the objective of providing a distributed flow of water without any water leakage, and figure 3.3 shows the diffuser after the modification.

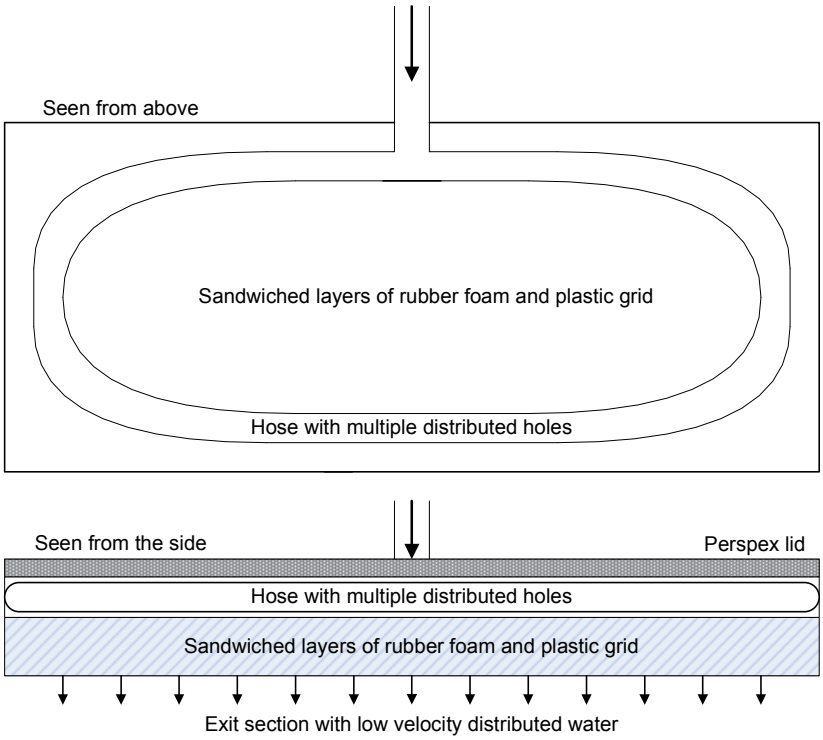

Figure 3.3. Perspex diffuser with several sandwiched layers of rubber foam and plastic grid to evenly distribute the incoming water. The exit section is meant to be slightly submerged into the water scale model.

The hose was connected in a closed circuit aiming to provide an even distribution of pressure and a distributed flow rate through the drilled holes. These holes were added while testing the flow rate, so that they could compensate for any low-pressure zones. Water flowing out of the hose was then passed through a series of interior components of rubber foam and plastic grids, further distributing the flow.

After completing the contents of the diffuser, a Perspex lid was added and sealed with silicone rubber. Another challenge described by Hough [15] related to the mechanically ventilated experiments was to regulate the out flow at the bottom of the water scale model.

3.1.2 Regulating valves

In order to maintain steady-state during experiments, it was essential for the outflow to match the inflow. Previously the out flow had been controlled by a drain valve, and for each experiment this valve had to be finely adjusted to match the sum of the incoming membrane and diffuser flows [15]. The present author devised a modification that made the water scale model's water level self regulating. This modification is shown in figure 3.4.

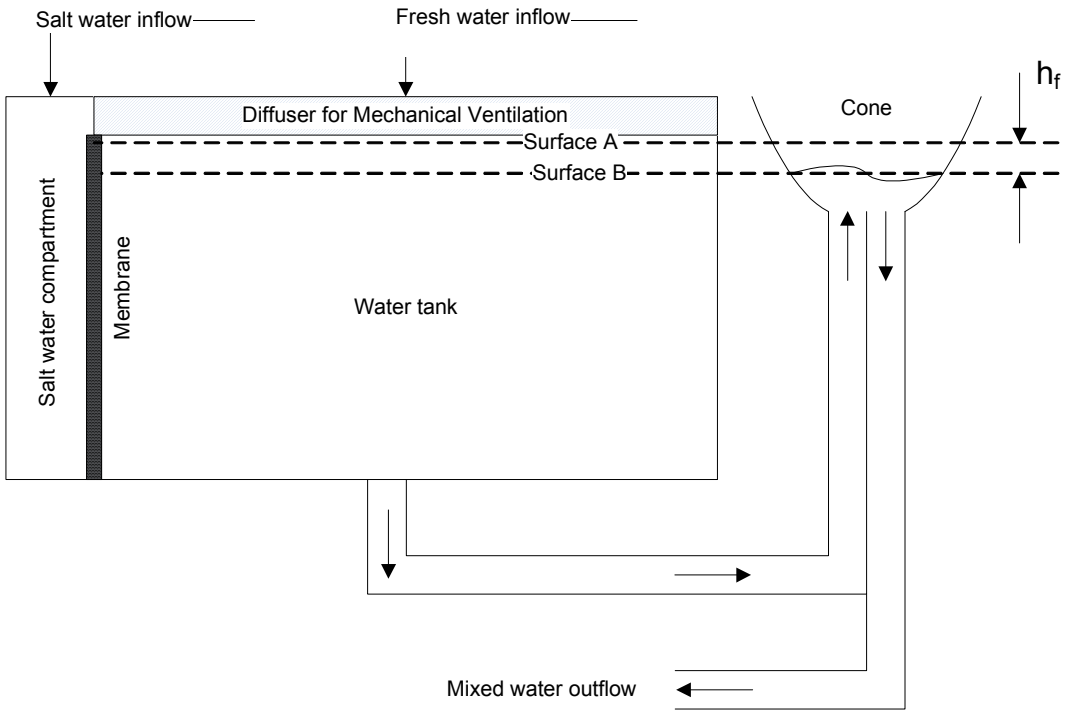

Figure 3.4. The water scale model with a modified outlet valve (not to scale). Surface A is the water tank level and surface B is the cone water level. The height of the cone was adjusted so that any height of surface A could be provided. The water in the cone was exposed to atmospheric pressure.

The theoretical principle of this can easily be expressed with the steady-flow energy equation as

$$p_A + \frac{1}{2}\rho v_A^2 + \rho g h_A = p_B + \frac{1}{2}\rho v_B^2 + \rho g h_B + \rho g h_f \qquad (3.1)$$

following a streamline from one surface to the other. The concept of this design is that the pressures at both points equalize, hence equation (3.1) reduces to $h_f = h_B - h_A$ where h_f is the sum of the pressure losses[3] [17]. In other words, the cone can be lowered a height of h_f, and the flow will regulate itself. In practice, the height of the cone was adjusted to provide

[3] This is the sum of pressure losses caused by friction, inlets, outlets and bends.

the required steady-state surface level for the water scale model, slightly submerging the diffuser.

3.2 The conductivity probe

Another significant modification in terms of accuracy was done by analysing the conductivity probe in terms of an electrical resistance analogy. These calculations and modifications are presented in appendix B and the results are repeated here.

3.2.1 Principle

The principle behind conductivity probe measurements is that the conductivity of the sampled fluid in the nozzle-section of the probe is representative of the conductivity of the liquid drawn into the tip of the probe. The probe consisted of two concentric stainless steel tubes that are separated by an insulator. When the probe was submerged, the electrical resistance of the water could be measured according to its salt content by applying a voltage and measuring the current using a conductivity meter. The purpose of the electrical resistance analogy analysis was to investigate the accuracy of this process (P. Cooper, *pers. comm.*). The modification that this analysis resulted in is presented in figure 3.5, showing the nozzle section of the probe.

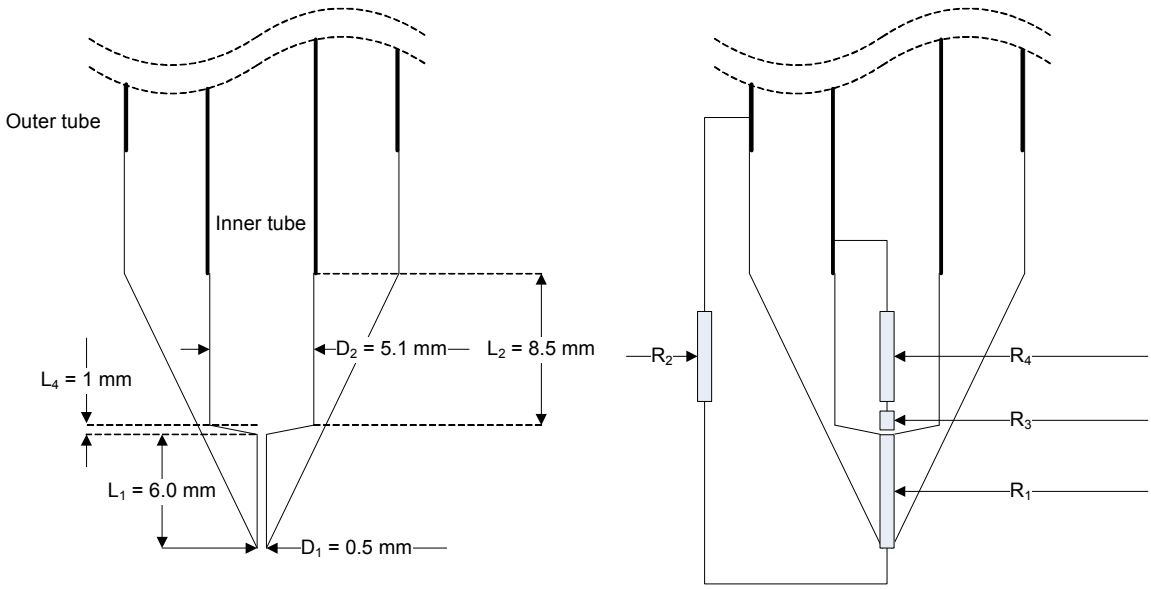

Figure 3.5. Lower section of the probe, with the right figure showing the main component of the electrical resistance analogy. The nozzle section was made of plastic and did not conduct electricity. The potential difference was applied between the inner and outer stainless steel tubes.

Two copper wires were installed, one inside and one outside the probe. The outside copper wire reduced resistance R_2 and the inside removed resistance R_4 entirely. The outside copper wire also rendered measurements closer to the top of the water scale model possible, as contact with water could be made further down, thus increasing the range of the probe. In addition, it provided means to control the condition of the inner copper wire as both the wires were exposed to the same oxidizing environment.

3.2.2 Probe calibration

Calibration of the probe was done using a Anton Paar DMA 35N density meter. The probe was inserted into a cylindrical cup filled with fluid. Water of constant salt concentration was then injected into the cup and mixed using a syringe. The voltage reading from the PM2 was then recorded in LabVIEW, and at the same time the Anton Paar was used to sample liquid right next to the nozzle. Several samples were taken for each concentration to ensure that the density was uniform. This setup is illustrated in figure 3.6.

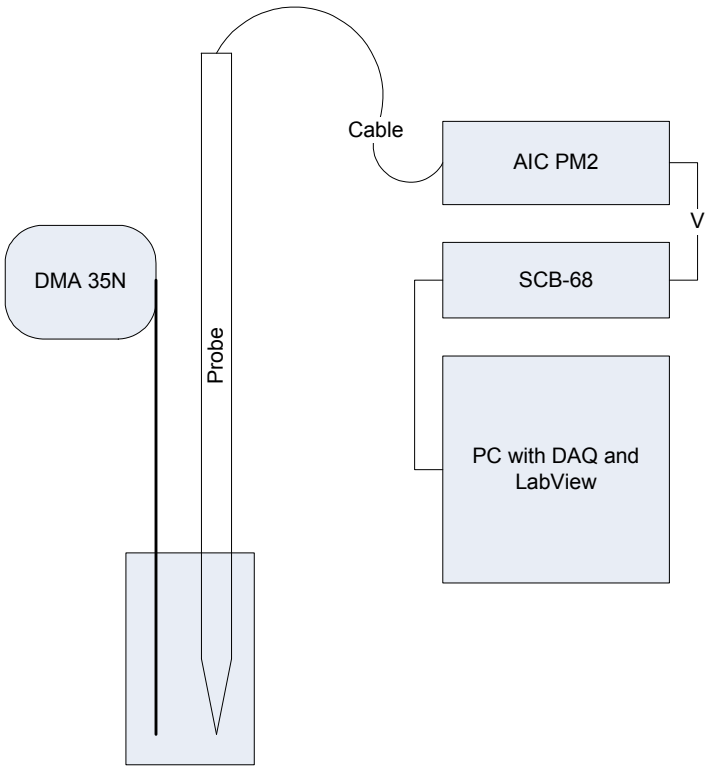

Figure 3.6. Calibration procedure for the conductivity probe, using a Anton Paar DMA 35N density meter as a reference to the readings from the conductivity meter in LabVIEW.

The most important result of this calibration process was that there was a linear relationship between the voltage readings and the actual density (see appendix B.4). Accordingly, linearity was assumed for calibrating the probe readings to density and consequently fewer samples were needed to obtain a full profile. This represented a huge advantage in experimental procedures, as the probe was calibrated before each experiment for accuracy. It was also found that the probe saturated at densities above 1070 kg/m^3. For this reason, only ambient stratifications with densities up to this level could be measured.

3.3 Performing a traverse

Since the resolution of the PM2 conductivity meter was limited to one reading every other second, each traverse was slowed down to the minimum allowed by the available torque from the 12 volt electric motor running the probe. This was done using a variable voltmeter, resulting in an average time of 4.5 minutes to complete one traverse.

During a traverse, sampling with the probe was done through continuous siphoning of ambient fluid. This fluid went through the probe nozzle and a rubber hose before entering a drain bucket positioned lower than the water scale model. Moreover, the probe had to be descending for sampling stratified fluid. This was a consequence of the boundary layer that developed around the ascending probe, polluting the sample. Also, if the probe was moving upwards in a stratified fluid where the density is decreasing with height, it was suspected that there was a flow pattern as in figure 3.7.

In addition, the diameter of the inner tube was one order of magnitude larger than the nozzle, thus the volume flux though the nozzle is very small compared to the volume of fluid already in the probe. During ascent, this fluid would have a higher density than the newly sampled fluid which could cause some of the denser fluid to descend and the newly sampled fluid to mix, or channel through, the denser one. These effects are also illustrated in figure 3.7.

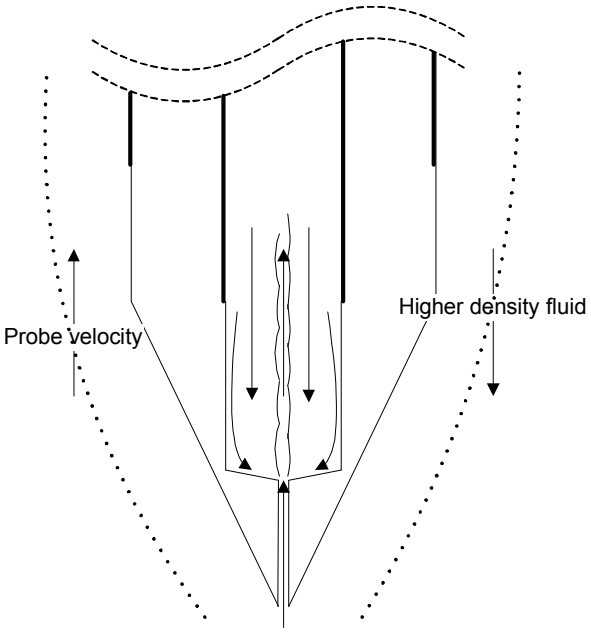

Figure 3.7. Suspected pattern of mixing in probe including a surrounding boundary layer created during the ascent of the probe. The area between the dotted lines and the probe represents the region where some fluid has been transported through the boundary layer. This was removed by gently stirring the probe.

Consequently, these effects resulted in a "quarantine period" between experiments, as the dense fluid had to exit the probe before an unpolluted sample could be taken. The pause required between experiments was significantly reduced after the probe modifications of removing of resistance R_4. It was then only limited by fluid following the boundary layer of the probe during ascent. This effect was observed both visually and through readings from the PM2, but could be avoided by gently stirring the probe before a new traverse commenced.

3.3.1 Sampling and stratification profile

The conductivity probe siphoned ambient fluid which constantly ran through it for sampling. Due to the scope of this thesis, it was assumed that the sampling at a given height corresponded to the density at that height, as mentioned in the previous section.

A more realistic approach is that the density of the sample is dependant on the local stratification, as described by Wood [18,19] and Bryant and Wood [20], but this approach is beyond the scope of the present work. However, it should be mentioned that a linear stratification would provide the optimal conditions for sampling.

For observing these sampling procedures, the stratifications and flow patterns, a shadowgraph was used.

3.4 Shadowgraph technique

A shadowgraph converts phase differences into amplitude differences, making them observable [21]. As the refractive index of a liquid changes with its density, shadows of the changes in salt concentration are cast onto the tracing paper. This method was used for both of the linearly stratified and mechanically ventilated experiments and it is illustrated in figure 3.8.

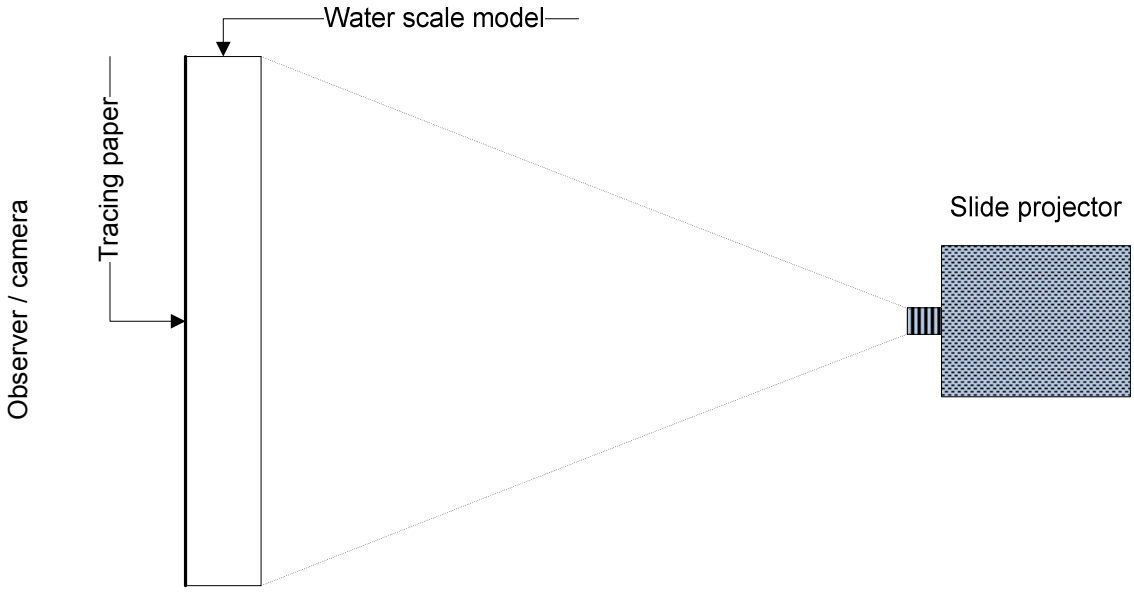

Figure 3.8. Creating a shadowgraph by covering up one side of the water scale model with tracing paper and shining light on the other side of the model using a slide projector as a light source. As seen from above.

The shadowgraphs were produced using a slide projector as a light source on one side of the water scale model, covering the other side of the model with two sheets of A3 tracing paper. This allowed for observing flow patterns resulting in changes in density. These changes would be largest during the beginning of an experiment, and the next section explains how the mechanically ventilated filling box experiment was started.

3.5 Mechanically ventilated filling box

To start an experiment, valve *S* in figure 3.9 was regulated together with valve *M* to provide the required Δh for membrane flow and flow rate for the diffuser, respectively. Additionally, Δh_{outlet} was set at a height to regulate the water level in the water tank so that the lower part of the diffuser was slightly submerged. The system was then allowed to reach steady-state.

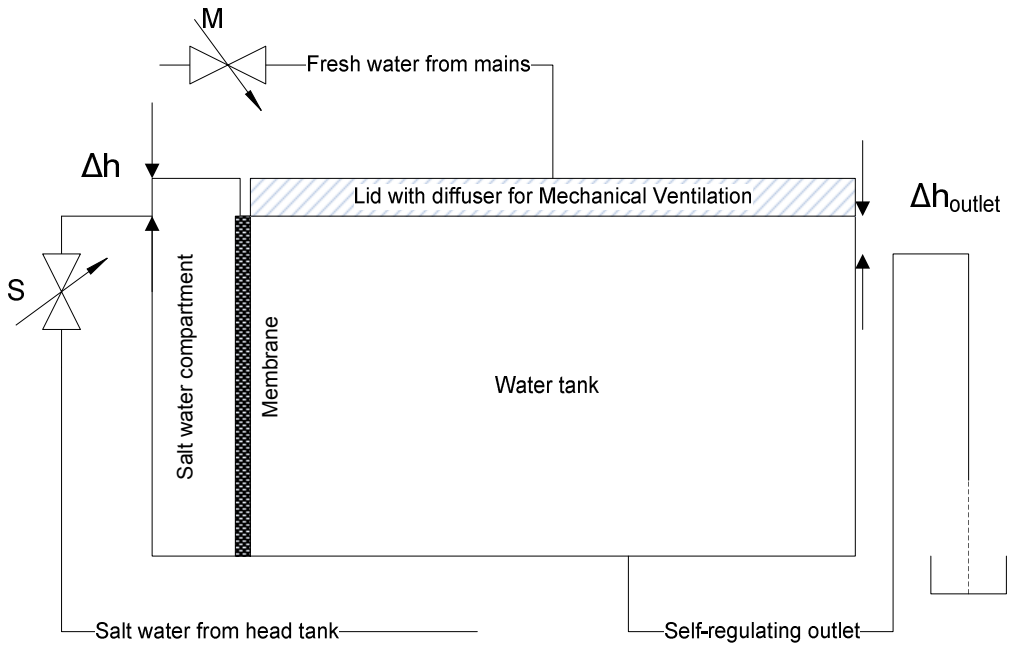

Figure 3.9. The mechanically ventilated water scale model with the self-regulating outlet, the salt water from the head tank and the slightly submerged diffuser for incoming flow. The top section of the self-regulating outlet was exposed to atmospheric pressure.

Two main techniques for measuring the flow rates through the membrane and the diffuser were examined. One method was to use flow meters to monitor membrane and diffuser flow, but they had to be calibrated before each experiment due to density differences. The most sensible and precise method was to use a measuring cup and a stopwatch to determine the outgoing flow rate from the water scale model (this would also be the method of calibrating the flow meters; hence the applied method prevented two additional manual reading). The outgoing flow rate was measured at two points: during the experiment and afterwards, turning the membrane flow off but leaving the diffuser flow unchanged. The membrane flow could then be found by continuity. At each point, the flow rate was measured using the average of multiple measurements.

All the mechanically ventilated experiments were performed when the stratification was at steady-state. To ensure that steady-state was reached, multiple traverses were performed and it was assumed that the system was in steady-state when the conductivity traverses overlapped, i.e. that the stratifications of traverses *n + 1* and *n + 2* were equal to that of stratification in traverse *n*. This procedure was also followed before each experiment of two reasons: for checking repeatability, and because the first traverse for each experiment could have traces of fluid from the previous experiment.

The conditions for each experiment were determined by varying three parameters: the density of the source, the flow rate from the source and the flow rate from the diffuser. Varying these parameters resulted in different density distributions, or stratifications, inside the water scale model.

When everything was set up to work efficiently, numerous traverses could be performed within the scope of one day. This was quite in contrast to the experiments requiring a linearly stratified environment.

3.6 Linearly stratified filling box

3.6.1 Creating a linear stratification

In order to test the effects of a vertical plane distributed source of buoyancy on a linearly stratified environment, the water scale model was set up with a linearly stratified ambient. There are several methods for achieving linear stratification [22], and in this work a double bucket method was preferred due to its simplicity and availability. Figure 3.10 illustrates the setup used, and in addition to the details there, the wiring and electronics were the same as in figure 3.1.

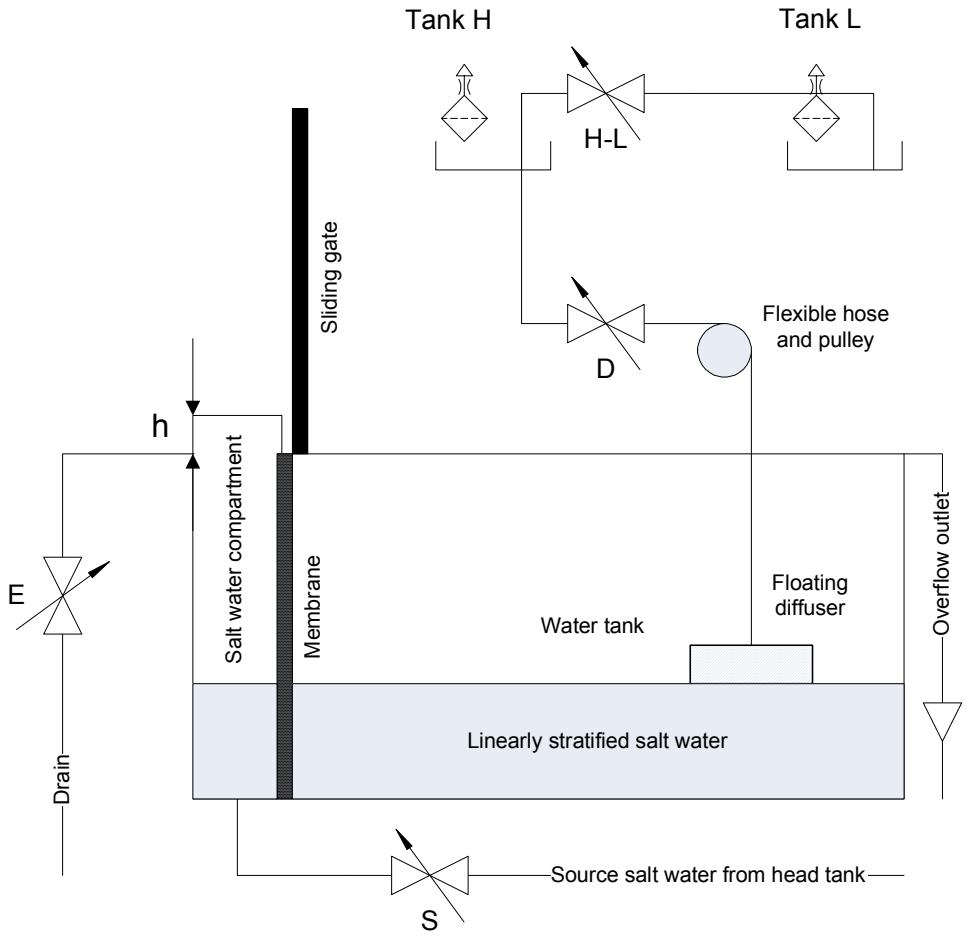

Figure 3.10. The linearly stratified water scale model displayed with a double bucket method, a sliding gate, a floating diffuser and an overflow outlet for the displaced water.

The two tanks *H* and *L* were elevated in order to provide sufficient head. Tank *H* contained high concentration salt water and tank *L* low concentration, typically fresh water. They were connected by a valve-controlled hose, valve *H-L*. In addition, tank *H* contained a bilge pump that provided sufficient mixing of the incoming water from tank *L*.

Tank H was then connected to a floating diffuser through valve *D* and a soft rubber hose going through a pulley. The pulley system ensured that the diffuser was allowed to float freely without having the weight of the hose suppressing any vertical movement, possibly disturbing the filling process.

Firstly, a floating diffuser had to be constructed, as those used by previous students had deteriorated due to salt and humidity. The construction was inspired by the previous model constructed by Eggebrecht [14] and used by Hough [15]. As displayed in figure 3.11, it was

constructed using rubber foam, a plastic mesh and Styrofoam, distributing water at a low velocity over a large surface, as displayed in figure 3.12.

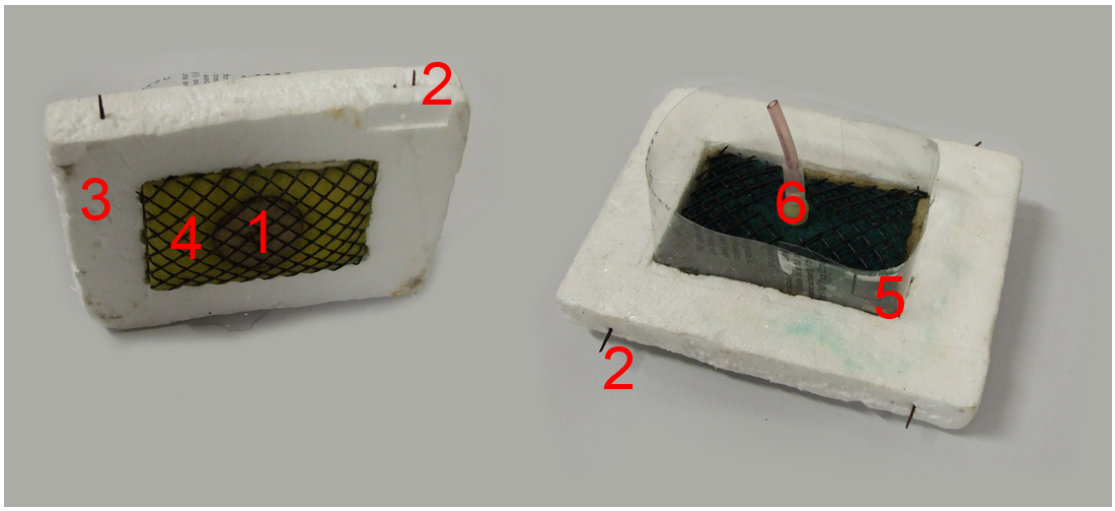

Figure 3.11. Floating diffuser used to set up the linearly stratified environment. Description as follows: 1. Momentum stopper. 2. Anti-stiction device made of wood. 3. Styrofoam frame. 4. Rubber foam covered in plastic mesh. 5. Barrier to prevent any overflowing fluid. 6. Rubber hose fitting.

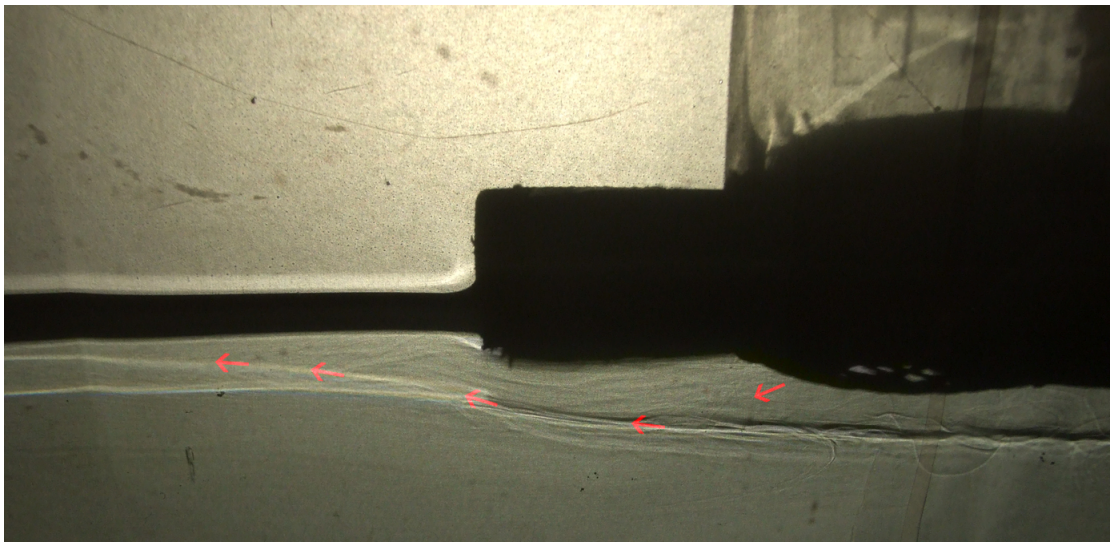

Figure 3.12. A shadowgram showing the flow from the diffuser to the ambient. The flow pattern had negligible transient effects and the red arrows indicate flow direction.

As the filling process started, valve *H-L* and valve *D* were opened simultaneously, allowing water to slowly fill up with the tank with decreasingly dense brine. After this process was completed, three conductivity traverses were performed, both to ensure that they were repeatable and that the stratification was linear.

A consequence of this filling procedure was that the salt water compartment behind the membrane filled up at the same time as the main section of the water tank.

3.6.2 The salt water compartment

To completely flush this compartment of stratified fluid to provide a uniform density from the source at the start of each experiment, salt water was supplied from below by carefully controlling valve *S*, using a similar method as Hough [15]. The highly dense source then displaced the stratified fluid, and ideally this flow should have a piston-flow pattern. An image of this is in figure 3.13, the red arrow indicating flow direction.

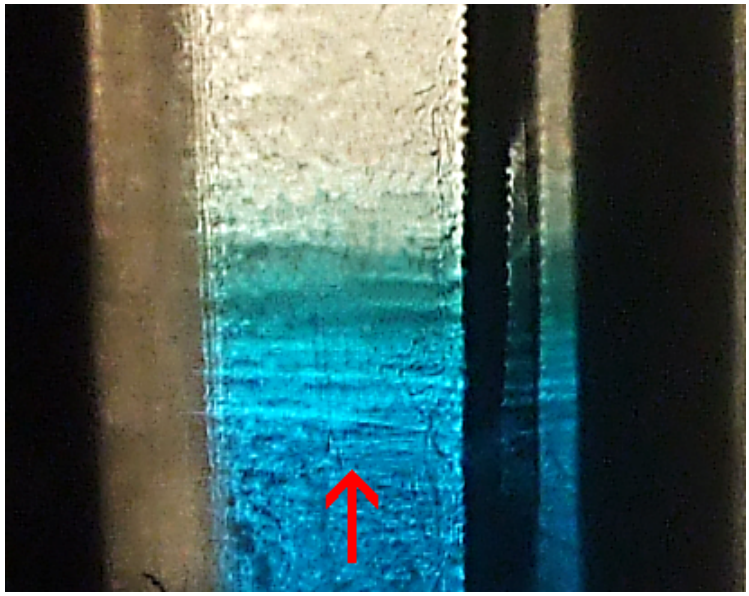

Figure 3.13. A shadowgram of the displacement flow in the supply compartment. The interface of the supply fluid's (blue dye) advancing front is indicated by the bright horizontal lines. Right above, mixing between stratified fluid and supply fluid can be observed indicated by the slightly green colour.

This flow pattern indicated that the supply liquid displaced the stratified liquid, completely filling this supply compartment as the front moved upwards. While doing this, the stratified liquid was drained from the top of the supply chamber through carefully controlling valve *E*, keeping *h* at zero. This process was monitored using shadowgraph technique to ensure that entrainment was minimal and that a negligible amount of membrane flow occurred. In addition, a blockage was positioned slightly above the supply opening at the bottom to prevent any fountains [3,23] entraining the already present stratified fluid.

When the supply chamber was full of supply fluid, the drain valve *E* was closed and the supply valve *S* regulated such that a constant head was produced and the steady flow through the membrane to the main part o the tank was achieved.

3.6.3 Actuation

This constant head forced liquid through the membrane, thus actuating the plume. After a certain time, usually less than two minutes, valve *S* was closed and valve *E* opened. Stopping the remaining supply fluid in the supply compartment to flow through the membrane without disrupting the ambient stratification was done by using a thin plastic sheet, sliding it down on the supply side of the membrane. Following this, a conductivity traverse was performed to see the change in conductivity and thus the change in ambient density.

The experimental methodologies for the mechanically ventilated and the linearly stratified experiments have been described in this chapter. The next chapter continues by presenting the numerical methodology used for solving the plume equations developed by Cooper et al. [1] for a plane vertically distributed source of buoyancy.

4 Numerical Methods

This chapter explains how the plume equations are solved and the modifications done to the program that solved them. The motivation behind these modifications was to increase the modularity of this program and thus make is possible to implement new features, such as a better routine for modelling intrusions and the modelling of a dimensional environment.

Numerical solutions of the plume equations for a vertically distributed source had been done previously by using a computer program written in Fortran 77 by Paul Cooper [1]. This program, hereinafter referred to as *Distran*, was written specifically for the purpose of solving these plume equations for the vertically distributed source in a filling box situation, using a technique similar to that of Germeles [8] and Worster and Huppert [9].

4.1 Distran

After conversations with P. Cooper (P. Cooper, *pers. comm.*), it was decided to implement *Distran* with new functionality. Firstly, when implementing changes into an already complex code, it is an advantage having a modular and thus flexible code. *Distran* as developed by Cooper was not modular; hence one motivation for revising the program was to create individual subroutines that could be controlled easily, allowing additional subroutines to be added without altering the entire code. Moreover, this modular approach would simplify the debugging process.

Distran was written using Fortran 77, which has now been replaced by Fortran 90/95[4]. Thus, for both flexibility and adaptability, a Fortran 95 free format was chosen for revising Distran. Moreover, the Salford FTN95 package [24] was used as an integrated developer environment, as it provided excellent debugging possibilities combined with a very robust compiler.

[4] A newer standard exists, Fortran 2003, but Fortran 95 is currently more established and widely supported by compilers, hence selected for re-writing Distran.

The Germeles approach to numerically solving the plume equations utilizes numerical layers for portraying the environment inside the box [8], as explained in chapter 2. The initialization process of this environment is as follows [1,8,9]:

The plume is assumed to be fully developed as it reaches the top of the box, and a numerical layer is formed in a defined time step. The reduced gravity at the height of the outflow from the plume sets the reduced gravity of this numerical layer, and the depth of the layer is calculated from the volume flux in the plume at the height of the outflow.

Between each time step, the plume entrains fluid from the first numerical layer. The original layer is reduced in thickness as it is displaced downwards by a numerical layer of greater buoyancy. The process starts again from the top and fills the box. The density is integrated over the numerical interfaces to find the driving pressure difference and to calculate the ventilation flow rate. Locally, the buoyancy of each numerical layer is compared to the plume's buoyancy. If the ambient buoyancy is greater, the plume's buoyancy flux, momentum flux and volume flux is set to zero and a new numerical layer with the buoyancy of the plume is formed (i.e. an intrusion into the ambient is formed).

Figure 4.1 shows a flow chart of this process in *Distran*.

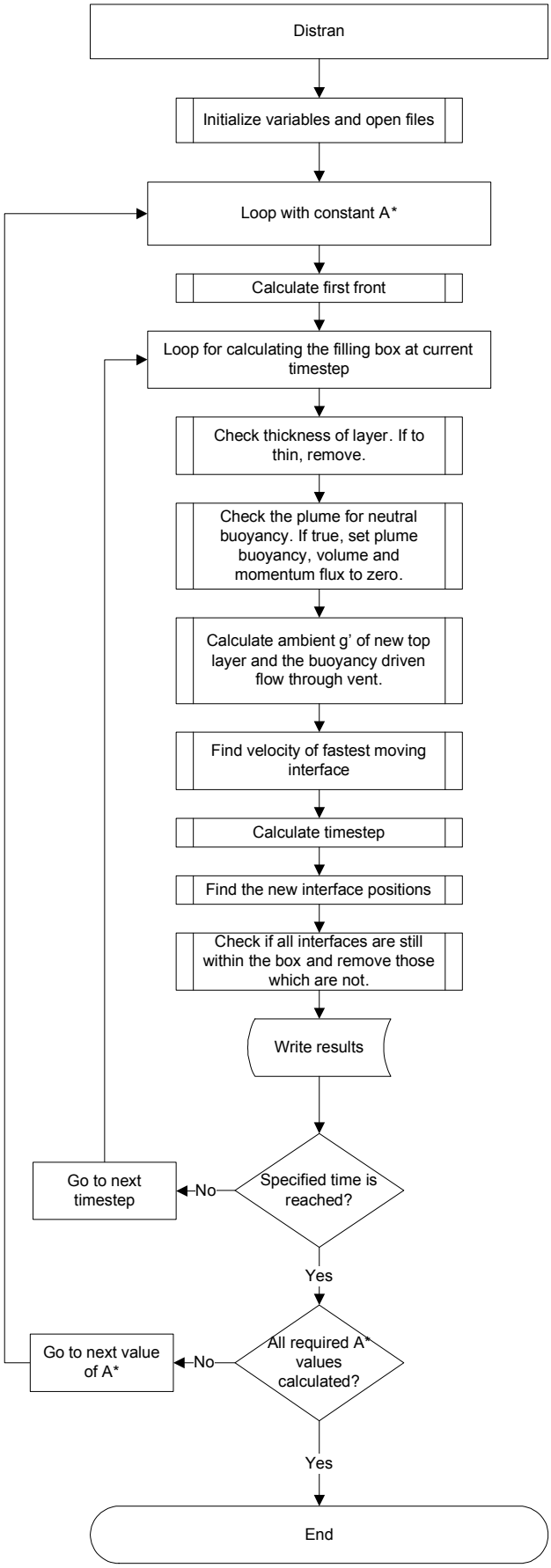

Figure 4.1. Top-down approach flowchart describing the architecture of Distran. Subroutines are displayed as double framed boxes.

The top down approach in figure 4.1 displays the main code that links the subroutines together and all of the double framed boxes in figure 4.1 are subroutines. The results from the numerical calculation were written to an external file in a way that simplified import of data to spreadsheet software. Most importantly, the modularity introduced to the code by the present author opened up the opportunity for programming a new intrusion routine: The way the program modelled ambient intrusions could be done in a way that smoothes out the detraining section, creating a horizontal velocity profile of Gaussian shape instead of immediately setting the plume velocity, volume flux and momentum flux to zero. However, before implementing this into *Distran* a theory for modelling a simplified intrusion had to be developed.

4.2 Detrainment

An (exaggerated) intrusion of a plume to a uniform ambient can be modelled being similar to figure 4.2, described by its three 'regions'.

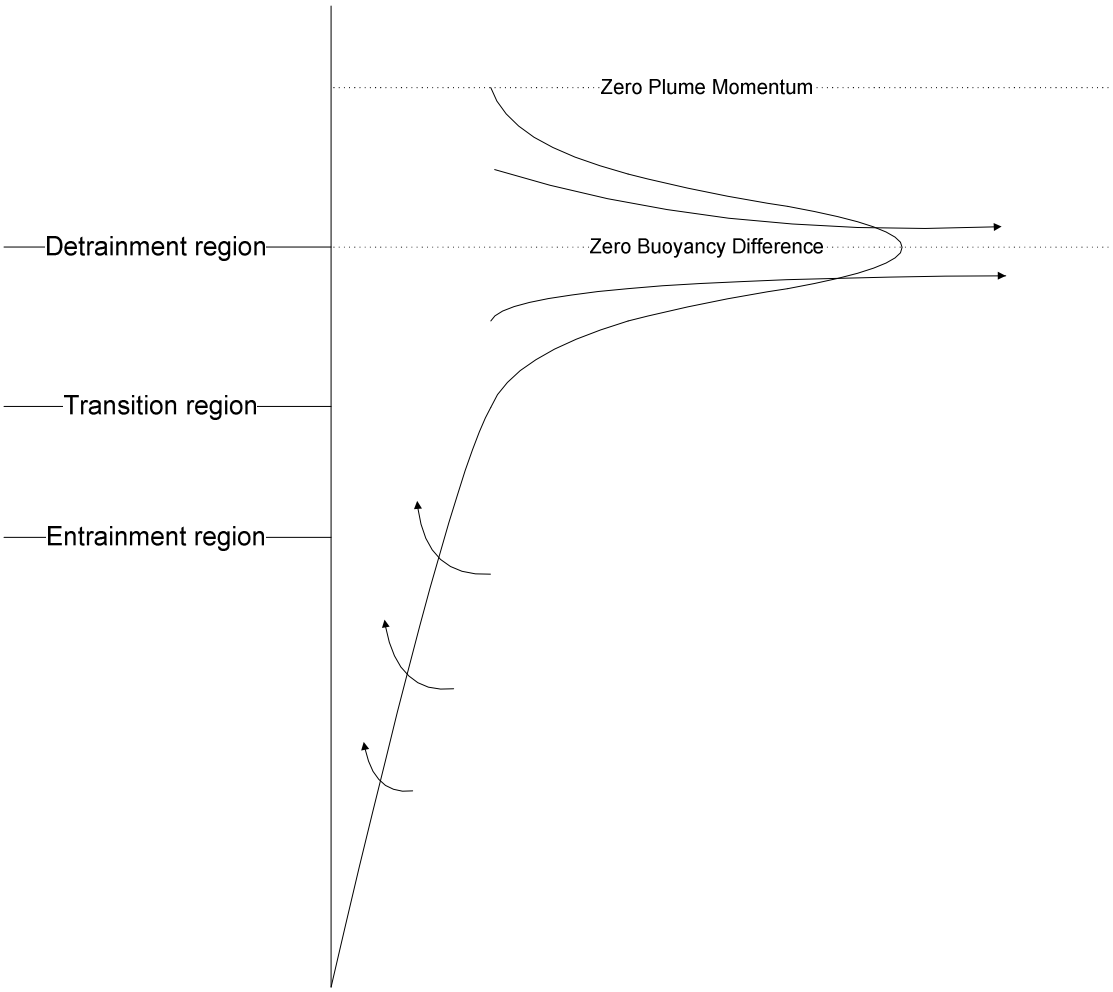

Figure 4.2. A plume detraining, showing the regions of entrainment, transition and detrainment. First, the rising plume entrains fluid from the ambient and at some point the buoyancy of the plume equals that of the ambient. This zero buoyancy difference causes the plume's momentum to decline and in the region between zero buoyancy and zero momentum the plume will spread out into the ambient forming an intrusion.

This intrusion can be modelled in a simple way by using the similarity solution for a uniform ambient presented in §2.3.1. This solution was used in order to relate the width of the plume to its vertical velocity, and the Gaussian shape was used to determine the horizontal velocity itself. Assuming that α is a constant with respect to height, and that the velocity profile of the detrainment is of a Gaussian shape, the horizontal velocity in the plume can be described as

$$v(z) = G(z) \times e^{-\frac{1}{2}\left(\frac{z-z_{nb}}{\sigma}\right)^2} \tag{4.1}$$

where v is the velocity, z is the current height, z_{nb} is the height of neutral buoyancy. $G(z)$ is a function and σ determines the width of the Gaussian curve:

$$\sigma_{nb} = f\left(b(z_{nb}), \left.\frac{dM}{dz}\right|_{z_{nb}}, N^2 \ldots \right)$$

where b can be found by combining equations (2.17) and (2.20):

$$b = \frac{Q}{w} = \frac{\frac{3}{4}\left(\frac{4}{5}\right)^{1/3} \alpha^{2/3} F_0^{1/3} z^{4/3}}{\left(\frac{4}{5}\right)^{1/3} \alpha^{-1/3} F_0^{1/3} z^{1/3}} = \frac{3}{4}\alpha \times z$$

Accordingly, assuming that the width of the Gaussian curve is a function of the width of the plume, b at the point of neutral buoyancy can be expressed as

$$b_{nb} \sim \frac{3}{4}\alpha \times z_{nb} \tag{4.2}$$

An expression for the Gaussian width of the intrusion σ can then be found by assuming that $\sigma = B_{nb} b_{nb}$ where B_{nb} is a constant.

Returning to equation (4.1), it is sensible to assume that the maximum velocity is at the point of neutral buoyancy, since this is the centre of the detraining region. The total detrained volume of the plume can then be related to the maximum velocity and the area under a Gaussian curve.

Firstly, the total detrained volume flux per unit width can be found by integrating the velocity over the Gaussian distribution:

$$\begin{aligned} D_{tot} &= G(z) \int_{-\infty}^{\infty} e^{-\left(\frac{z - z_{nb}}{\sqrt{2}\sigma}\right)^2} dz \quad \left[\frac{\mathrm{m}^2}{\mathrm{s}}\right] \\ &= G(z) \times \mathrm{I} \end{aligned} \tag{4.3}$$

Integration by substitution yields $x = \frac{z - z_{nb}}{\sqrt{2\sigma}}$ and $\sqrt{2\sigma}\,dx = dz$, so substituting *dz* into integral (4.3) returns

$$\begin{aligned} \mathrm{I} &= \sqrt{2\sigma}\int_{-\infty}^{\infty} e^{-x^2}\,dx \\ &= \sqrt{2\sigma}\sqrt{\pi} \end{aligned}$$

Continuing, the horizontal velocity, $v_{dent,\max}$ is at the point of neutral buoyancy, where Q equals Q_{nb}. Therefore, it can be related to the total detrained volume as

$$v_{dent,\max} = \frac{Q_{nb}}{\mathrm{I}} = \frac{Q_{nb}}{\sqrt{2\pi\sigma}} \tag{4.4}$$

Furthermore, the horizontal velocity of the detraining region (at the mid-height along the Gaussian curve) can be expressed in terms of the maximum velocity as

$$v_{dent}(z) = v_{dent,\max} e^{-\frac{1}{2}\left(\frac{z - z_{nb}}{\sigma}\right)^2}$$

which again can be combined with equation (4.4) giving

$$v_{dent}(z) = \frac{Q_{nb}}{\sqrt{2\pi\sigma}} e^{-\frac{1}{2}\left(\frac{z - z_{nb}}{\sigma}\right)^2} \tag{4.5}$$

Assuming that the velocities can be superimposed, the combined horizontal velocity of the entrainment and detrainment may be written as

$$v_{net}(z) = v_{ent}(z) - v_{dent}(z) \tag{4.6}$$

By inserting equation (4.5) into equation (4.6), the complete expression for the horizontal velocity becomes

$$
\begin{aligned}
v_{tot}(z) &= v_{ent}(z) - \frac{Q_{nb}}{\sqrt{2\pi\sigma}} e^{-\frac{1}{2}\left(\frac{z-z_{nb}}{\sigma}\right)^2} \\
&= \alpha w_{mean}(z) - \frac{Q_{nb}}{\sqrt{2\pi\sigma}} e^{-\frac{1}{2}\left(\frac{z-z_{nb}}{\sigma}\right)^2}
\end{aligned}
\tag{4.7}
$$

where the integral in equation (4.7) must be solved numerically. Assuming that the simple detrainment procedure developed in this chapter is applicable to all scenarios and not only for the uniform ambient, it was implemented into Distran as a subroutine.

Such a subroutine is presented in figure 4.3, showing the iterative process of solving equation (4.7).

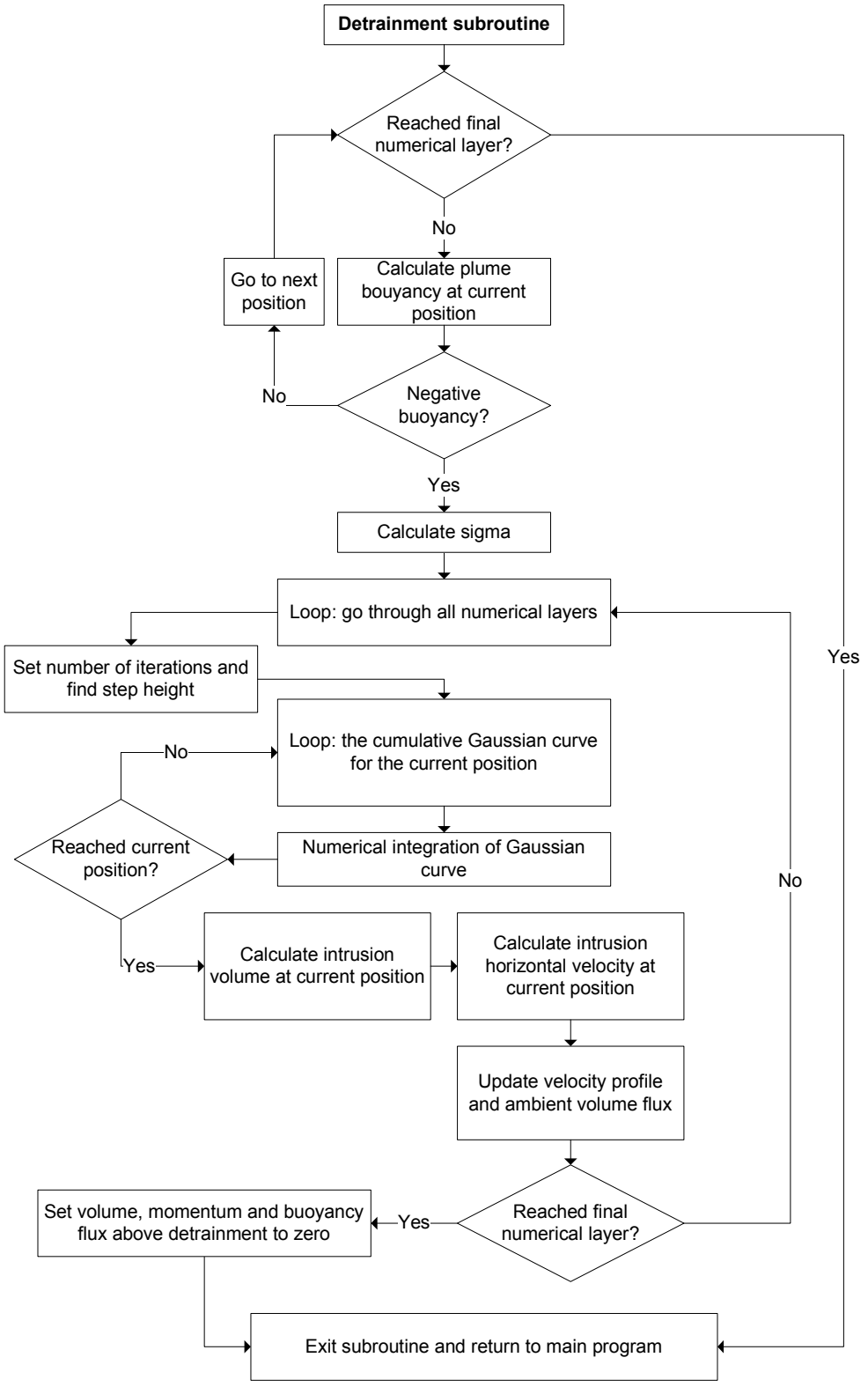

Figure 4.3. A flowchart describing a simple detrainment subroutine. The subroutine was written in Fortran 95 as a part of the program *Distran* described in §4.1.

This subroutine was then implemented into *Distran*, along with the routine described in the next section.

4.3 Varying buoyancy flux

The original version of *Distran* was non-dimensional and in order to compare experimental and numerical results, *Distran* had to be modified so that the dimensional aspects of the experiment were correctly modelled.

Previously, it was shown by Eggebrecht [14] that buoyancy flux through the membrane in the water scale model varied significantly with height. By assuming a linear stratification throughout the water scale model, he found that the volume flux per unit area through the membrane can be expressed as

$$Q_s''(z) = \frac{1}{2} c \times g\left(\rho_s - \rho_{e,0}\right) z^2 + c \times p_0 z \quad \left[\frac{m}{s}\right] \tag{4.8}$$

where $\rho_{e,0} = \rho_e\left(z = 0\right)$ and c is the membrane coefficient. As the buoyancy flux is linked to the volume flux and consequently to the pressure distribution, finding an expression for the pressure distribution was the first objective. Volume flux per unit area through the membrane as a function of height is proportional to the pressure difference between the water chamber and the salt water chamber, depending on the membrane coefficient:

$$Q_s''(z) = c\left[p_s(z) - p_e(z)\right] \quad \left[\frac{m}{s}\right] \tag{4.9}$$

where p_s is the pressure at the salt water side and p_e is the pressure in the water tank. $p_{s,0}$ is the pressure in the source at z = 0, and $p_{e,0}$ = 0 due to cancellation of atmospheric pressure:

$$p_s(z) = p_{s,0} + \rho_s g z \quad [Pa] \tag{4.10}$$

$$p_e(z) = \int_0^z \rho_e g dz \tag{4.11}$$

Equation (4.11) can be conveniently rewritten by introducing equation (2.4) for ambient buoyancy, using $\rho_{e,0}$ as the reference density ρ_∞.

$$p_e(z) = g\int_0^z \left(\frac{\rho_{e,0}}{g}\Delta_e(z) + \rho_{e,0} \right) dz$$
$$= \rho_{e,0}\int_0^z \Delta_e(z)\,dz + \rho_{e,0} gz \tag{4.12}$$

As a result, the expression for the volume flux per unit area through the membrane in equation (4.8) becomes

$$Q_s''(z) = c\left[p_{s,0} + (\rho_s - \rho_{e,0})gz - \rho_{e,0}\int_0^z \Delta_e dz \right] \quad \left[\frac{m}{s}\right] \tag{4.13}$$

The integral in equation (4.13) needs to be solved numerically for a given ambient buoyancy distribution. Accordingly, the corresponding expression for the buoyancy flux per unit area is

$$F_s(z) = \Delta_{s-e}(z) \times Q_s''(z) \quad \left[\frac{m^2}{s^3}\right] \tag{4.14}$$

where the buoyancy of the source relative to the ambient is

$$\Delta_{s-e} = g\frac{\rho_s(z) - \rho_e(z)}{\rho_{e,0}} \quad \left[\frac{m}{s^2}\right] \tag{4.15}$$

The source density $\rho_s(z)$ does not vary with height, so $\rho_s(z) = \rho_s$. Inserting equation (2.4) into equation (4.15) yields

$$\Delta_{s-e} = g\frac{\rho_s - \left[\rho_{e,0}\frac{\Delta_e}{g} + \rho_{e,0}\right]}{\rho_{e,0}} = g\left[\frac{\rho_s}{\rho_{e,0}} - 1 - \frac{\Delta_e}{g}\right]$$

Therefore equation (4.14) can be written in terms of Δ_e as

$$F_s(z) = Q_s(z) \times g\left[\frac{\rho_s(z)}{\rho_{e,0}} - 1 - \frac{\Delta_e}{g}\right] \tag{4.16}$$

or fully as

$$F_s(z) = c\left[p_{s,0} + (\rho_s - \rho_{e,0}) gz - \rho_{e,0} \int_0^z \Delta_e dz \right] \times g \left[\frac{\rho_s}{\rho_{e,0}} - 1 - \frac{\Delta_e}{g} \right] \quad (4.17)$$

Equations (4.13) and (4.16) were then implemented into *Distran* by adding a new subroutine, “Pressure distribution”, displayed in figure 4.4.

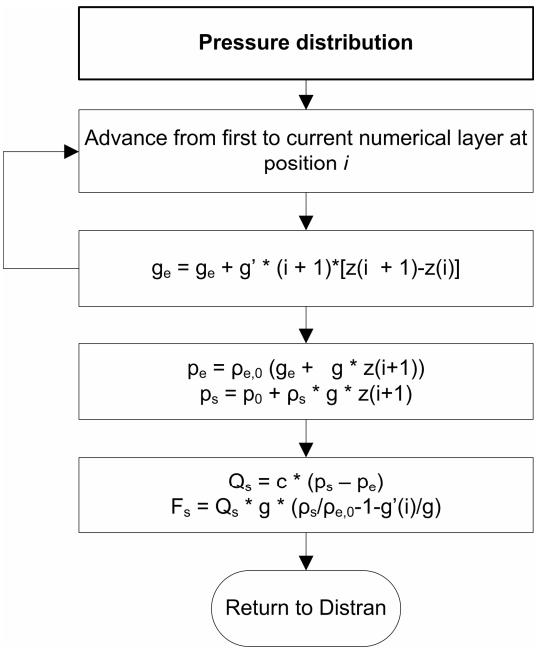

Figure 4.4. Flowchart describing the subroutine ‘pressure distribution’. The subroutine solves for the varying buoyancy flux related to the experimental results of the water scale model.

4.3.1 Other alterations

Other alterations made to *Distran* were as follows:

- Two distinct versions of Distran were developed. One dimensional and one non-dimensional.
- Several ‘bugs’ in the original code were found and corrected by the author and P. Cooper (P. Cooper, *pers. comm*.) during the work of this thesis. The ones of highest importance were related to how the detrainment mechanism affects the ambient stratification.
- A subroutine for establishing a linearly stratified environment using dimensional parameters was developed and implemented into *Distran*.

- Turning different features on and off can be done by changing initial conditions, such as varying buoyancy flux, simulating a linearly stratified environment or using the Gaussian routine for detrainment.

After implementation of the varying buoyancy flux, the detrainment and the other alterations as subroutines in *Distran, Distran* went through an extensive round of debugging followed by comparing results with those presented by Cooper et al. [1].

In order to test the numerical code against experiments in the water scale model, a series of experiments for a ventilated filling box were performed. These results are presented in the next chapter

5 Results

This chapter firstly presents the results from the ventilated filling box followed by the results for the linear stratification. After this, non-dimensional numerical results are presented followed by the dimensional, comparing experimental and numerical results.

Several runs were conducted for the mechanically ventilated and linearly stratified experiments, but the ones selected for data analysis had to meet certain requirements, especially when it came to repeatability when using the conductivity probe: if a repeat of a non-transient conductivity traverse proved impossible, the results were discarded. Typically, the first few runs of each category were discarded as experimental procedures were acquired from performing experiments. The repeatability of the steady-state mechanically ventilated experiments is presented as charts in appendix C.

5.1 Mechanically ventilated filling box

5.1.1 Results

One typical development of steady-state for the mechanically ventilated filling box is presented in figure 5.1.

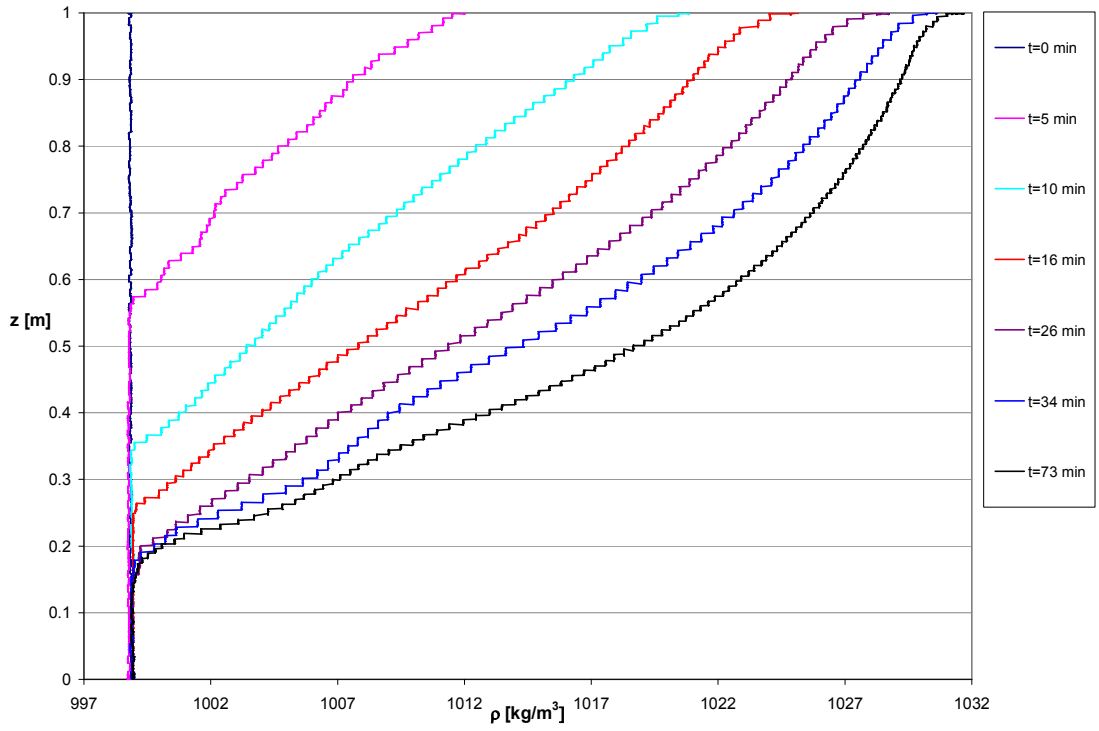

Figure 5.1. The development of steady-state stratification for mechanically ventilated experiment 12 where z [m] is height and ρ is density [kg/m^3]. The lower section consists of a uniform area of fresh water and the upper section consists of stratified regions. The legend displays the time in minutes after the experiment started.

A completely uniform stratification can be seen at t = 0 in figure 5.1 as the water scale model only contained fresh water. This uniform area reduces as the first front emerges down when brine enters over the different time scales, and at steady-state (t = 73 min) the uniform area is approximately 7.5 cm high. A conversion table for water density to salt contents can be found in appendix F.

The development in the stratification in figure 5.1 was quite typical for the experiments, but the strength and position of the first front varied according to densities and volume flows through the membrane and diffuser.

No strong interfaces were observed for when the mechanically ventilated water scale model was at steady-state. A strong interface for the first front was observed in the beginning of some of the experiments, but this was a transient effect and was no longer visible when steady-state reached. This 'transient' first front is displayed in figure 5.2.

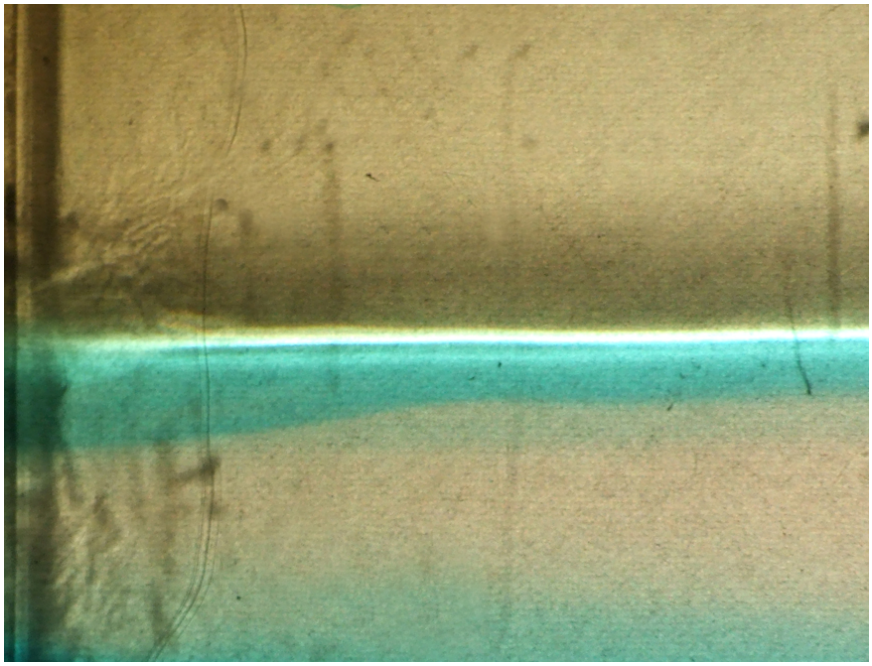

Figure 5.2. Interface for the first front during the development of steady-state for experiment 12 at t = 8 min. This first front was a transient effect and disappeared before steady-state was achieved due to vertical mixing and smearing.

Attainment of steady-state was examined by comparing three stratification measurements: When these three stratifications were equal, it was assumed that the system was at steady state. These measurements were also a good indicator for the repeatability of the measuring equipment. Figure 5.3 shows the results from steady-state experiment 12 before calibration, demonstrating steady-state and excellent repeatability.

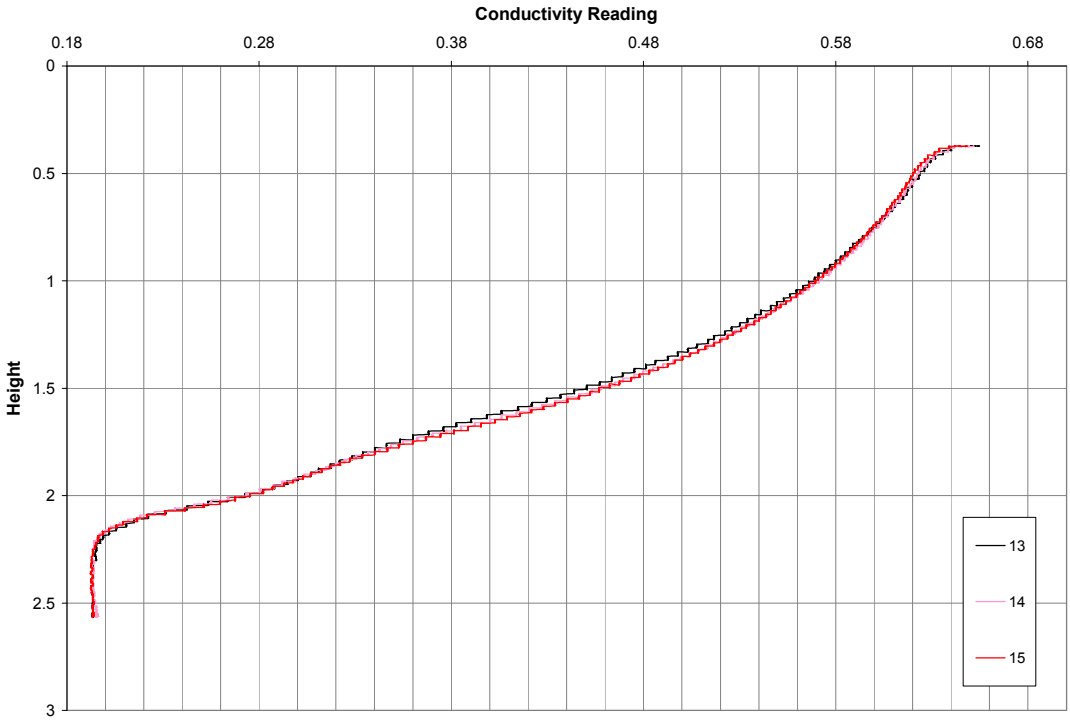

Figure 5.3. Mechanically ventilated steady-state experiment 12. Maximum deviation between the stratifications at any point was found to be within 1 % using error bars. The results are plotted as direct readings from LabVIEW and are not calibrated to density or height.

By normalizing the experimental results with regards to maximum density, all the results may be plotted in the same graph, as in figure 5.4. A figure showing height against the ambient buoyancy instead is presented in appendix C.

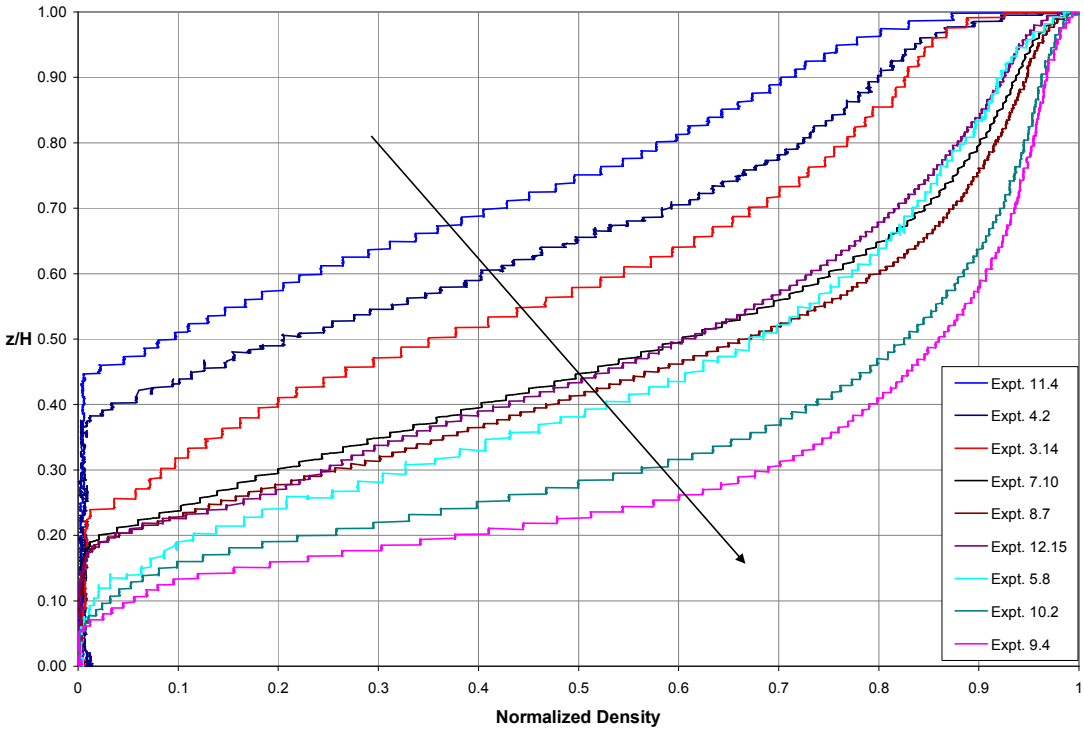

Figure 5.4. The stratifications of all steady-state mechanically ventilated experiments, showing the vertical stratification using the normalized density. The legend displays the experimental run in which the stratification was at steady-state. The arrow indicates decreasing flow rate through the diffuser.

The first fronts in figure 5.4 varied from the normalized height of 0.6 to 0.44 according to the volume flow that was applied through the diffuser. An increased volume flow increased the position of the first front, corresponding to an increased 'equivalent' value of the effective vent area. As the effective vent area equivalent was reduced, the stratification in the water scale model became decreasingly linear with a weak stratification right after the first front which grew stronger towards the ceiling of the box. This can be seen in figure 5.2, especially for experiments 9.4 and 10.2, in which there is a strong increase in density from $0.08 < z/H < 0.30$. The parameters used for the experiments are in table 5.1 below.

Experiment	ρ inlet [kg/m3]	ρ source [kg/m3]	ρ outlet [kg/m3]	Qtot [m3/s]
Expt. 3	998.4	1022.6	1016.2	2.884E-05
Expt. 4	998.5	1020.4	1010.0	3.817E-05
Expt. 6	998.8	1037.4	1030.1	3.294E-05
Expt. 7	998.8	1033.3	1033.3	3.726E-05
Expt. 8	998.8	1033.3	1033.3	3.660E-05
Expt. 9	998.8	1030.7	1029.6	4.167E-05
Expt. 10	998.8	1030.7	1029.6	3.687E-05
Expt. 11	998.8	1029.8	1013.4	5.556E-05
Expt. 12	998.8	1037.5	1031.7	3.671E-05

Table 5.1. Parameters used for the steady-state ventilated filling box experiments.

Experiments 5 and 6 were discarded due to noise produced by the experimental set up as the potentiometer experienced a short circuit due to faulty wiring and vibration caused by the traversing probe. Experiments 1 - 3 were trials, and thus not included in any data analysis due to lack of accuracy in experimental procedure.

5.1.2 The effective vent area

The mechanically ventilated water scale model did not have the two vent areas required to calculate the effective vent area by using equation (2.36). However, the stratification inside the water scale model does not see the diffuser or the drain valve. It sees the relationship between the volume flux in the plume and the net flow of fluid through the box. Whether this flow of fluid is caused by differences in external buoyancy to the local ambient or a pressure difference due to the pressure of the incoming flow from the mains is irrelevant as long as the incoming water is at a sufficiently low velocity to avoid turbulent mixing.

Based upon this assumption, the effective vent area can theoretically be calculated by reformulating equation (2.38) to

$$A^* = \frac{Q_{vent}}{\left(\int_{z_0}^{H} \Delta_e dz\right)^{\frac{1}{2}}} \tag{5.1}$$

Integrating the density distribution would then give an approximate result for the actual value of A^* experienced by the stratification in the water scale model. This variation of A^* can be referred to as the effective vent area equivalent.

Using this approach to find an estimate for A^*, the mechanically ventilated experiments could be simulated in Distran and compared to the density profiles of the actual experimental data. However, for most of the time it was not possible to calculate the integral in equation (5.1). Another aspect is that there was a considerable amount of flow through the membrane for several of the mechanically ventilated experiments, and this is not accounted for in Q_{vent} in equation (5.1).

When comparing the experimental results presented in this chapter to the numerical results from *Distran*, the effective vent area was found by matching the steady-state volume flow out of the box in the numerical simulation to the actual volume flow used in the experiment.

As a result, it was necessary to have the steady-state ventilation flow rate in order to calculate the effective vent area equivalent numerically.

Calculation of effective vent area was not necessary in the next section, which considers the effect of the membrane flow on a linearly stratified environment.

5.2 Linearly stratified filling box

5.2.1 Results from conductivity probe traverse experiments

Setting up a linear stratification using the double-bucket method and the floating diffuser worked very effectively, producing linear stratifications with linear best fit curves up to R^2 = 0.999 and a filling time of around 90 minutes. A typical intrusion experiment is displayed in figure 5.5, showing the density profiles of before and after the intrusion.

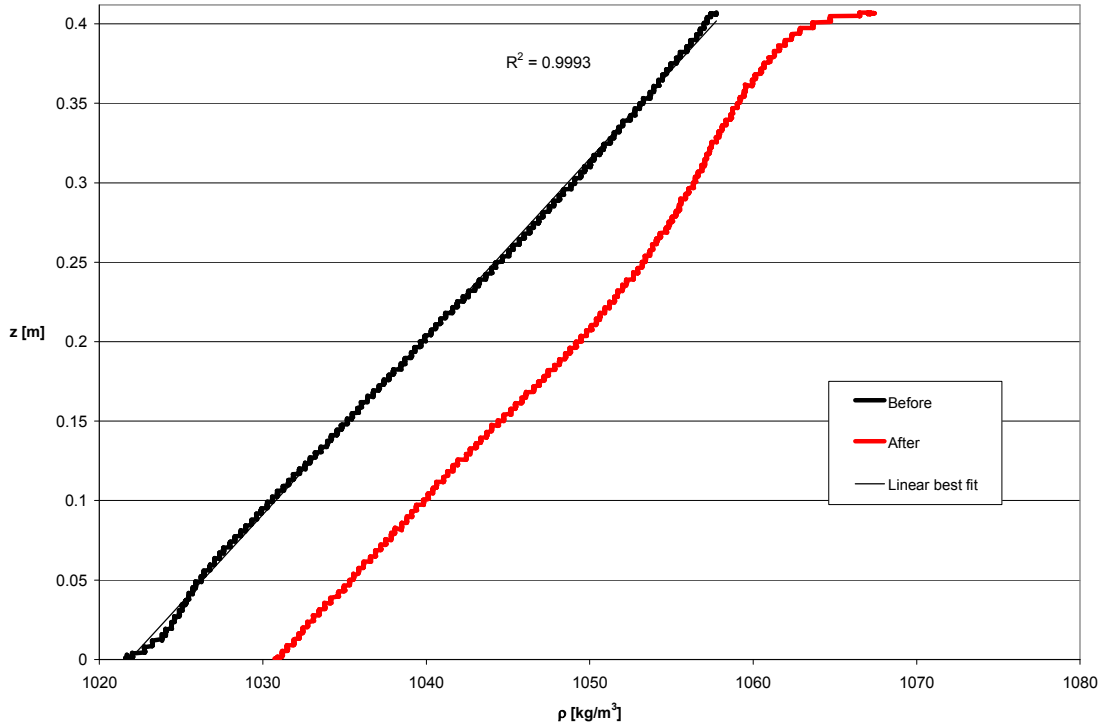

Figure 5.5. The density profiles for before and after the intrusion process in the water scale model for experiment 8 of the linearly stratified environment. The after profile has been shifted to the right due to the increased density of the membrane flow compared to that of the ambient.

A total of seven experiments were performed, but only five of these met the accuracy requirements for the stratification profiles and repeatability when it came to the conductivity probe.

The process of extracting information located in the difference between the two profiles in figure 5.5 is not intuitive. In order to analyse this information and thus interpret the results,

the net downward flow was found by an analysis based upon the one presented by Baines [25].

5.2.2 Net downward flow

A stratified environment consists of density surfaces whose heights shift when an intrusion occurs. This change of height for a certain density surface represents the flux of fluid which has penetrated that surface, and can be used to find the net downward flow at height *z*. This effect on the ambient stratification can be found by differencing the initial and final stratification profiles. Baines [25] expressed the net downward flow as

$$Q(z) = Q_0 \int_{\rho_i(z)}^{\rho_f(z)} \tilde{Q}(\rho) \frac{d\rho}{\rho_f(z) - \rho_i(z)} \quad \left[\frac{\mathrm{m}^2}{\mathrm{s}}\right] \tag{5.2}$$

where subscripts f and i represents values from final and initial stratification, respectively. Equation (5.2) can be averaged to produce

$$Q(z) \approx \frac{1}{2} Q_0 \left[\tilde{Q}(\rho_f(z)) + \tilde{Q}(\rho_i(z))\right] \quad \left[\frac{\mathrm{m}^2}{\mathrm{s}}\right] \tag{5.3}$$

where the previously mentioned change of height has been scaled with the initial volume flux Q_0 to produce $\tilde{Q}$. Equation (5.3) is arguing that the net downward flow as a function of height is equal to the average of the change in height for the final and initial density surfaces where both of them are a function of the same height *z* as $Q(z)$.

Before equation (5.3) could be applied to the measured stratification profiles, the recorded data had to be sorted. This was a consequence of analogue and continuous recording of data, meaning that there were no directly equivalent values for height and density represented for the initial and final density profiles. Accordingly, heights and densities had to be linearly interpolated in order to find the movement of a certain density surface. Furthermore, it was assumed that the error represented by the interpolation was negligible since the sets of data had a high resolution compared to that needed by the linear

interpolation. Three different interpolations (indicated by *hat* '^') were needed to achieve this, where subscripts *f* and *i* represents final and initial profile reading, respectively:

- $\hat{\rho}_f\left(h_i(z)\right)$, the interpolated density for the final density profile corresponding to the initial height.
- $\hat{h}_f\left(\rho_i(z)\right)$, the interpolated height for the final density profile corresponding to the initial density.
- $\hat{h}_f\left(\hat{\rho}_f\left(h_i(z)\right)\right)$, the interpolated height for the final density profile corresponding to the interpolated density for the final profile found for the initial height.

An explanation of $\hat{h}_f\left(\rho_i(z)\right)$ is in table 5.2.

$h_i(z)$	**ρ_i**	**$\hat{h}_f(z)$**	**h_f**	**ρ_f**
h_{i1}	$\rho_i(h_{i1})$	$\hat{h}_{f1}(\rho_i(h_{i1}))$	h_{f1}	$\rho_f(h_{f1})$
h_{i2}	$\rho_i(h_{i2})$	$\hat{h}_{f2}(\rho_i(h_{i2}))$	h_{f2}	$\rho_f(h_{f2})$
~	~	~	~	~
h_{iy}	$\rho_i(h_{iy})$	$\hat{h}_{fy}(\rho_i(h_{iy}))$	h_{fy}	$\rho_f(h_{fy})$
h_{iy+1}	$\rho_i(h_{iy+1})$	$\hat{h}_{fy+1}(\rho_i(h_{iy+1}))$	h_{fy+1}	$\rho_f(h_{fy+1})$

Table 5.2. Interpolation example for $\hat{h}_f(z)$. In the table $h_{iy} \neq h_{fy}$ as "y" indicates array position. $\hat{h}_{fy}$ finds the unknown array position for the two h_f-values where the two corresponding values of $\rho_f(h_f)$ are close, but not exactly equal to of $\rho_i(h_{iy})$. The values are therefore interpolated.

The changes in height for a density surface and thus the flux of fluid that penetrated that surface were then found as

$$\Delta h_i(z) = h_i(z) - \hat{h}_f\left(\hat{\rho}_f\left(h_i(z)\right)\right) \tag{5.4}$$

$$\Delta h_f(z) = h_i(z) - \hat{h}_f\left(\rho_i(z)\right) \tag{5.5}$$

According to (5.3), the net downward flow for a density surface can then be expressed as

$$Q(z) \approx \frac{1}{2}\left[\Delta h_f(z) + \Delta h_i(z)\right] \left[\mathrm{m}^2\right] \tag{5.6}$$

where the scaling with respect to initial volume flux was not used, as the Q_0 used by this experiment differs from that of Baines[5]. $Q(z)$ then represents the shift in height of a density surface.

It is important to note that not all the densities in the before and after density profiles are included in (5.6) for net downward flow. This is a consequence of the displacement of fluid inside the water scale model. As more fluid is added through the source membrane, continuity forces the same volume of fluid to leave the top of the box, and thus the range of the conductivity probe. This fluid's density is not present in the final density profile, and will consequently not be represented in the net downward flow. The same applies for any gravity current that reaches the bottom of the water scale model. As this gravity current has a density that was not a part of the initial density profile, it would not be a part of the net downward flow. The parameters for the experiments are in table 5.3.

Run	Time [s]	ρ_t [kg/m^3]	ρ_b [kg/m^3]	N [1/s]	ρ_s [kg/m^3]	Q [m3/s]
3	100	1023.4	1053.9	0.85	1079.5	2.36
5	106	1031.0	1058.5	0.80	1089.6	4.45
8	160	1021.6	1058.0	0.93	1079.2	3.18
9	143	1007.0	1045.1	0.95	1079.2	3.73

Table 5.3. Parameters for the linearly stratified experiments where N is the buoyancy frequency for the initial linear stratification and 'time' is the number of seconds of which the source was turned on.

The net downward flow for run 6 of the linearly stratified environment is displayed in the figure 5.6 below (z is positive downwards).

[5] Baines investigated a plume adjacent to a wall released from a horizontal line source at the top of an enclosure, whereas this work investigates the plume from a vertically distributed source.

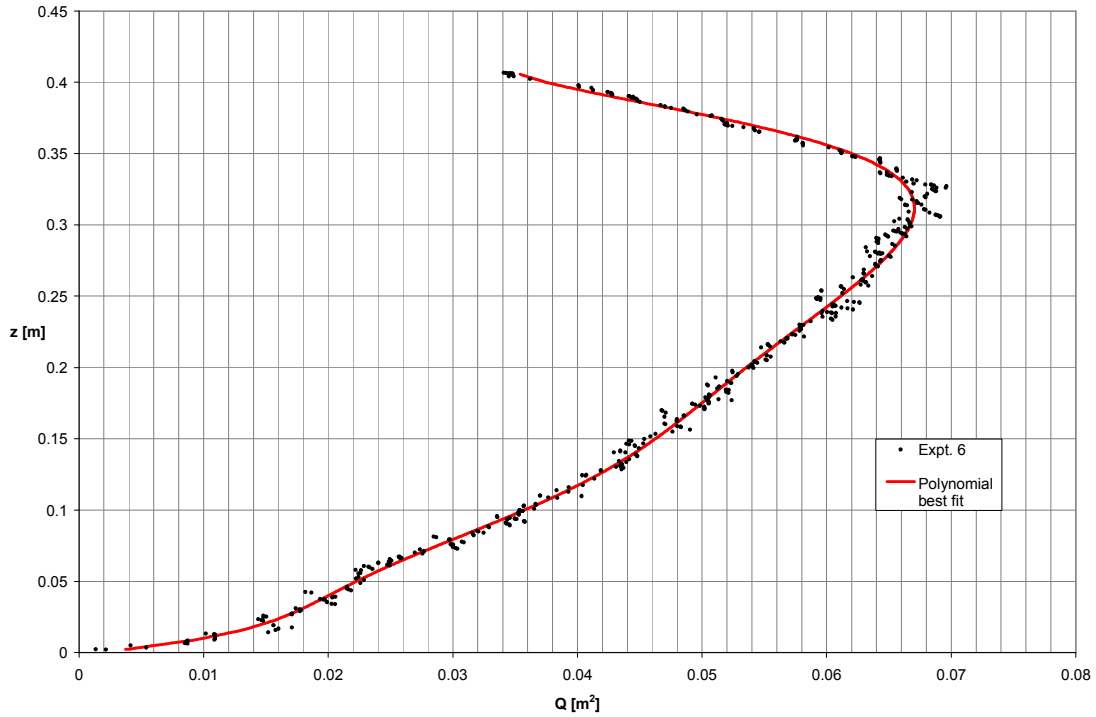

Figure 5.6. Net downward flow Q of linearly stratified experiment no 6. Q = [m^2/s] × [s], the total time for experiment 6. The red line is a high order polynomial with R^2 = 0.996.

The data was smoothed using a polynomial best-fit, shown as the red line in figure 5.6, in order to remove the significant level of noise from the data. The mean outward velocity could then be found by using (5.7) applying the same technique as Baines [25].

$$v(z) = -\frac{dQ(z)}{dz} \tag{5.7}$$

It is possible to solve equation (5.7) by applying a Douglas-Avakian numerical differentiation method [26] to the smoothed curve in figure 5.6. This method fits a fourth order polynomial to a moving set of seven data points and from this it determines the mid point value. The solution of equation (5.7) for experiment 6 is in figure 5.7.

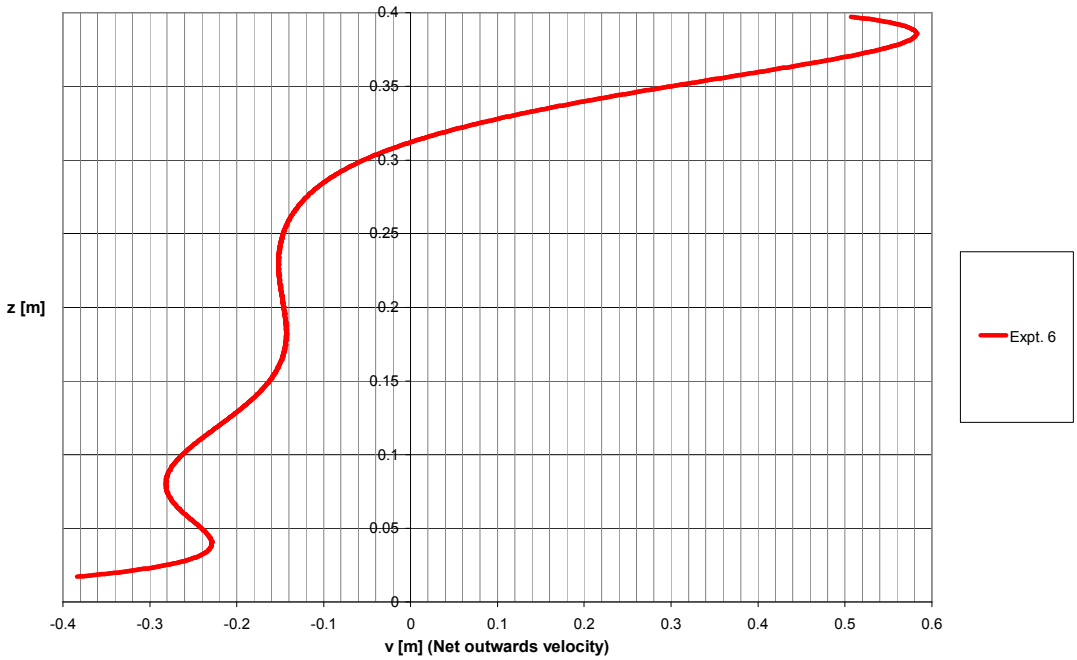

Figure 5.7. Mean outwards horizontal velocity v(z) for linearly stratified experiment 6, found by differentiating the best fit of the net downward flow by equation (5.7) using Douglas-Avakian numerical differentiation method.

The velocity of the net downward flow gives a better representation of the occurring flow pattern as the regions of entrainment and detrainment can be seen as positive and negative horizontal in velocities, respectively. Note that this velocity represents the total movement; hence it is not time dependent. This was preferred as it was the total change that was measured (time dependent velocity can be found by dividing by the time in table 5.3). The results for the remaining experiments are presented over the next two pages in figures 5.8 and 5.9 for net downward flow and outwards velocity, respectively.

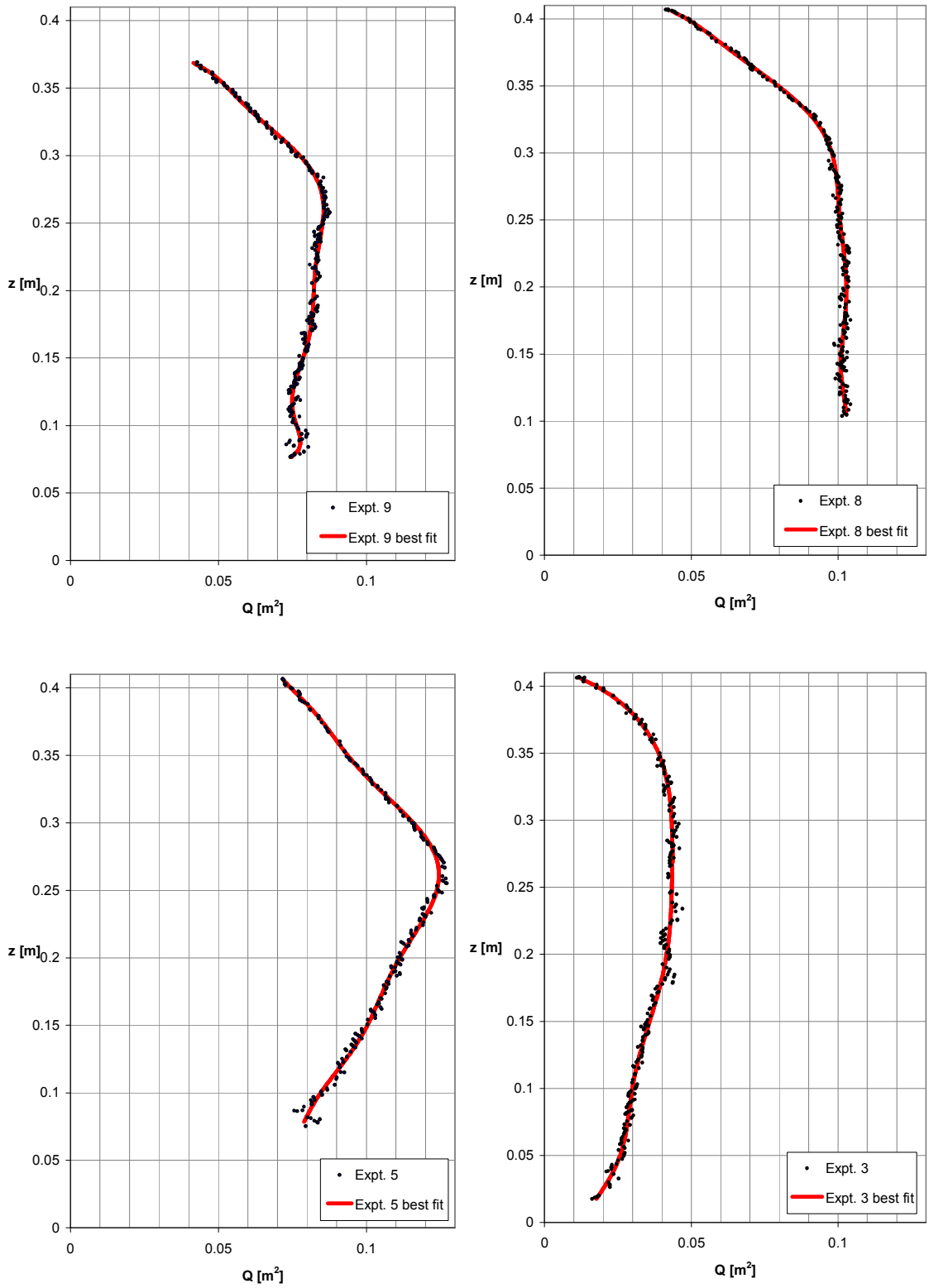

Figure 5.8. Net downward flow of linearly stratified experiments no 9, 8, 5 and 3. The red line is a high order polynomial best fit line to the experimental data points, represented by the black markers.

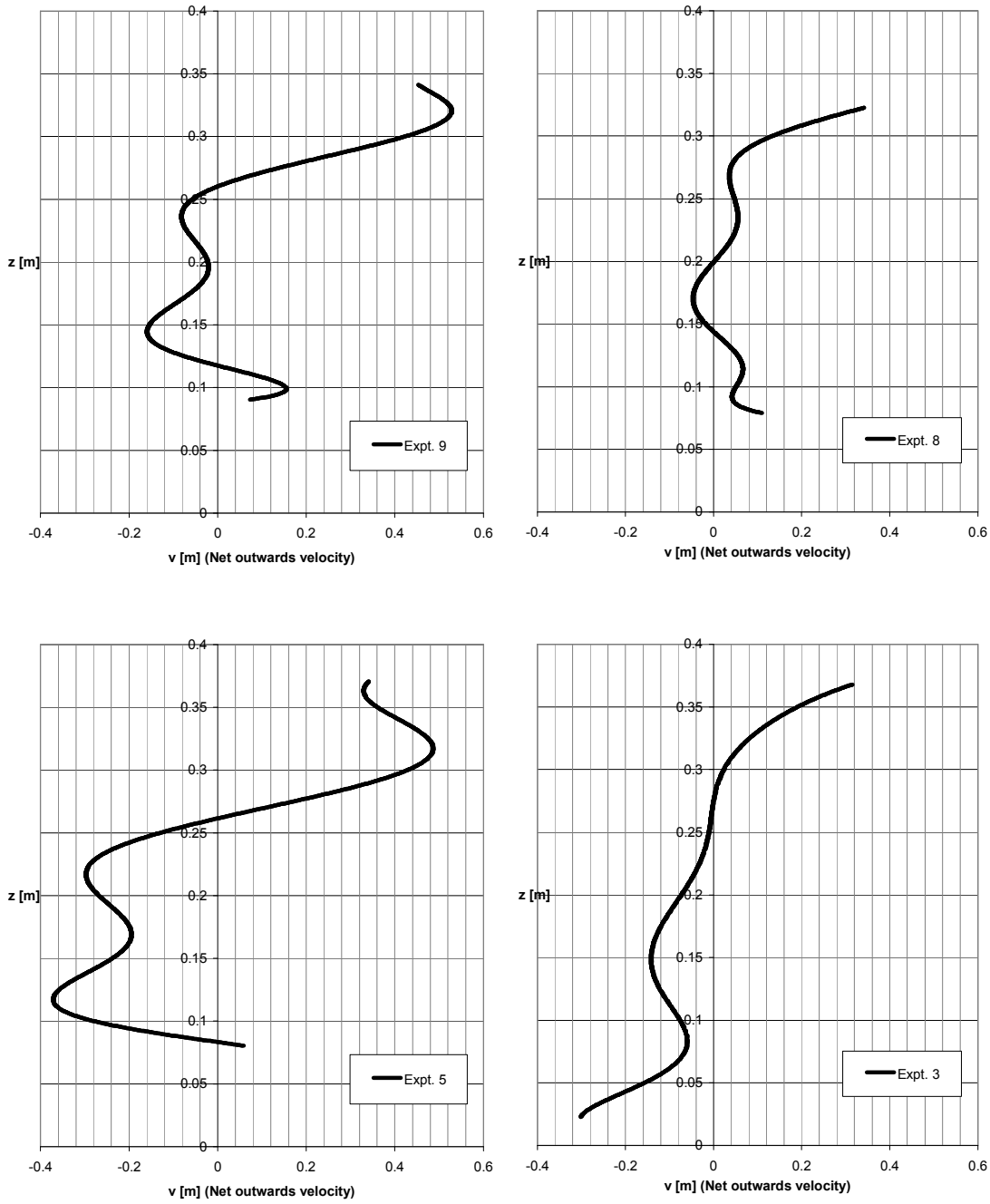

Figure 5.9. Height z [m] versus mean outwards velocity *v(z)* for linearly stratified experiments 9, 8, 5 and 3 found by differentiating the best fit of the net downward flow by equation (5.7) using Douglas-Avakian numerical differentiation method.

The parameters for the best fit lines for the net downwards flow differentiated to produce the velocities in the figure above can be found in appendix D. For experiment 8, the data is compared to a photograph from the experiment in figure 5.10.

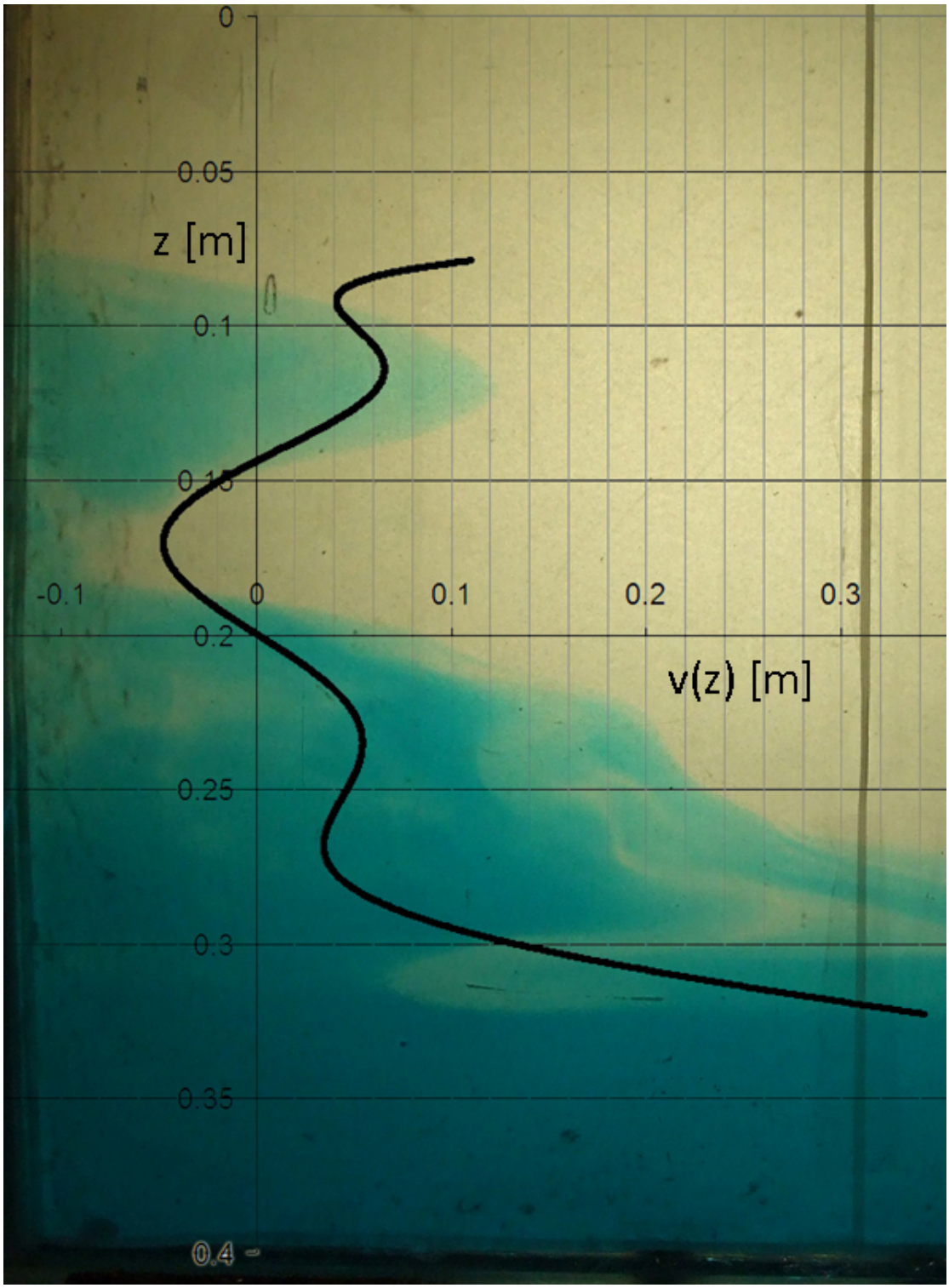

Figure 5.10. Height z [m] versus mean outwards velocity *v(z)* from the downward flow from experiment 8, found by differentiating the best fit of the net downward flow by equation (5.7) using Douglas-Avakian numerical differentiation method. The background photograph is from experiment 8 after the membrane flow was stopped and the system was at rest. The right movement of the top section is describing entrainment strengthened by the endpoint effect of the high order polynomial fit. The relationship between the gravity current and intrusion flow from expt. 8 is also portrayed. The source flow was coloured with blue food dye, and a light colour indicates dilution by entrainment.

A trend can be observed for the velocities: Before making the distinct movement to the right at the top which is related to the gravity current, there is a section where the velocities go to the left, then right then left again. These turning points of these locations indicate maximum entrainment and detrainment, and are highlighted in table 5.4.

Experiment no.	Max left movement (entrainment)	Right movement (detrainment)
9	0.14	0.19
8	0.17	0.23
6	0.07	0.17
5	0.13	0.17
3	0.15	0.24 (very weak)

Table 5.4. Results from the linearly stratified experiments, indicating the locations for maximum entrainment and detrainment.

Again, it is important to emphasize that the units for the velocities are in metres as a result of showing the total change in velocity. This reflects the measurements; the difference between two stages. It can be thought of as a velocity which is multiplied with the time elapsed between the initial and final density profile.

The gravity current seemed to have a large influence on the results for the linearly stratified experiments. To investigate this observation further and discuss the effects of this influence, an analysis of the total volumetric plume flow was performed.

5.2.3 Total volumetric plume flow

The total flow exhibited during the linearly stratified experiments can be found by integrating the areas under the net downwards flow curves (figure 5.8). These curves display the movement of a density surface ([m^2]), and by integrating these density surfaces over their respective height, the total change in volume caused by these density surfaces ([m^3]) can be found. In other words, the volume of the moving density surfaces can be found by integrating the area under the curves of net down flow, as this represents volume flow of a surface.

In addition, a fraction of the source fluid that entered the box formed a gravity current. This displaced the ambient fluid above it at the bottom of the experimental tank. This gravity current was not a part of the volume exhibited by the moving density surfaces, because the density of the gravity current was higher than the ambient densities. Accordingly, the gravity current was not a part of the initial density surfaces and is of this reason not a part of the volume flows that can be calculated by integrating the curves in figure 5.8. Consequently, the difference between the total net downward flow of in figure 5.8 and the total volume flow from the source has to correspond to the gravity current.

Taking this difference for all of the experiments, a relationship between the gravity current and the entrained fluid can be found, and is displayed in figure 5.11.

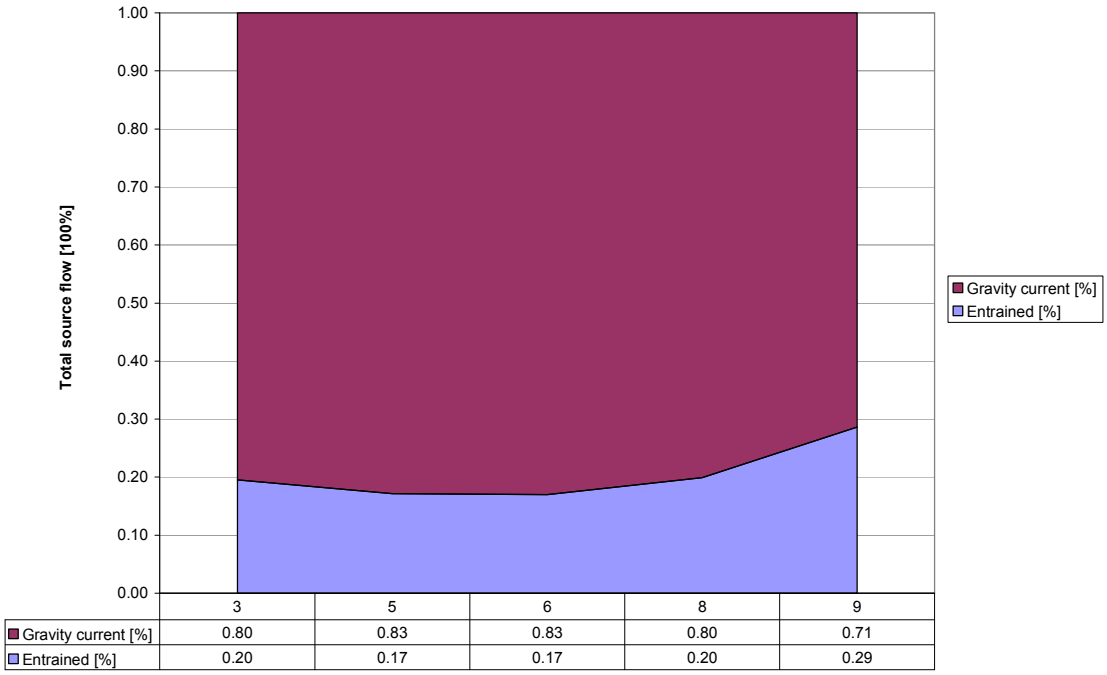

	3	5	6	8	9
Gravity current [%]	0.80	0.83	0.83	0.80	0.71
Entrained [%]	0.20	0.17	0.17	0.20	0.29

Figure 5.11. The relationship between the gravity current and entrained flow as a percentage of the total volume of source fluid that entered the water scale model.

As observed in figure 5.11 there is a clear trend throughout the linearly stratified experiments that the gravity current had a very strong influence on the flow in the water scale model, amounting to approximately 80 % of the total flow through the membrane. This trend could also be observed during the experiments, as the source fluid was coloured using blue food dye (figure 5.10).

The flow patterns in figure 5.11 explains the velocity profiles presented §5.2.2. They indicate that the flow was dominated by the gravity current, disturbing the intrusion flow and thus the accuracy of the measurement related to the velocity profiles of the intrusion. In addition, the profiles presented in §5.2.2 went through rigorous processing in order to produce net downward flow curves and the corresponding velocity profiles. This process included several complex steps susceptible to incorrect data treatment. Of this reason, the experimental procedure was calibrated to investigate whether or not the processing of data was valid.

One approach to check the validity of the result analysis was to use the method of selective withdrawal, similar to that described by Wood [18,19]. By extracting a certain amount of fluid from a known stratification, the change in height of density surfaces would produce a change in volume that could be compared to the actual extracted volume.

5.2.4 Calibration of experimental procedure

As a calibration procedure for the linearly stratified experiments, a linear stratification was again established in the water scale model. This time, a small hose was fitted inside the tank so that fluid could be extracted from the stratification. In addition, a clamp was fitted onto the hose so that the volume flow could to be controlled and fluid from the stratification could be siphoned out into a measuring cup. This was performed using a low flow rate (two litres per hour), ensuring that the siphoned fluid was extracted from a narrow range of density surfaces. Additionally, the membrane was sealed so that no unexpected flow related to the membrane and supply chamber could occur. The process is illustrated in figure 5.12.

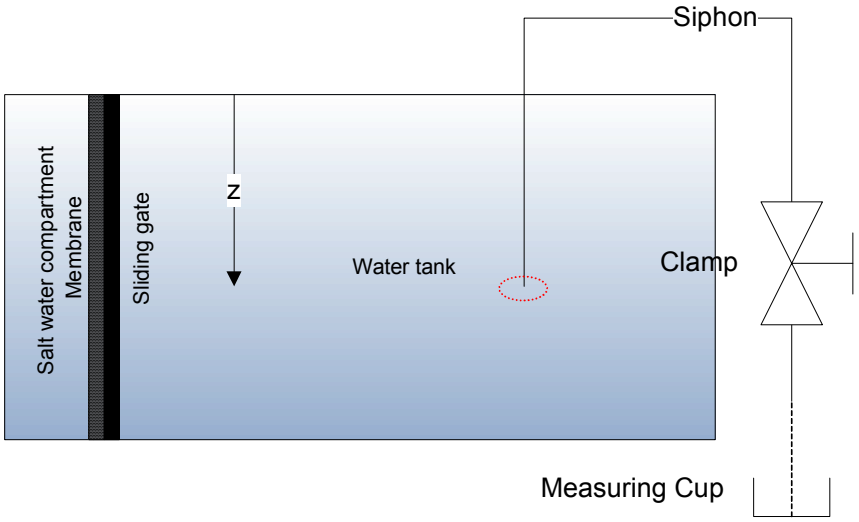

Figure 5.12. The extraction process for the calibration procedure. The environment in the water scale model is linearly stratified and the point of extraction is at the beginning of the siphon (z = 0.22 m) as indicated by the red circle.

This allowed for a very controlled way of changing the stratification where the results could be predicted with a high degree of confidence, as point of extraction, the volume extracted and the initial stratification was known. The results from the processing of data could then be compared to the predictions. If they coincided, it would be a strong indicator for the validity of the data analysis for the intrusion experiments.

The process of extraction was monitored using shadowgraph, and an interface started to appear after the extraction of approximately one litre. This interface grew stronger as more fluid was siphoned out, indicating that fluid was extracted within a certain horizontal density range. A total of 2.0 and 2.5 litres were extracted for the first and second extraction experiment, respectively. The density profile for this first extraction is displayed in figure 5.13, showing the initial and final conductivity probe traverse as “before” and “after”, respectively.

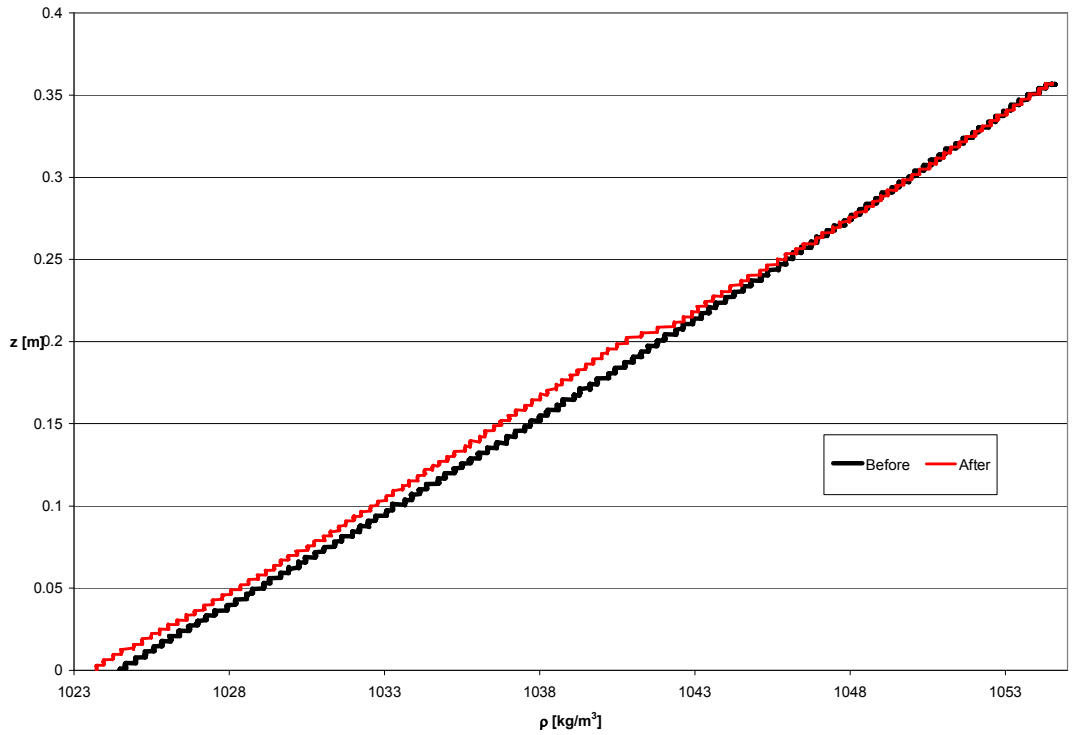

Figure 5.13. Extraction (no. 1) of fluid from a linearly stratified environment. The two density profiles "before" and "after" are the initial and final stratifications for the extraction process of 2.00 litres of fluid at z=0.22. The before profile had a linear best fit of R^2 = 0.9996.

The same analysis as in §5.2.2 was then applied, differencing the profiles to find the net downward volume flow. The change in volume could then be calculated, and is plotted for both extractions in figure 5.14.

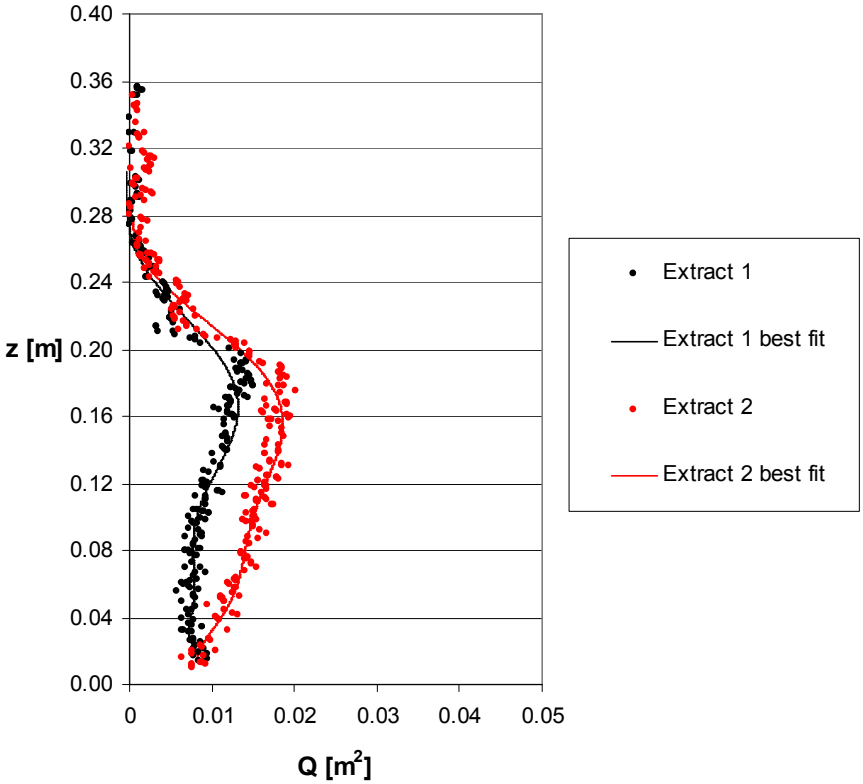

Figure 5.14. Outwards velocity profile, showing total change for extract 1 and 2. The fluid was extracted at z = 0.22 for both extractions.

The area under this curve would then correspond to the total volume, as several density surfaces are integrated over a height. This area was found by integration of the curve and the results are in table 5.5, showing good correlation to the actual volume.

Extraction no.	Actual volume	Volume by integral	Error [%]
1	2.00 litre	1.96 litre	-2.0
2	2. 50 litre	2.64 litre	5.6

Table 5.5. The results from the extraction of fluid from a linearly stratified environment in the water scale model compared to the calculated change in volume using calculations similar to Baines [25].

As the experimental results for both the mechanically ventilated and linearly stratified experiments have been presented, the next section moves on to present the numerical results from the simulations in *Distran*.

5.3 Numerical methods

5.3.1 Non-dimensional results

The plume equations for a mechanically ventilated box were solved using Distran as described in chapter 4. In order to relate the dimensionless vent area a^* to the range of parameters, the plume equations were solved numerically several times with variation of those parameters. The results were plotted as points only; hence the connecting lines shown in the figures are lines of best fit for the respective datasets.

The solution presented in figure 5.15 demonstrates the relationship between dimensionless vent area and position of the first front. In a ventilated environment, the area below the first front would then be of uniform ambient.

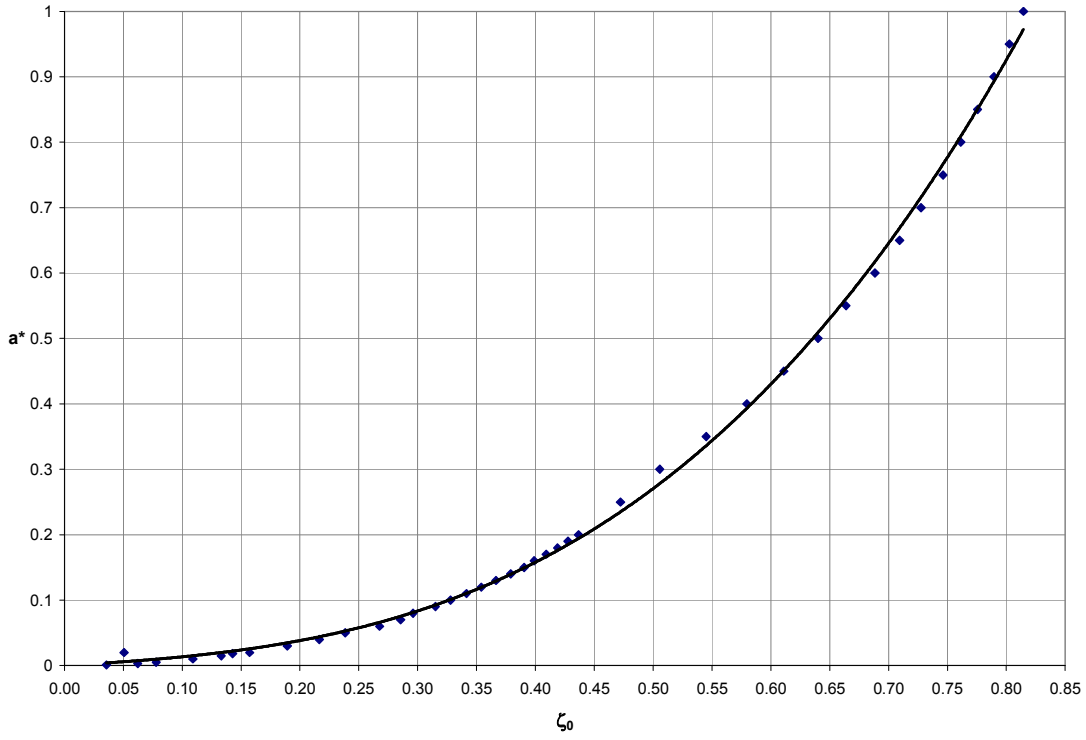

Figure 5.15. Relationship at steady-state for a ventilated filling box between the dimensionless vent area and the position of the first front for $\tau = 150$. The individual points were recorded using multiple solutions and the connecting line is a polynomial best fit forced through the origin.

Within the range displayed in figure 5.15, an excellent prediction of a^* to the steady-state position of the first front was found by the polynomial best fit

$$a^* = \frac{37}{25}\zeta_0^3 + \frac{13}{100}\zeta_0^2 + \frac{53}{500}\zeta_0 \qquad (5.8)$$

which can be used to calculate the position of the first front given the vent area. Results for other useful relationships can be found in appendix E. For a ventilated filling box at steady-state, figure 5.16 describes solutions for the density distribution for various values of a^*. These values were selected as they illustrate the difference in behaviour for the ventilated box conditions.

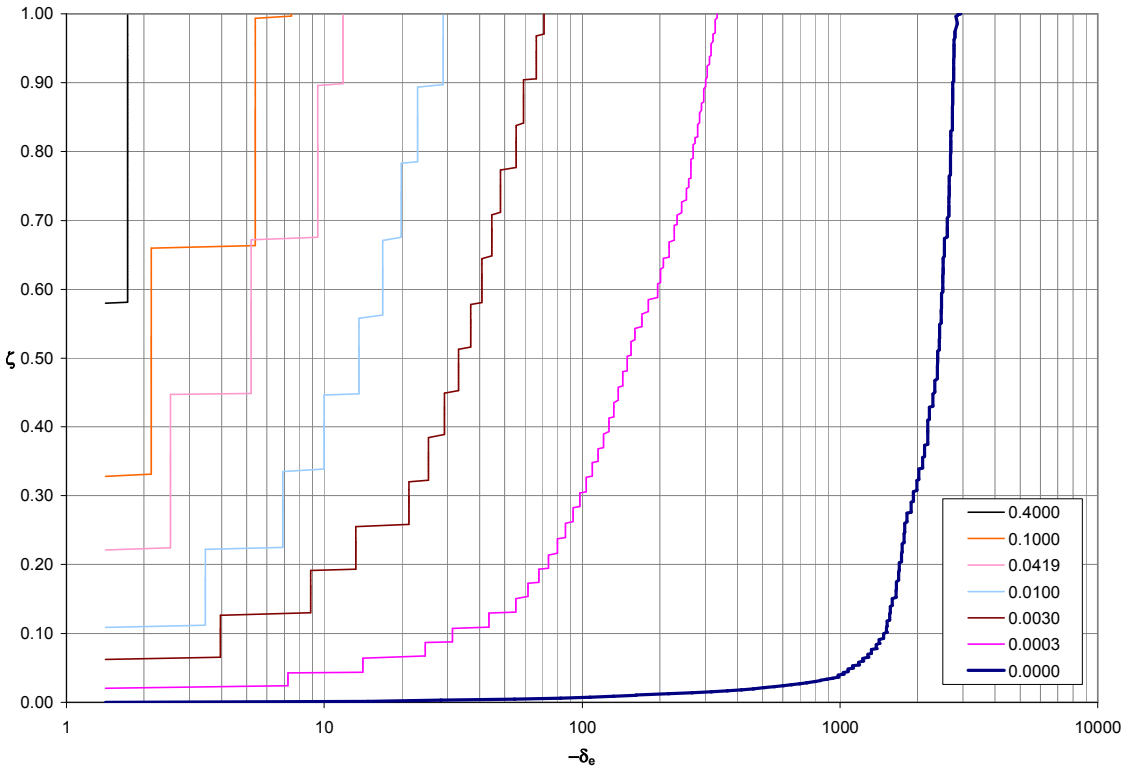

Figure 5.16**.** The ambient stratification generated within a ventilated filling box at steady-state (τ = 180) by a plane, vertically distributed source of buoyancy as a function of the non-dimensional vent area of $A^*/(\alpha HL) = a^*$.

Figure 5.16 illustrates how the number of interfaces increase as the value of a^* decrease. Smaller a^* also reduces the height of the first front (ambient layer), and the profiles become decreasingly linear. Three values of a* similar to those presented in figure 5.16 were used to illustrate plume behaviour, which follows in the next section.

5.3.2 Non-dimensional results for specific vent areas

For the purpose of presenting an appropriate range of solution for the results in figure 5.15, vent areas with a difference of one order of magnitude were selected: 0.1, 0.04 and 0.003. Each of them is representative for the solution in that respective region, and they are presented in figure 5.17.

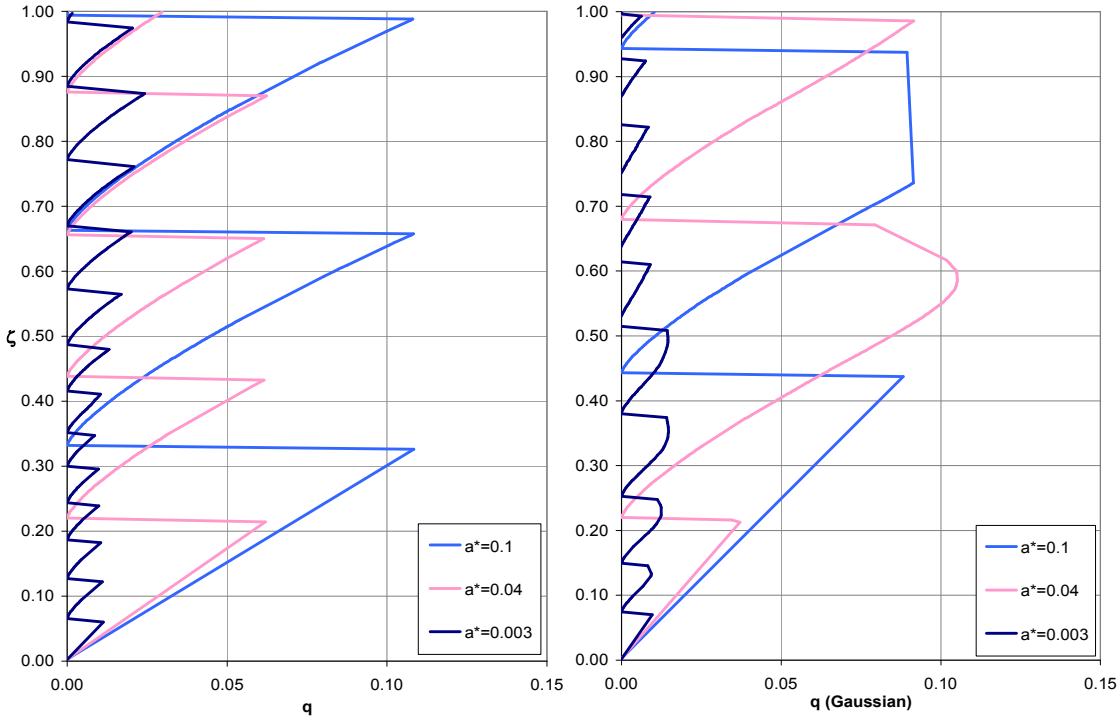

Figure 5.17. The relationship between the dimensionless height and plume volume flux plotted for the dimensionless vent areas of 0.1, 0.04 and 0.003. The Gaussian routine was enabled for figure (b).

Several plumes can be seen detraining into the ambient, and the volume flux is set to zero after intrusions as a part of the numerical scheme. This abruptness can be avoided to some extent by enabling the Gaussian routine: In the left figure of figure 5.16 the smoothing effect of the Gaussian routine prevents the plume from immediately being set to zero after the detrainment.

However, it was not clear by interpreting numerical results whether or not there was conservation of buoyancy when the Gaussian routine was enabled. Therefore, the Gaussian routine was turned off for comparing Dimensional results to experimental results.

5.3.3 Dimensional results and the mechanically ventilated experiment

The dimensional version of Distran was given the parameters of the experimental results and matched against the ventilation flow rate. For experiment 12, the results were as in figure 5.18.

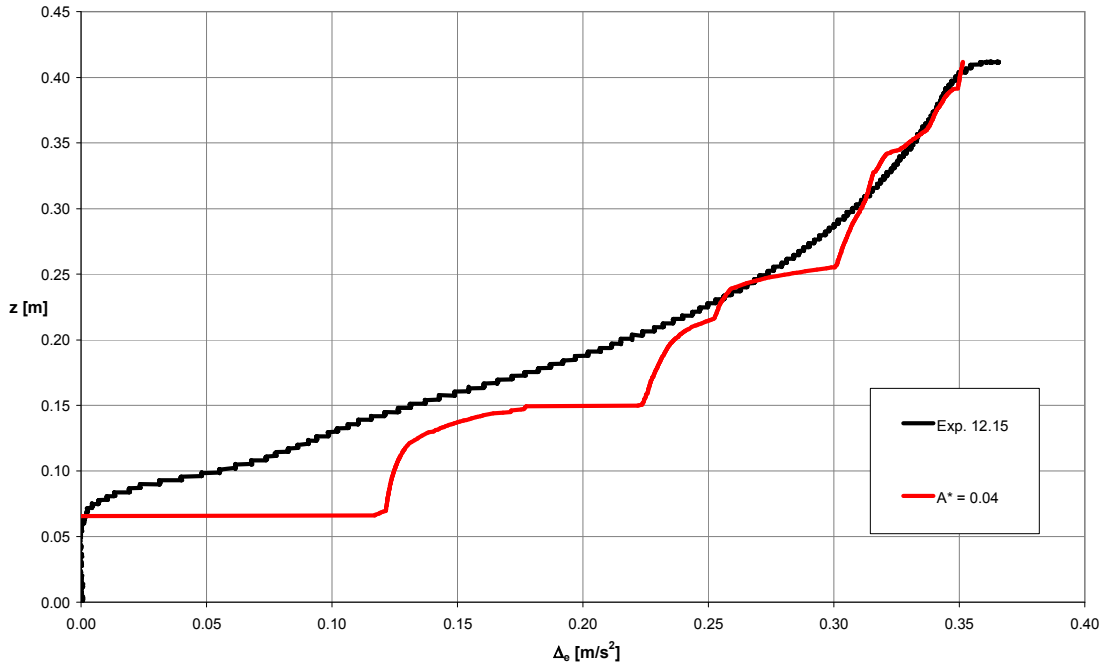

Figure 5.18. The stratification curves of experiment 12.15 and the results from a numerical simulation in Distran with A^{*} = 0.04 and ρ_s = 1037.5 kg/m^3 at t = 4000 s. Δ_e is the ambient buoyancy and the membrane coefficient was set to c = 1/3.28e5 * (3.21/4.15) [m^3s/kg].

A summary for the comparison in figure 5.18 between the numerical and experimental results for experiment 12 is presented in table 5.6.

	Mechanically ventilated experiment 12 (steady state)		
	Experimental	Distran (dimensional)	Error
Q_{vent} [m^3/s]	3.67E-05	3.36E-05	-9.23 %
$\Delta_{e,max}$ [m/s^2]	0.161	0.353	-3.68 %
First front [m]	0.068	0.067	-1.77 %

Table 5.6. The differences between the experimental results and the numerical results from the dimensional version of Distran for linearly stratified experiment 12.

In addition, figure 5.18 displays the ambient buoyancy of the numerical results for the ventilated filling box in figure 5.19 versus its plume's buoyancy flux, demonstrating several regions of detrainment effectively creating the interfaces for the ambient buoyancy.

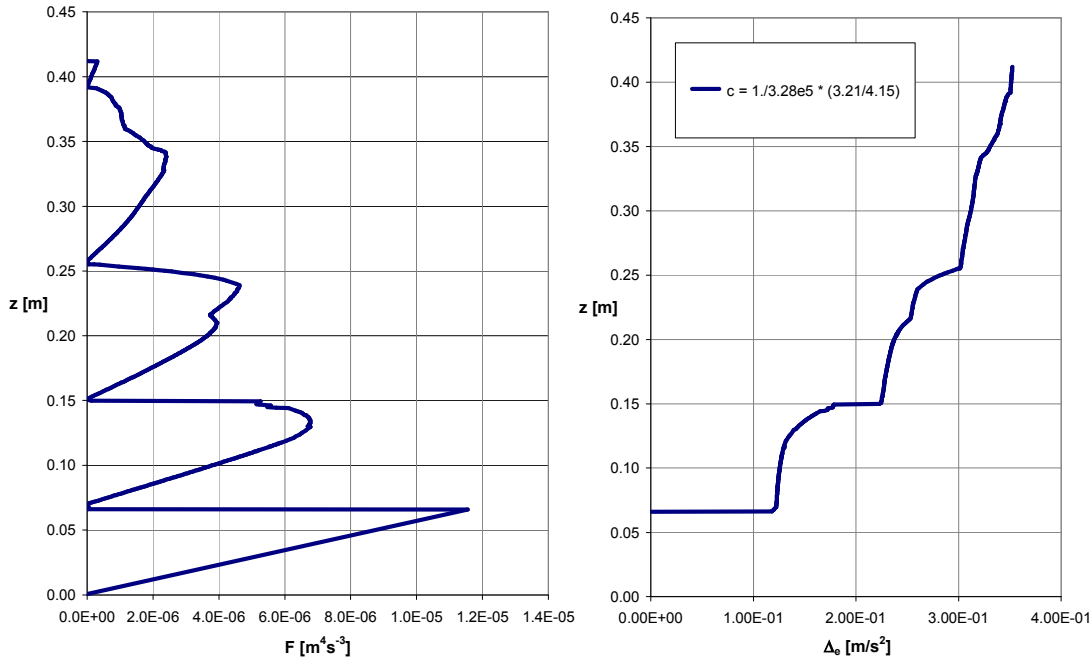

Figure 5.19. The buoyancy of the plume (left) and the ambient buoyancy (right) for the dimensional numerical solution using the parameters from steady-state experiment 12 at t = 4000 s. The detrainment of the plume clearly contributes to the ambient buoyancy. Membrane coefficient c = 1/3.28e5 * (3.21/4.15) [m^3s/kg].

When the plume detrains, the buoyancy of the plume is added to the ambient indicating conservation of buoyancy in the filling box, satisfying conservation of buoyancy. This was not obvious with the Gaussian detrainment routine enabled, thus the experimental results were compared to the dimensional version of *Distran* without this feature turned on to be certain of conservation of buoyancy.

The results from comparing numerical results to the experimental results for mechanically ventilated steady-state experiment 11 are in figure 5.20.

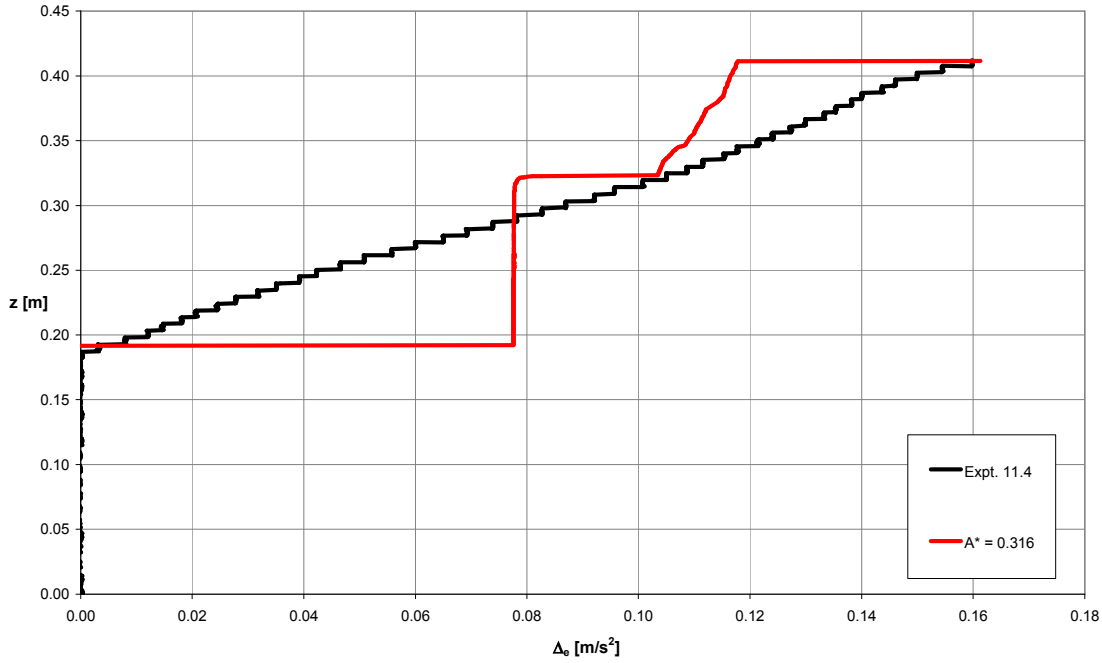

Figure 5.20. The stratification curves of experiment 11.4 and the results from a numerical simulation in Distran with $a^* = 0.00039$ and $\rho_s = 1029.8$ kg/m^3. Δ_e is the ambient buoyancy and the membrane coefficient c = 1/3.28e5 * (3.21/4.15) [m^{3}s/kg].

A summary of this comparison is presented in table 5.7.

	Mechanically ventilated experiment 11 (steady state)		
	Experimental	Distran (dimensional)	Error
Q_{vent} [m^3/s]	5.55E-05	5.63E-05	1.42 %
$\Delta_{e,max}$ [m/s^2]	0.161	0.162	0.62 %
First front [m]	0.18	0.1917	6.10 %

Table 5.7. The differences between the experimental results and the numerical results from the dimensional version of Distran for linearly stratified experiment 11.

5.3.4 Dimensional results and the linearly stratified experiment

Comparing the transient stratifications produced by the linearly stratified environment experiments to the numerical solutions proved difficult and was not successful. This was due to several reasons, mostly related to the gravity current produced by the incoming mass flux from the membrane. This incoming mass flux as a gravity current was not accounted for in the numerical modelling.

6 Discussion

This chapter discuss of how the results produced in the present work is given and provides answers and greater understanding. Firstly, the comparison between the dimensional numerical results and the experimental results is presented.

6.1 Dimensional results and the mechanically ventilated experiment

6.1.1 Similarities

There was a good quantitative agreement between the solutions from the dimensional version of *Distran* and the steady-state experimental results for the mechanically ventilated water scale model.

The results demonstrated agreement in relation to the total change in ambient buoyancy, where experiment 11 and 12 deviated 0.62 % and 3.68 % respectively. The prediction of the first front was also excellent with an error of 6.10 % and 1.77 % for experiment 11 and 12 in §5.3.3, respectively.

The total ventilation flow rates were matched in order to compare effective vent areas for the mechanically ventilated experimental and numerical results. When these ventilation flow rate correlated, the position of the first front and the strength of the ambient buoyancy correlated accordingly, indicating that the numerical and experimental results had the same values of the effective vent areas.

There was also a good qualitative agreement with regards to the shape of the ambient stratification. The deviations between these profiles were related by the appearance of interfaces for the numerical results. These deviations and other differences between experimental results and the theoretical predictions are discussed in the sections that follow.

6.1.2 Interfaces

The shape of the stratification for the ventilated filling box at steady-state results from *Distran* was as expected. This was because the filling box was calculated in a manner that produces interfaces [10]. These interfaces were a consequence of the numerical detrainment process where any vertical transport of fluid have to occur through the plume [1,10]. The buoyancy of this detraining numerical plume is added to the ambient (as it detrains), and the following intrusions form a new numerical layer that corresponds to the buoyancy lost by the plume, as demonstrated in figure 5.19.

The realistic behaviour of an intrusion, for instance as described by Manins [27], is very complex and not accounted for in *Distran*. Neither the simple detrainment mechanism of setting the plume flow to zero nor the Gaussian routine can properly describe this behaviour, as a detrainment is expected to affect the entire ambient above the point of neutral buoyancy [27].

In addition, free convection theory describes a transition from laminar to turbulent flow on a vertical surface by a critical length. Accordingly, the lower section of the boundary layer created by the plume is dominated by laminar flow before it can become turbulent, depending on ambient conditions [28]. This transition was also expected for the experimental result.

One experimental observation related to this transition was that the plume did not fully detrain after the point of intrusion. Instead, the outer section of the plume became negatively buoyant and detrained, whilst inner sections closer to the source remained positively buoyant and continue to ascend. Accordingly, when the plume was turbulent in the water scale model, the turbulent outer-layer became negatively buoyant as it entrained ambient fluid and the laminar sub-layer remained positively buoyant and thus continued to descent.

This behaviour related to the laminar layer was not accounted for in the theory of Cooper et al. [1], as they assumed fully turbulent flow for the entire plume, a deviation from the top-hat assumption used in *Distran*.

Because of these differences, the largest deviations between experimental and numerical results for the mechanically ventilated box were essentially expected to be related to this inconsistency.

Instead of the multiple interfaces predicted by the numerical solution, the steady-state stratification results for the mechanically ventilated water scale model can be described using a two-section model. The bottom section was an area of uniform buoyancy containing fresh water and the upper section consisted of weakly stratified regions where the distribution of salt water increased with height. This is indicated for mechanically ventilated steady-state experiment 8 in figure 6.1.

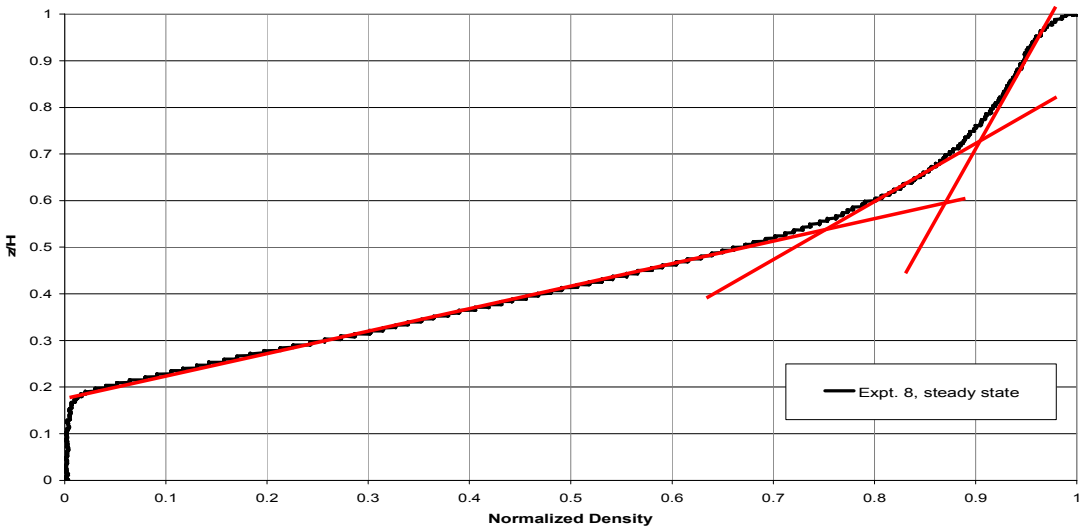

Figure 6.1. The upper section of mechanically ventilated steady-state experiment 8, which indicates weakly stratified regions where the stratification is close to linear at some stages.

The weakly stratified region in the upper section of a steady-state ventilated filling box has also been reported in literature. Chen et al. [4] noted that if intrusions occur over a range around the interface (and not only at specific points) and that entrainment occurs at a low level within each stratification layer, the effect would be a smoothing of the multi-layer stratification. This fits well to the description of what was observed in the mechanically ventilated experiments, having weak stratifications in the upper areas. Regions of weak stratification after the first front were also reported by Etheridge and Sandberg [3], Chen and Cardoso [29] and Chen et al. [13].

Linden et al. [10] did not observe any interfaces experimentally for the vertical line source except for the first front, and suggested that the lack of interfaces was due to vertical mixing

or smearing. Chen et al. [13] also lacked any experimental results to support Linden et al.'s [10] predictions, but supported their assumptions of vertical mixing as the dominant factor for this discrepancy.

Moreover, the fluid mechanics of a ventilated filling box as described by Cooper et al. [1] and Linden et al. [10] only allows for vertical movement of fluid in the box through the plume, as mentioned previously: As the plume move upwards, it entrains ambient fluid and detrains at a certain height. Thus, any movement of fluid across interfaces will not occur unless there is some sort of smearing.

6.1.3 Smearing

Vertical movement, as described by Linden et al. [10] and Chen et al. [4,13] was observed during the water scale experiment for the ventilated filling box. A shadowgram displaying the effect of smearing at steady-state caused by turbulent mixing in the vertical region at the position of the first front is in figure 6.2.

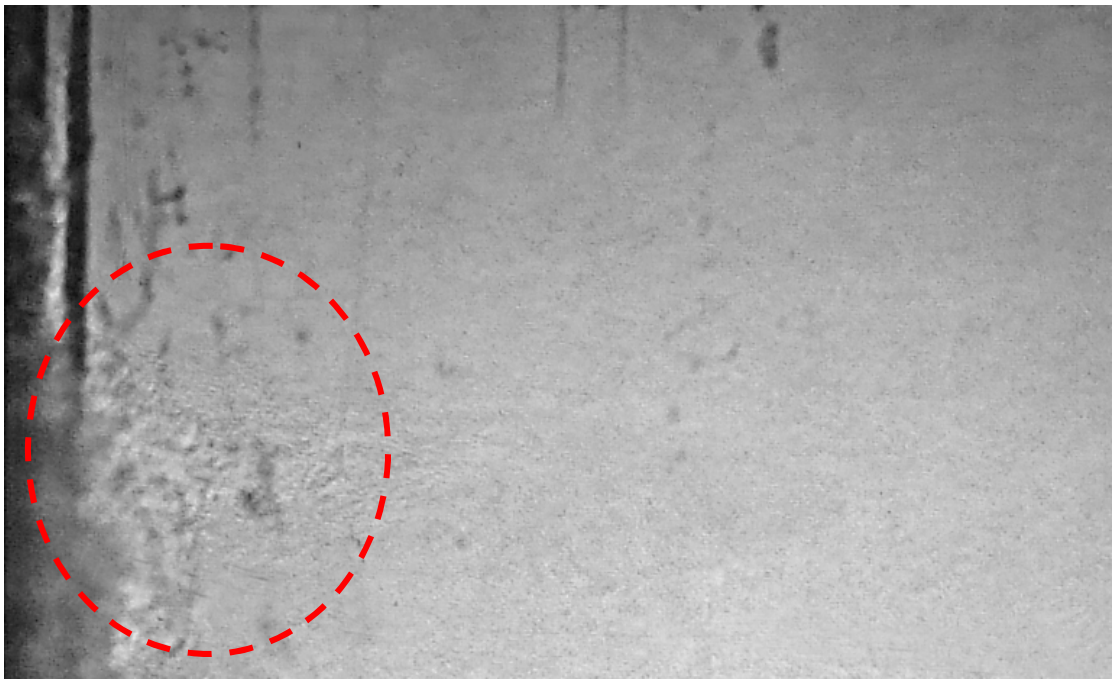

Figure 6.2. A shadowgram at the position of the first front during expt. 12 at steady-state indicating smearing and vertical movement. A sharp interface was initially observed as a transient effect, but it was reduced going towards steady-state due to this indicated effect (no interface was apparent using shadowgraph at steady-state).

The strength of the mixing appeared strongest at this position, but it was also observed for several regions along the vertical source of buoyancy (the membrane). As the interface for the first front was time dependent (figure 5.2), it also suggested that smearing occurred and prevented any steady-state interfaces.

In agreement with Linden et al. [10] and Chen et al. [4,13], this effect presents one explanation of why sharp interfaces were not observed, especially for the first front where the mixing was very turbulent.

6.2 Dimensional results and the linearly stratified experiment

In the linearly stratified experiments, the gravity current accounted for 80 % of the total volume flow. This severely biased the experimental results to the numerical results. A consequence of this was that the transient behaviour of the intrusion could not be measured accurately using two slow conductivity probe traverses. Accordingly, the traverses could only be used to find the total change in an initial and final stratification profile. The comparisons between the experimental and numerical results were inconclusive because of this. Nevertheless, the parameters from the linearly stratified experiments can still be examined numerically by comparing the dimensional and non-dimensional results from *Distran*.

6.2.1 Verification of the dimensional plume equations

As it was not possible to compare the linearly stratified experiments of §5.2.1 to the theory predicting intrusion heights as shown in figure 2.3 as the source buoyancy flux was not uniform and the results heavily influenced by gravity currents. Therefore, Distran was used to compute the theory using parameters from the experiments to validate whether the dimensional code was working correctly.

To control that *Distran* was solving the set of equations correctly, the dimensional volume flux of the plume was tested against the best fit line of the non-dimensional volume flux, using the parameters of linearly stratified experiment 9.

Firstly, a numerical solution was produced using a constant buoyancy flux modelling. Secondly, the varying buoyancy flux was used instead of the constant buoyancy flux. In this scenario, the membrane constant was set to a low value and the initial pressure high, such that the volume flow through the membrane was independent of height. The results were then non-dimensionalized by equations (2.21) to (2.24), and plotted against the non-dimensional volume flux of equation (2.28), displayed in figure 6.3.

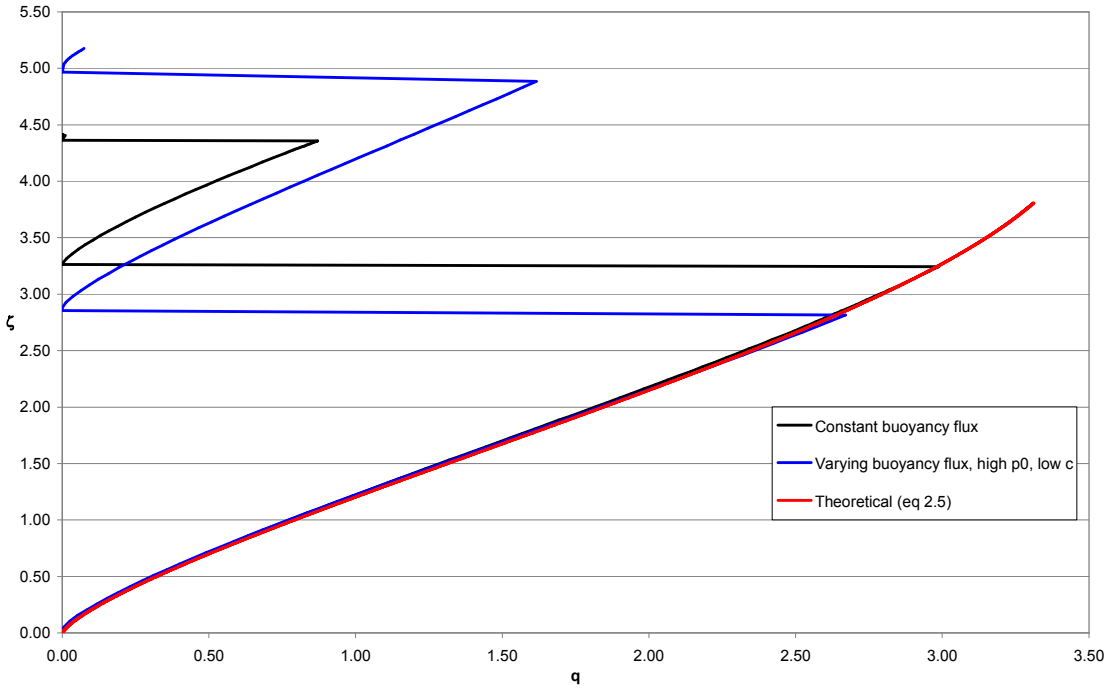

Figure 6.3. The non-dimensional volume flux of equation (2.28) against the results from the dimensional version of *Distran* at $\tau = 4$, using the parameters from linearly stratified experiment 9. The results were non-dimensionalized using equations (2.21)-(2.24). Both plumes detrains within the region $2.70 < \zeta < 3.60$ as predicted by Cooper et al. [1].

The results are perfectly correlating to the theoretical calculations by Cooper et al. [1], which is a strong indication that the dimensional code is solving the plume equations correctly. Moreover, the occurrences of intrusions were validated against the predicted intrusion height, all of them being within the region of $2.7 < \zeta < 3.6$.

6.2.2 Membrane constant

Several numerical solutions where the membrane coefficient was varied were calculated to study the effects of the membrane constant on the volume flux in the plume. The general results are presented in figure 6.4.

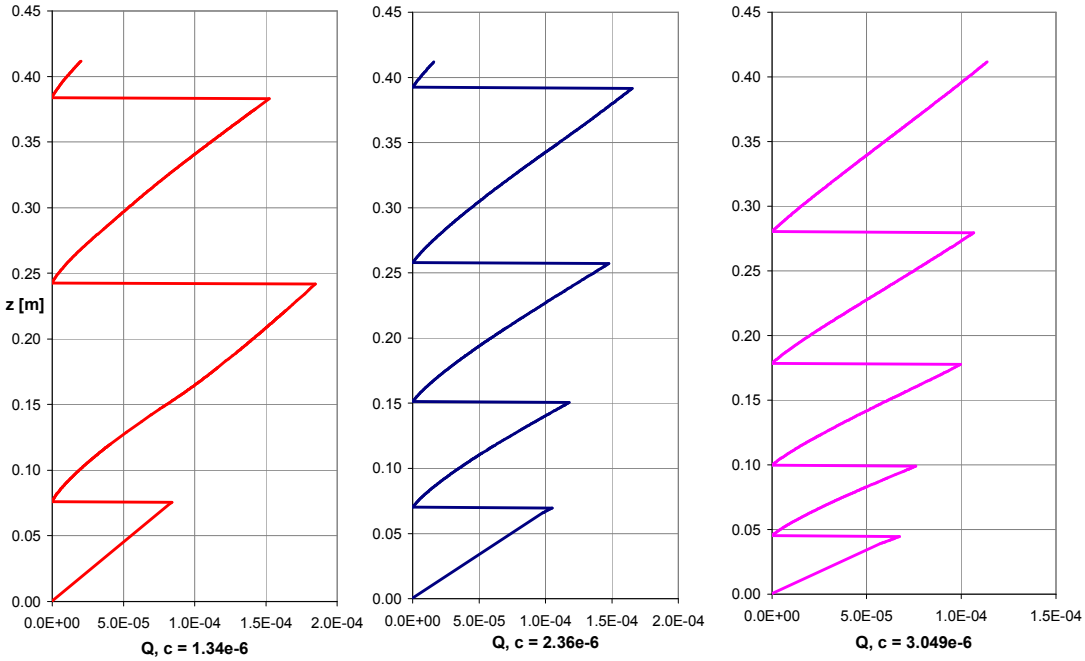

Figure 6.4. The effect of varying the membrane coefficient on the volume flux in the plume for the dimensional version of Distran. A decrease of the membrane coefficient caused a decrease of the plume volume flux and an increase in the number of detrainments. The parameters of steady-state experiment 12 were used for this simulation. (c is in [m^3s/kg] and Q in [m/s]).

When the membrane coefficient is decreased, the volume flux in the plume is intuitively reduced. In figure 6.4 there is a trend that decreasing the membrane coefficient increases the number of detrainments in the plume. This result is quite interesting for many reasons, one related to the design of the water scale model. The lack of proper observable intrusions and domination of the gravity currents in the water scale model could be a consequence of having a too large membrane coefficient.

In the numerical results from *Distran* for the ventilated filling box at steady state, a membrane coefficient of c = 2.358 x10^{-6} [m^3s/kg] was used in order to fit experimental and numerical results for the flow rate. This is in contrast to the initial experimental findings of the membrane coefficient for the membrane, which was c = 1.134x10^{-6} [m^3s/kg] (P. Cooper, *pers. comm.*). This difference could be explained by environmental factors, as it was several years since the membrane was calibrated. The importance of calibrating the membrane coefficient and its influence on the water scale model has not been discussed in detail previously, and as it was not within the scope of this work, it should be given attention in future research.

6.3 Numerical results

6.3.1 An example calculation

The non-dimensional results for the ambient stratification presented in figure 5.16 represent generalized solutions that can be used for design purposes. By applying the plume equations in §2.3.3, these non-dimensional stratification profiles can be made dimensional and therefore used to determine the temperature stratification in a room based on any design criteria, as in the following example (the details of the calculation are in appendix E).

Consider a room where a single wall is 4.8 metres high, 5 metres wide and heated by a 20 W/m^2 convective heat source. Assuming that all the other walls are adiabatic, the temperature stratification for this room can be predicted as presented in figure 6.5.

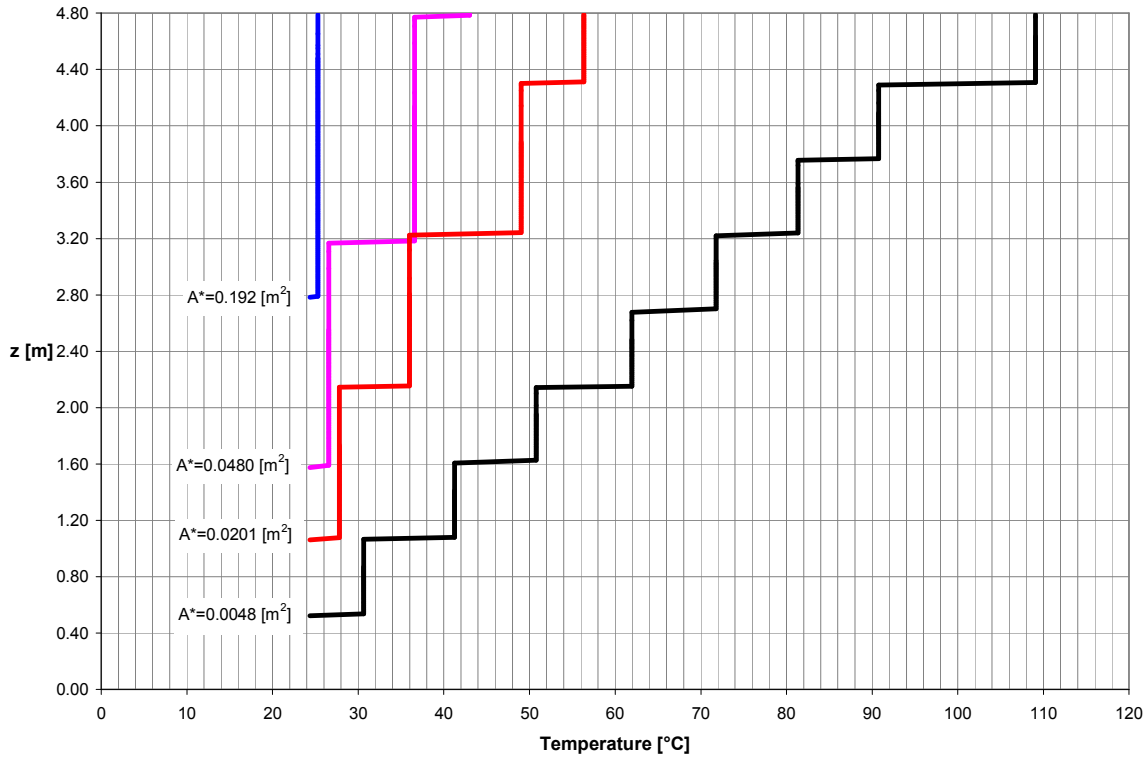

Figure 6.5. The temperature stratification for a naturally ventilated room as calculated by Distran. The room is 4.8 m high and 5 m wide with one wall representing a 20 W/m^2 convective heat source. The other walls are considered adiabatic.

This example represents a simple scenario where it is assumed that convection is the only mechanism of heat transfer inside the ventilated space, i.e. the effects of radiation and

conduction are neglected [1]. Some of the results are in need of an explanation related to the behaviour of *Distran* and the numerical scheme:

The highest value of the effective vent area in figure 6.5, $A^* = 0.192\ m^2$, represents an effective opening of approximately $0.3 \times 1.6\ \text{m}^2$. *Distran* predicts that the first front will be at 58 % of the total height, which is not expected for such a high value of the effective vent area [3]: In a realistic example, such a value of A^* would represent an enclosure having a uniform temperature or at least a very high position for the first front.

This discrepancy for the numerical result is a consequence of the non-mixing characteristics of the numerical scheme not accounting for the complex flow patterns experienced in a real scenario (§6.1.2). Accordingly, the movement of the first front is calculated because of a very small temperature difference: There is only a weak indication of a first front and the stratification above the first front is uniform with a temperature very similar to the one below. In other words, *Distran* predicts a nearly uniform temperature stratification, as would expected for a real scenario. In addition, and for the same reasons, the presence of the strong and distinct interfaces in figure 6.5 is not expected for a real scenario.

Table 6.1 compares these numerical interfaces of the example in figure 6.5 to those predicted by Linden et al. [10] for a vertical line source.

a*	**A* [m^2]**	**Number of interfaces**	
		Figure 6.16	Linden et al. [10]
0.4	0.192	1	2
0.1	0.0480	3	3
0.0419	0.0201	4	4
0.01	0.0048	8	7

Table 6.1. The results for the example calculation in figure 6.5 compared to the results for the number of interfaces for a vertical line source in a ventilated filling box as presented by Linden et al. [10], using the same parameters and strength of the buoyancy source.

The results show a good correlation between the number of interfaces predicted by *Distran* for a plane vertical source and Linden et al. [10] for a vertical line source.

6.3.2 Dimensional results

The shape of stratification for the dimensional results of *Distran* deviated from the non-dimensional due to the modelling of the varying buoyancy flux. There are still strong interfaces in the stratification as displayed in figure 5.18 and 5.20, especially for the first front which has a large jump in ambient buoyancy compared to the uniform lower layer.

Moreover, the layers are not perfectly mixed for the dimensional results, quite in contrast to the non-dimensional results. This indicates that the varying buoyancy flux causes smearing of the ambient buoyancy, giving non-uniform contributions to the stratification of the ventilated filling box. This is demonstrated in figure 6.6 where the buoyancy of the plume is compared to the buoyancy of the source.

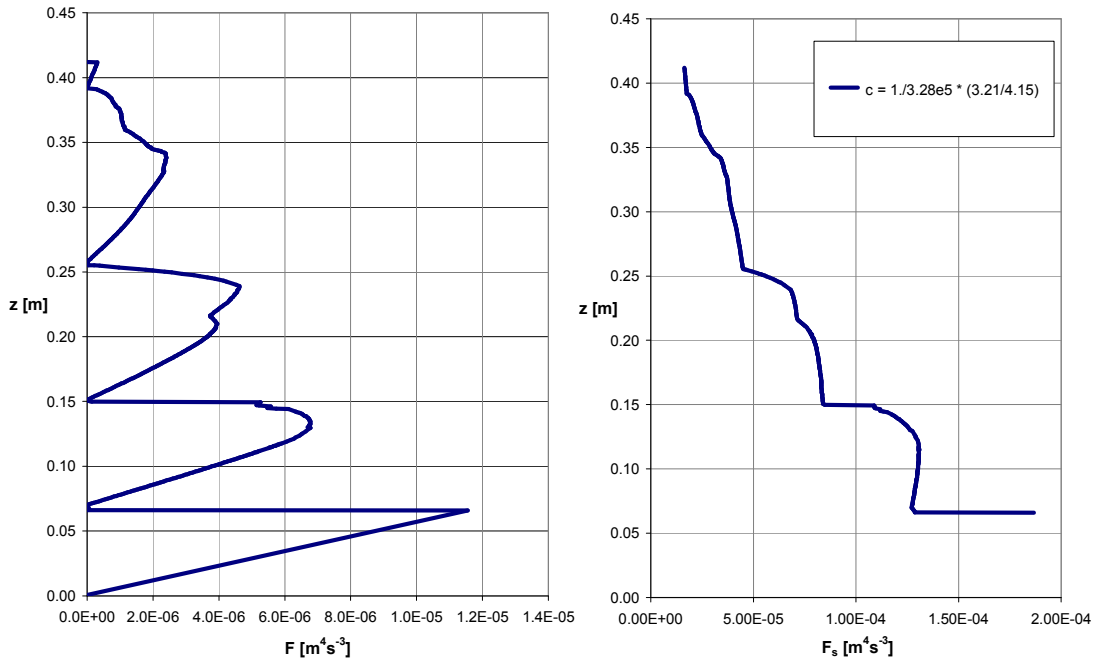

Figure 6.6. The dimensional buoyancy flux of the plume and source to the left and right, respectively (c is in [m^3s/kg]). The comparison demonstrates the influence of the buoyancy from the source on the buoyancy of the plume, explaining the difference between the non-dimensional and dimensional ambient buoyancy. The dimensional parameters from steady-state experiment 12 were used for these results.

In addition, the results from *Distran* demonstrated an increase in ambient volume flux at successive detrainments as the flow from the membrane was modelled correctly. The modelling these detrainments with the Gaussian routine developed in §4.2 is discussed in the next section.

6.3.3 Detrainment

The Gaussian routine worked in the manner it was purposely designed for smoothing the detrainments of the plume's volume flux, consequently smoothing out the buoyancy flux and the momentum flux. The initial motivation for this behaviour was to remove the 'noise' in the ambient stratification produced by Cooper et al. [1] (figure 2.7). However, it was discovered during the revision of *Distran* that this noise was produced by an error in the code, and consequently the Gaussian routine was no longer needed for that purpose.

The second motivation for the Gaussian routine was to decrease the strength of the distinct interfaces, thus making the numerical results comparable to the experimental by introducing a more realistic behaviour of detrainment. As the dimensional version of *Distran* was successfully modelled with a varying buoyancy flux, the ambient stratification behaved accordingly to the buoyancy flux of the source. In addition, the modification of the plume equations by a Gaussian curve made the control of conservation of buoyancy extremely difficult. Also, a Gaussian routine does not properly describe a realistic intrusion [27]. For these reasons it was decided that the Gaussian routine should be turned off during the comparisons between experimental and numerical results for the mechanically ventilated filling box.

It is suggested that alternative methods for enhancing the detrainment routine of *Distran* on the plume equations to be investigated in future studies. These detrainment procedures should not be considered as a realistic modelling, but rather an improvement to the already existing detrainment routine in *Distran*.

6.4 Mechanically ventilated filling box

The mechanically ventilated steady-state experiments produced high quality measurements of the ambient stratifications and the measurements demonstrated excellent repeatability as differences in steady-state stratification profiles were within 1 %[6]. This was made possible through the self-regulating valve and extensive control of the conductivity probe, calibrated before each experiment against the *Anton Paar* density meter to ensure accurate readings.

[6] Using the Y Error Bars in Excel and 1 % Error Amount

One of the negative consequences of the water scale model as experienced during the mechanically ventilated experiments was to find the effective vent area.

6.4.1 Effective vent area

The difficulties of calculating the effective vent area is a negative aspect of using a mechanically ventilated water scale model, with the need of introducing *an effective vent area equivalent* as mentioned in §5.1.2. However, using the ventilation flow rate to match the numerical and experimental results at steady-state provided a good replacement for calculating an implicit value of A^*.

One interesting aspect of the effective vent area which can be observed from interpreting the results from the mechanically ventilated experiment, relates to Linden et al.'s [10] assumption that the stratification in a ventilated box is dependent on the value of the effective vent area only. In other words, the curvatures of the results in figure 5.4 are the only relevant factor when comparing the shapes of the stratifications. This suggests that normalizing the profiles which have the same effective vent area should give the same slopes.

Experiments 12.15 and 7.10 could serve as an interesting observation to this assumption as they had very similar ventilation flow rates. It was therefore expected that they would have similar values of the effective vent area equivalent, indicating that their normalized curves should be of the same shape. Their respective curves in figure 6.7 support this assumption.

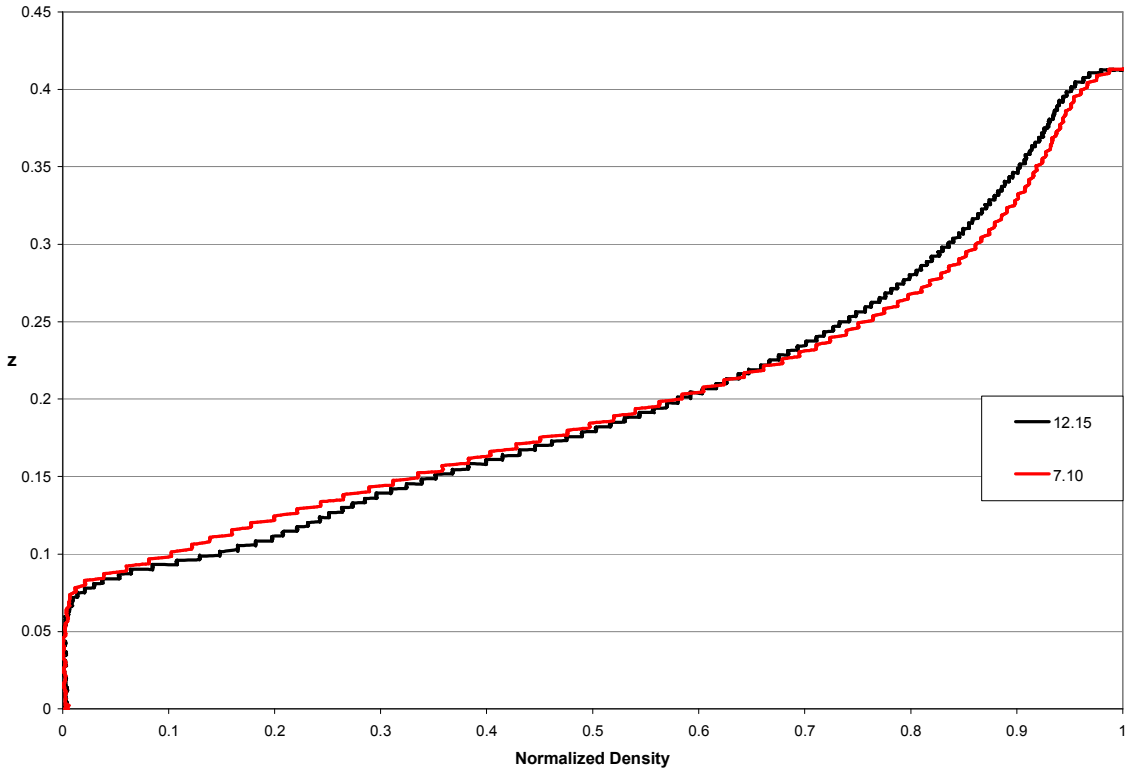

Figure 6.7. The normalized steady-state stratification profiles for the results from experiments 12 and 7, run 15 and 10, respectively. The profiles show a similar shape due to a similar ventilation flow rate through the diffuser producing similar values of the effective vent area. This corresponds to the predictions of Linden et al. [10].

It can also be seen in figure 6.7 that there are two distinct sections: one lower section where there is a uniform density and an upper section which has regions of weak stratifications. The strongest indication of an interface is the first front separating these two sections.

In addition to deviations in the steady-state mechanically ventilated experiments, the physics of the water scale model affected the linearly stratified experiments

6.5 Linearly stratified filling box

The linearly stratified experiments did not correlate to the numerical results from *Distran* because of the influence of the gravity current.

The effects caused by the gravity current could have been reduced by performing the linearly stratified experiments over a shorter time scale, effectively reducing the total amount of source fluid entering the main compartment of the water scale model and

consequently reducing the amount of gravity current. This alteration was also suggested by P. Cooper (pers. comm.) as a potential solution, but it was not successfully carried through for the linearly stratified experiments.

The most significant reason for this was related to the procedures of starting and stopping each of these experiments. Several valves had to be adjusted to avoid a change in initial pressure for the membrane flow as described in §3.6, and at the same time data had to be recorded, such as writing down flow information and documenting flow patterns. These adjustments and procedures alone required approximately one minute, effectively preventing measurements to be performed under less than one minute without reducing accuracy; It was also observed that measurements was already affected by the gravity current after one minute.

In addition, reducing the time scale would not only have resulted in lower gravity current flow, but also a proportionally smaller intrusion. The intrusion found when observing the volume flow and velocity charts of section §5.2.2 was significantly smaller than the gravity current (figure 5.10). Reducing the total flow could thus reduce the possibility of measuring the intrusion. Another aspect was small leakages from the source fluid in the source compartment into the ambient environment in the main compartment after the experiment was finished. These leaks were very small, but if the linearly stratified experiment was to be performed at significantly shorter timescale, the leaks would affect the results inversely proportional to the reduction time. This was a consequence of having a source compartment of constant volume (same total amount of source fluid that could enter the main compartment regardless of the total source flow) and the time required for a conductivity probe traverse.

Despite the problems related to the gravity current, the measurements for the linearly stratified experiment were excellent and the double-bucket method produced excellent linear stratifications with linear best-fit lines up to $R^2 = 0.9999$.

Additionally, the verification process in §5.2.4 proved useful to increase the confidence in the data analysis process. As the extractions were performed in a very restricted environment, the results were a strong indicator that the numerical treatment of the results was satisfactory. Consequently, it was reasonable to assume that the accuracy of the

intrusion-calculations were good predictions to the actual environment in the water scale model.

Another aspect of the data processing procedures was the use of best fit lines in order to find the velocity profiles. The endpoints of the best fit lines were treated very carefully to avoid some of the large fluctuations found in those areas; one example worth mentioning is the lower section of linearly stratified experiment 9 in figure 5.8 and 5.9.

6.6 Comparison to previous results

Linden et al. [10] predicted a multi-layer stratification to form at steady-state as described in §2.2.4. Cooper et al. [1] used a similar analytical approach as Linden et al. [10] to the ventilated filling box containing a plane source of buoyancy, thus the numerical solutions presented in this work had a similar stratification consisting of several interfaces.

It was discovered that full steady-state is not necessarily achieved at $\tau = 40$ as reported by Cooper et al. [1] in figure 2.7, which explains some of the shifts in ambient stratification between the curves: A lower value a^* increases the time to reach steady-state, and for $a^* = 0.0007$ steady-state was not observed before approximately $\tau = 120$. The reduction of the 'noise' from figure 2.7 to figure 5.16 was due to removal of errors during the revision in the numerical scheme.

Moreover, as an interesting note, the temperature profiles for a displacement ventilated room as reported by Bouzinaoui et al. [30] is displayed in figure 6.8 have similar stratification profiles as in figure 6.5 and 5.4, although they did thermocouple measurements using heat sources in a ventilated space (more details in appendix B.3).

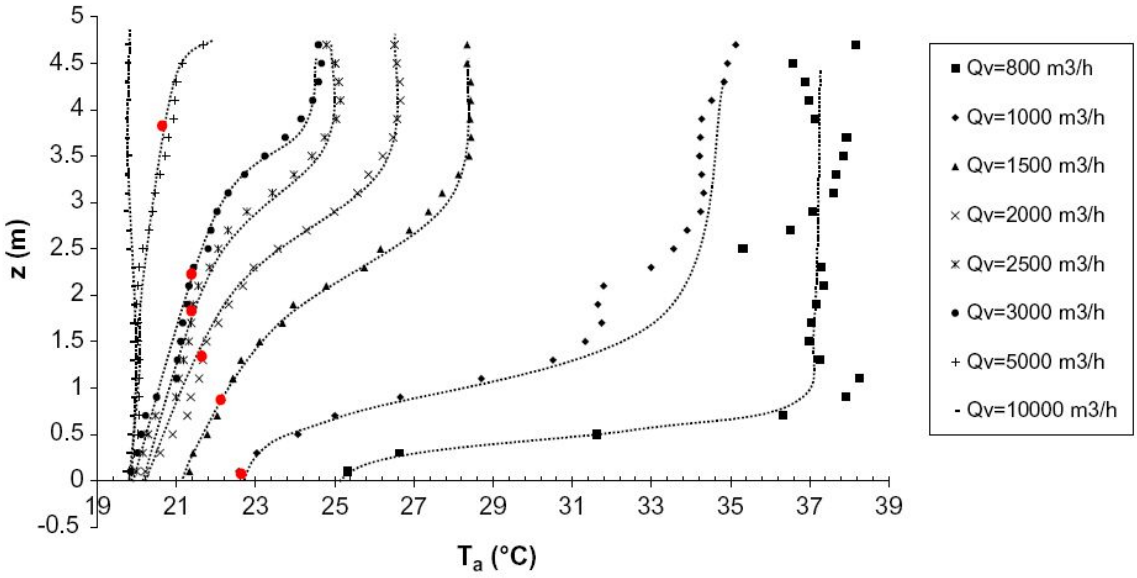

Figure 6.8. Vertical temperature profiles outside the plume (T_s=200°C, D_s=1.54m). Interface height calculated from Skåret's proposed law [31]. Reproduced from Bouzinaoui et al. [30].

Direct comparisons with figure 6.8 from Bouzinaoui et al. [30] are not possible, but the same qualitative characteristics are seen for the stratifications. It would be interesting to compare the non-dimensional stratification profiles to such a dimensional scenario, and an example that demonstrates the applicability for the non-dimensional results is presented in the next section.

6.7 Evaluation of the water scale model

Chen et al. [13] criticized the use of salt water to model buoyancy flows, noting that "the introduction of salt solution through the membrane may give rise to additional driving pressure, since the initial velocity of the salt solution could be relatively significant if the permeability of the wall is small."

Any possible initial conditions were found insignificant related the steady-state experimental results of obvious reasons. Nevertheless, could be interesting to investigate this claim for future experiments involving the water scale mode.

Chen et al. [13] also noted that one of their theoretical assumptions associated to the ratio of volume fluxes was not valid for a water scale model similar to the one used in this work,

as the flow through the membrane was about half the volume flux through the opening. For some of the experiments presented in this work, the volume flow was more than half of the total volume flux. As a consequence of this, their theoretical model could not be applied for this water scale model.

6.8 Discussion summary

The theory presented by Cooper et al. [1] for a plane vertically distributed source of buoyancy correlates with the ventilation flow rate and ambient buoyancy for the experimental results. The differences in stratification profiles were as expected due to vertical mixing and complex flow patterns that was not accounted for in *Distran*.

Distinct interfaces as predicted by the simple detrainment process proposed by Linden et al. [10] and Cooper et al. [1] for the steady-state ventilated filling box were not observed. Instead, a two layer model was observed where the upper region above the first front had areas of weak stratification, some of which were close to linear.

Lastly, direct comparisons to the linearly stratified environment were not successful as the influence of the gravity current in the water scale model was found to be 80 % of the total flow from the source.

7 Conclusion

In this work, experimental results from measurements in a water scale model have been compared to numerical results based on a theory developed by Cooper et al. [1]. The experiments provided good quantitative results for the stratified environment and demonstrated good correlation between the strengths and shapes of the ambient buoyancies. No multi-layer stratification was observed for the experimental results as predicted by the theory; instead two-section stratification was observed where the upper section had weak stratifications.

The deviations related to multi-layer stratifications as predicted by the numerical results could be explained by the fact that the initial laminar region of the plume and its laminar sub-layer was not accounted for in the theoretical assumptions. Vertical mixing was observed to have a smoothing effect on any sharp interfaces. Detrainment was also observed to occur over a significant depth, not only at a single location as modelled by Distran.

In the linearly stratified experiments, a gravity current formed at the bottom of the tank which was fed by the descending plume. This gravity current accounted for approximately 80 % of the total flow through the membrane. This meant that the measurements of the intrusions were compromised because of the vertical displacement of the ambient fluid throughout each experiment. For this reason, any comparisons to the numerical results were not successful. Moreover, the effect of the membrane coefficient on the membrane in the water scale model was examined theoretically, and it was found that it has a strong influence on the intrusions and the volume flux in the plume.

The modelling of a finite intrusion smoothed out the plume detrainments, influencing the ambient stratification produced by the numerical solution. As the modelling of varying buoyancy flux made the finite intrusion modelling redundant, it was not used when comparing numerical and experimental results. In addition, the numerical dimensional results for intrusions, without the finite intrusion modelling enabled, indicated good correspondence to the non-dimensional results by Cooper et al. [1].

Numerical non-dimensional results were found to be useful for predicting the temperature stratification in a ventilated space. The applicability of these results was illustrated by an example calculation for a dimensional scenario.

The experimental apparatus was successfully commissioned for both the mechanically ventilated and linearly stratified experiments. Measurements were carried out with satisfactory quantitative accuracy and the equipment was demonstrated to have worked efficiently. High quality steady-state stratification measurements were produced for the mechanically ventilated experiments using the traversing conductivity probe. The probe apparatus worked well within its limits showing good repeatability. This allowed for several experiments per day, demonstrating excellent repeatability at steady-state with the stratifications having only 1 % deviation.

The linear stratifications produced by the experimental setup were excellent with some linear stratifications having a linear best fit lines up to R^2=0.9999. The processing of the results to find the net outwards flow and produce horizontal velocity profiles was also promising, and was in good agreement with the verification procedure.

8 Suggestions for Future Study

This chapter presents suggestions for future research involving the water scale model and Distran. Firstly, suggestions related to the experimental materials and methods are presented, followed by suggestions for improving Distran.

8.1 Experimental

8.1.1 Membrane characteristics

For the water scale model to be analogous to the nature of a heated wall in contact with air, future experiments could be performed using a membrane that can provide uniform volume flux corresponding to a constant heat flux [28].

In order to provide such a buoyancy flux it would be necessary to have a very low membrane coefficient, such that the driving pressure becomes less dependent on height. However, these membranes become blocked by salt or particles quite easily due to the low permeability. Some experiments at Imperial College London were performed using sintered porous metal plates provided by GKN Sintered Metals (*G. R. Hunt, pers. comm.*). These plates can be soaked into an acid bath between experiments to ensure that the membrane is clean, thus lower membrane coefficients could be used.

8.1.2 Gravity currents

The implications of gravity currents in this present work were significant, as they were severely larger than the intrusions. Moreover, they shifted the ambient stratification upwards and thus disturbed the accuracy of the conductivity probe measurements.

A suggestion to avoid these problems in future research is to run the linearly stratified experiments for the shortest time possible while still achieving measurable intrusions. However, there are problems related to this in regards to starting and stopping procedures, especially stopping for the membrane flow.

An interesting modification to the water scale model related to this would be to divide the model into two interconnected chambers where the membrane is only in one of the chambers, effectively doubling the length of the tank allowing more time for observing intrusions, similar to the method Baines used for his plume and gravity driven flow experiments [25,32].

8.1.3 Conductivity probe

The density range of the conductivity probe could be increased so that the effects of using a higher density source fluid or a linearly stratified environment with a larger buoyancy frequency could be observed. One possible way of achieving this would be to modify the probe by installing a resistance between the probe and the conductivity meter.

Another interesting approach would be to construct a probe with smaller volume to observe any differences in responsiveness. By comparing the results using two different probes, the effects of sample size and any internal mixing in the probe could be investigated.

8.2 Numerical methods

It is suggested to further investigate the modelling of a finite intrusion accounting for more of the complex flow patterns encountered in the experimental procedures. Moreover, it would serve useful to model a routine that simulates a simplified scenario related to the vertical movement and smoothing observed during the experiments.

List of References

[1] Cooper P, Hunt GR, Linden PF. The ventilated filling box containing a vertically distributed source of buoyancy. Draft paper for Journal of Fluid Mechanics 2007.

[2] Skistad H, Nielsen PV, Seppänen O, Mundt E, Santoli L, Braham D, et al. Displacement Ventilation in Non-industrial Premises. RHEVA; 2001.

[3] Etheridge D, Sandberg M. Building Ventilation: Theory and Measurement. Chichester: John Wiley & Sons; 1996.

[4] Chen ZD, Li Y, Mahoney J. Experimental modelling of buoyancy-driven flows in buildings using a fine-bubble technique. Building and Environment 2000;36(4):447-55.

[5] Linden PF. The Fluid Mechanics of Natural Ventilation. Annual Review of Fluid Mechanics 1999;31(1):201-38.

[6] Morton BR, Taylor G, Turner JS. Turbulent Gravitational Convection from Maintained and Instantaneous Sources. Proceedings of the Royal Society of London Series A, Mathematical and Physical Sciences 1956;234(1196):1-23.

[7] Baines WD, Turner JS. Turbulent buoyant convection from a source in a confined region. Journal of Fluid Mechanics 1969;37:51-80.

[8] Germeles AE. Forced plumes and mixing of liquids in tanks. Journal of Fluid Mechanics 1975;71:601-23.

[9] Worster MG, Huppert HE. Time-dependent density profiles in a filling box. Journal of Fluid Mechanics 1983;132:457-66.

[10] Linden PF, Lane-Serff GF, Smeed DA. Emptying filling boxes: the fluid mechanics of natural ventilation. Journal of Fluid Mechanics 1990;212:309-35.

[11] Cooper P, Linden PF. Natural ventilation of an enclosure containing two buoyancy sources. Journal of Fluid Mechanics 1996;311:153-76.

[12] Linden PF, Cooper P. Multiple sources of buoyancy in a naturally ventilated enclosure. Journal of Fluid Mechanics 1996;311:177-92.

[13] Chen ZD, Li Y, Mahoney J. Natural ventilation in an enclosure induced by a heat source distributed uniformly over a vertical wall. Building and Environment 2001;36:493-501.

[14] Eggebrecht O. Two-dimensional plumes developing from a vertically distributed source of buoyancy in a linearly stratified environment. New South Wales, Australia: University of Wollongong; 2005.

[15] Hough CM. Investigations of buoyancy-driven flows from vertical surfaces. New South Wales, Australia: University of Wollongong; 2006.

[16] Logan P. Modelling natural displacement ventilation within an enclosure using a water filled scale model. Wollongong: University of Wollongong; 2000.

[17] White FM. Fluid Mechanics. 4 ed. New York: McGraw-Hill; 2001.

[18] Wood IR. Selective withdrawal from a stably stratified fluid. Journal of Fluid Mechanics 1968;32(02):209-23.

[19] Wood IR. Extensions to the theory of selective withdrawal. Journal of Fluid Mechanics 2001;448:315-33.

[20] Bryant PJ, Wood IR. Selective withdrawal from a layered fluid. Journal of Fluid Mechanics 1976;77:581-91.

[21] Settles GS. Schlieren and Shadowgraph Techniques: visualizing phenomena in transparent media. Springer; 2001.

[22] Econmidou M, Hunt GR. An alternative approach to the double-bucket method: Free-drain. Draft paper for Journal of Fluid Mechanics 2007 Jul 9.

[23] Baines WD, Turner JS, Campbell IH. Turbulent fountains in an open chamber. Journal of Fluid Mechanics 1990;212:557-92.

[24] Salford FTN95 [computer program]. Version 3.17 2004.

[25] Baines PG. Two-dimensional plumes in stratified environments. Journal of Fluid Mechanics 2002;471:315-37.

[26] Perry RH, Chilton CH. Chemical Engineers' Handbook. 5 ed. New York: McGraw-Hill; 1973.

[27] Manins PC. Intrusion into a stratified fluid. Journal of Fluid Mechanics 1976;74:547-60.

[28] Incropera FP, DeWitt DP. Fundamentals of Heat and Mass Transfer. 5 ed. New York: John Wiley & Sons; 2002.

[29] Chen MH, Cardoso SSS. The mixing of liquids by a plume of low-Reynolds number bubbles. Chemical Engineering Science 2000;55(14):2585-94.

[30] Bouzinaoui A, Vallette P, Lemoine F, Fontaine JR, Devienne R. Experimental study of thermal stratification in ventilated confined spaces. International Journal of Heat and Mass Transfer 2005;48(19-20):4121-31.

[31] Skåret E. Ventilasjonsteknikk [In Norwegian]. Trondheim: Inst. of Heating, Ventilation and Sanitary Techniques, NTH; 1986.

[32] Baines PG. Mixing in flows down gentle slopes into stratified environments. Journal of Fluid Mechanics 2001;443:237-70.

[33] Turner JS. Buoyancy Effects in Fluids. London: Cambridge University Press; 1973.

[34] Li Y, Shing VCW, Chen Z. Fine bubble modelling of smoke flows. Fire Safety Journal 2003;38(3):285-98.

[35] Maidment DR. Handbook of Hydrology. New York: McGraw-Hill; 1993.

List of Personal Communications

1 Cooper, P., Faculty of Engineering, University of Wollongong, Wollongong. In discussion. 2007.

2 Hunt, G. R., Department of Civil and Environmental Engineering, Imperial College London. In discussion. July 2007.

Appendices

Appendix A Experimental Equipment

A.1 Photographs of experimental equipment

This section presents photographs and screenshots describing experimental materials and methods, as depicted in figures A.1-A.5.

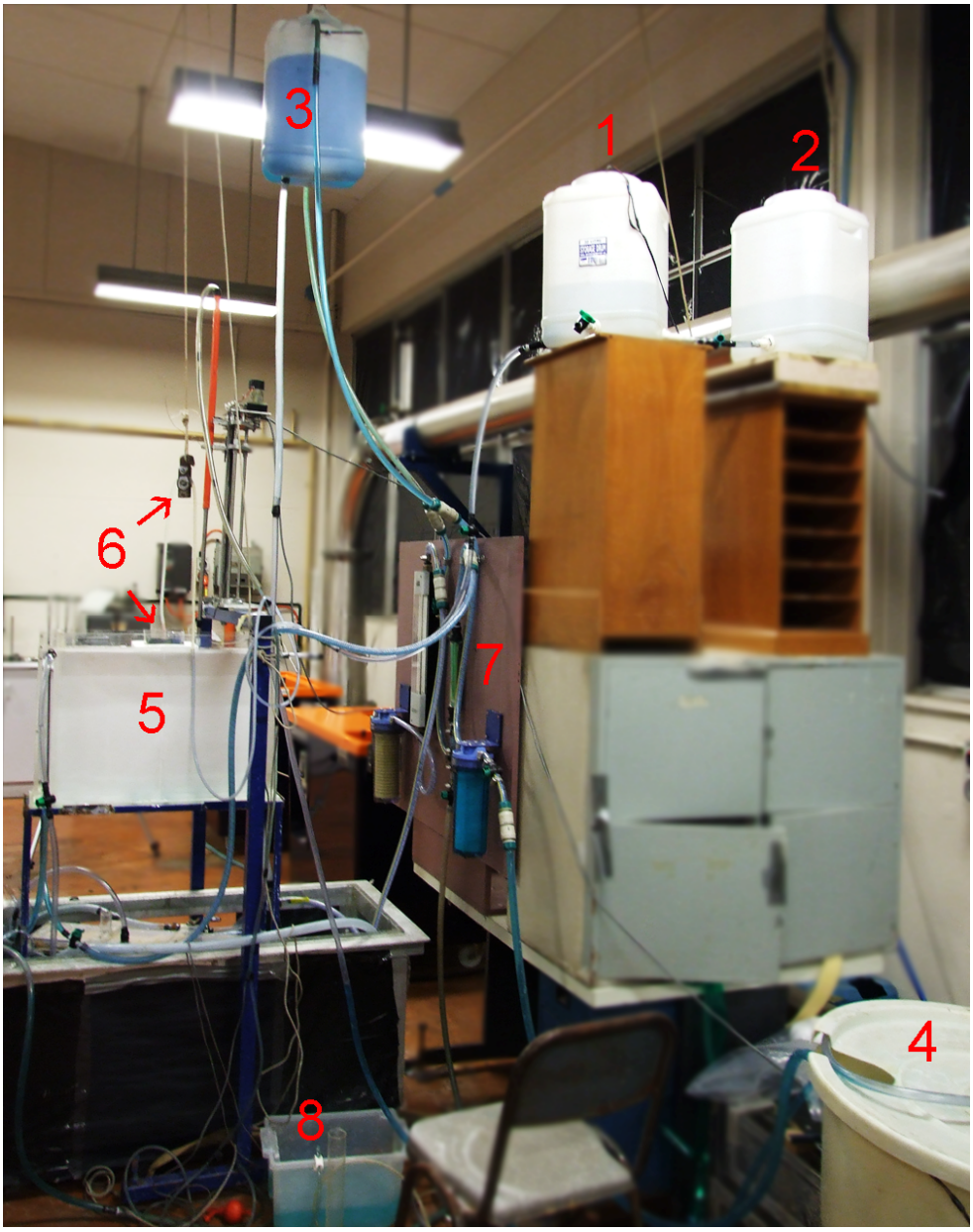

Figure A.1. Setup used for the linearly stratified experiments using a double-bucket system. 1. Bucket for water with high salt concentration, 2. Bucket for fresh water, 3. Constant head tank for high salt concentration supply water. 4. Supply tank for the constant head tank. 5. Water scale model, currently covered with tracing paper for shadowgraph. 6. Pulley system and diffuser. 7. Valves and filters.

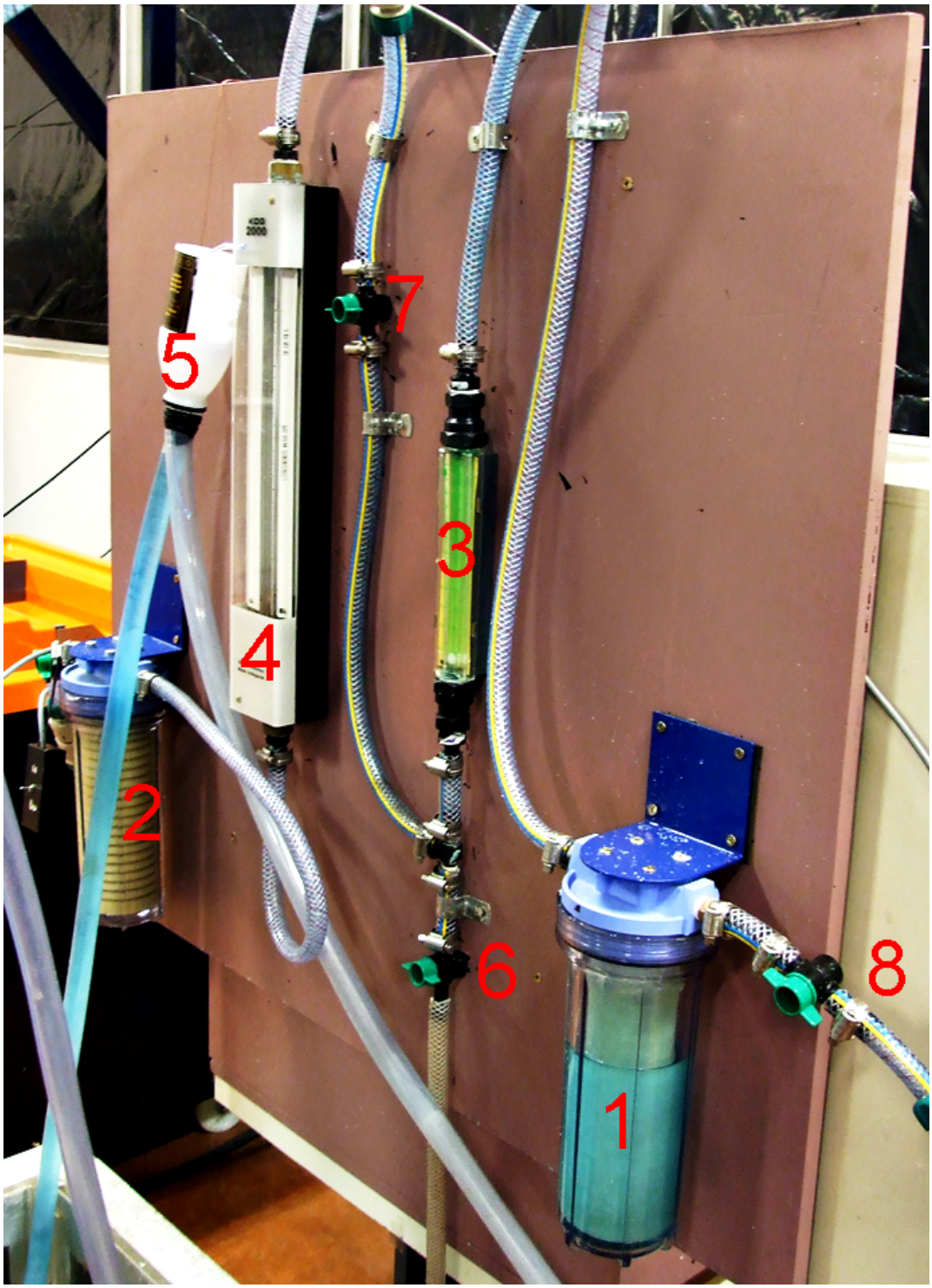

Figure A.2. Modular board for valve control. 1. 5-micron filter for brine. 2. Filter for fresh water. 3. Flow meter for brine. 4. Flow meter for freshwater. 5. Self-adjusting outlet for drainage from water scale model. 6. Pressure release valve. 7. Saltwater flow adjustment valve. 8. Head tank supply adjustment valve.

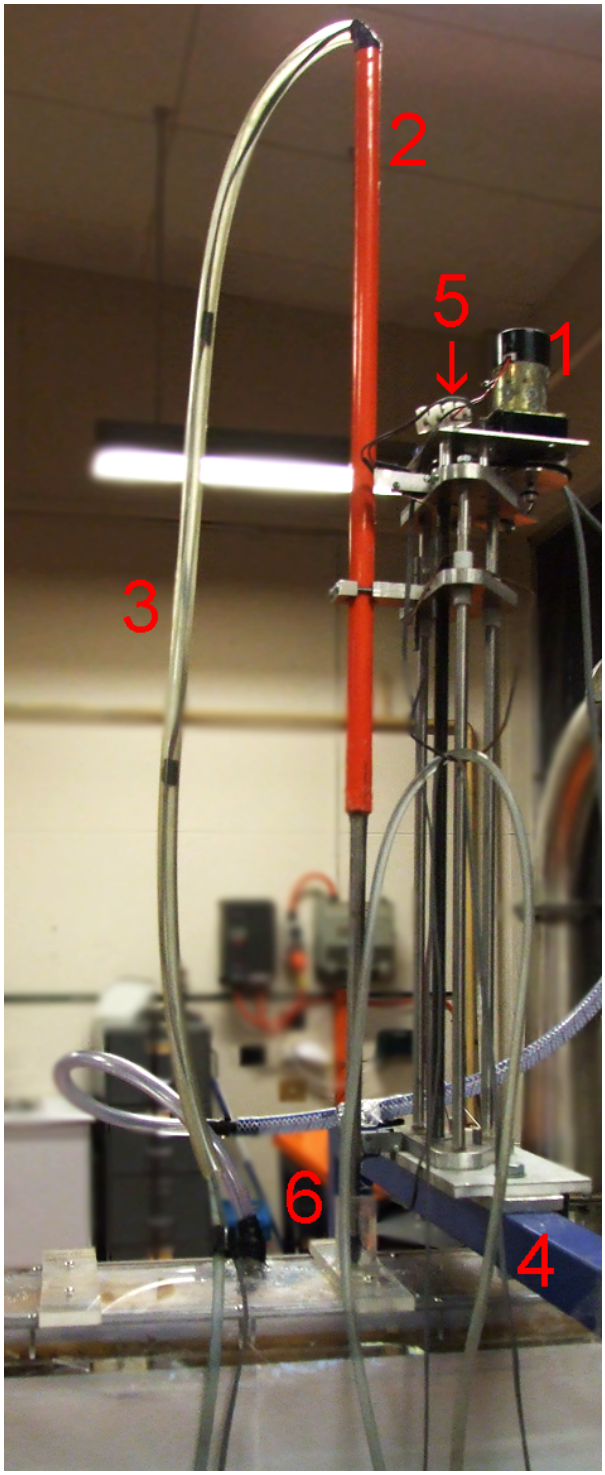

Figure A.3. Traverse mechanism used for performing traverses with the conductivity probe. 1. 12 V DC motor, 2. Conductivity probe, 3. Siphon, 4. Adjustable rig, 5. Potentiometer., 6. Fitted entrance for probe in the diffuser.

Figure A.4. Anton Paar DM 35n Portable Density meter.

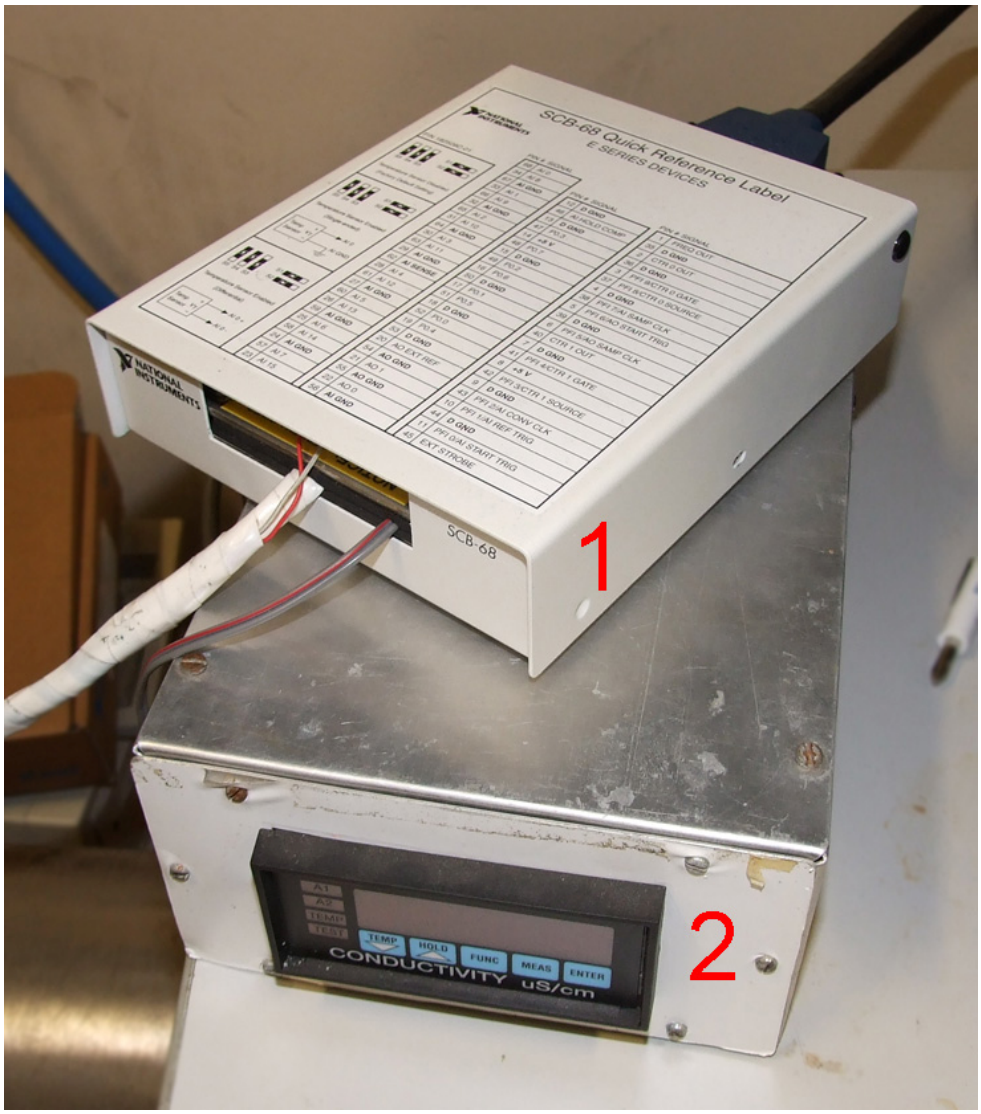

Figure A.5. 1. National Instruments SCB-68 DAQ. 2. Almagated Instruments Co. AIC PM2 Conductivity Meter.

A.2 LabVIEW program

The following program described in figures A.6 and A.7 was written in LabVIEW for recording data using a National Instruments DAQ.

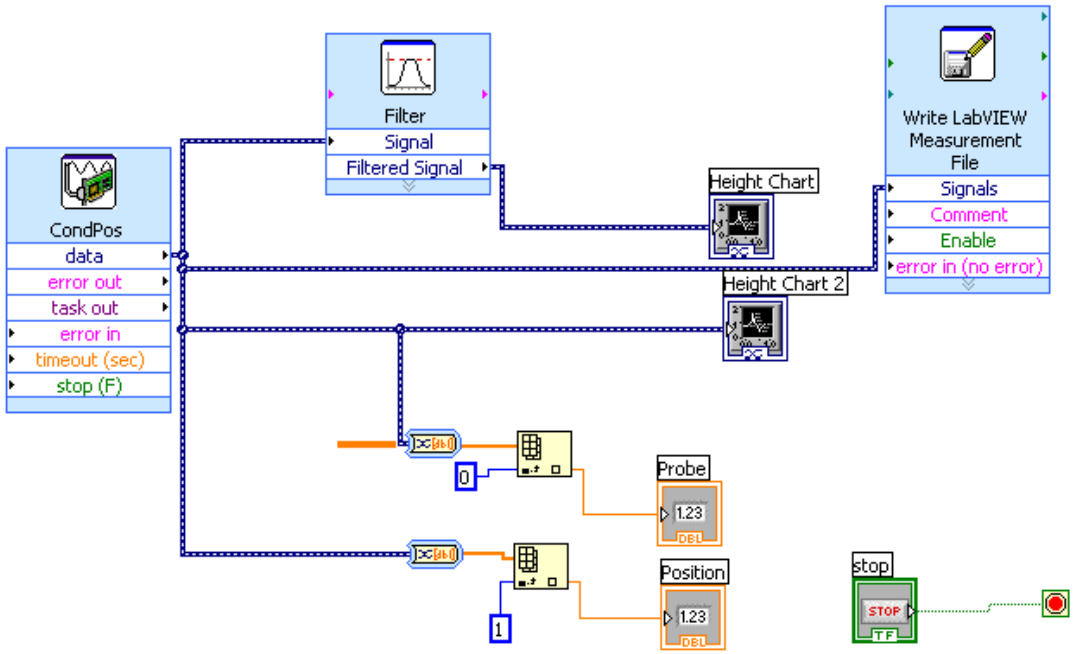

Figure A.6. LabVIEW setup for data acquisition from a DAQ. The program displays the recorded data with and without filtering while writing it to a file. This screen is for configuration.

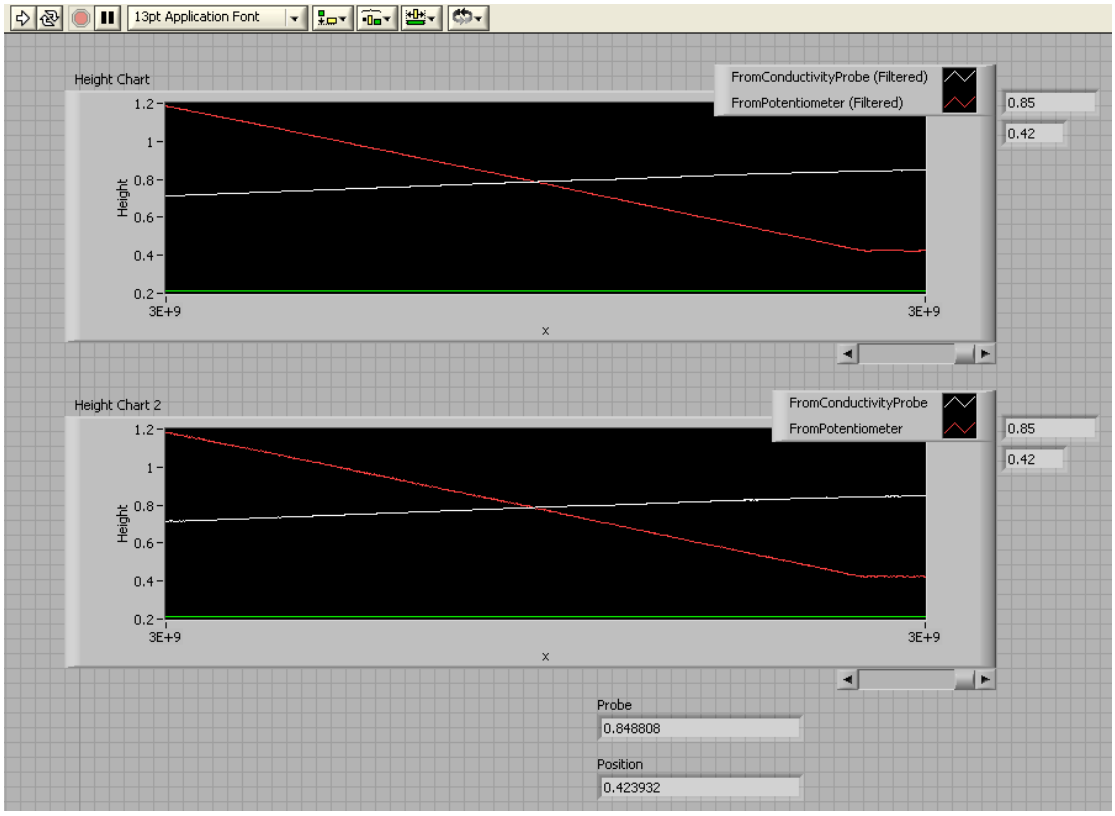

Figure A.7. LabVIEW program for data acquisition from a DAQ. The program displays the recorded data with and without filtering while writing it to a file. This screen is for displaying live results.

Appendix B Analysis

B.1 The conductivity probe

The conductivity probe consisted of two concentric stainless steel tubes separated by an insulator. By siphoning brine through the tip of the probe whilst applying a voltage between the outer and inner tube, the resulting current through the brine could be measured using a conductivity meter. The intensity of the current increases depending on the concentration of salt. The meter used alternating current to avoid any of the electrodes to become contaminated due to electrolysis.

B.1.1 Principle

The principle behind conductivity probe measurements is that the conductivity of the sampled fluid in the nozzle-section is representative for the measured conductivity. To investigate this claim, it is appropriate to introduce an electrical resistance analogy analysis (P. Cooper, *pers. comm.*). If successful, this analysis would return that the resistance of the nozzle section is some orders of magnitude greater than the other relevant probe resistances.

B.1.2 Order of magnitude consideration

The nozzle-section of the probe is illustrated in figure B.1.

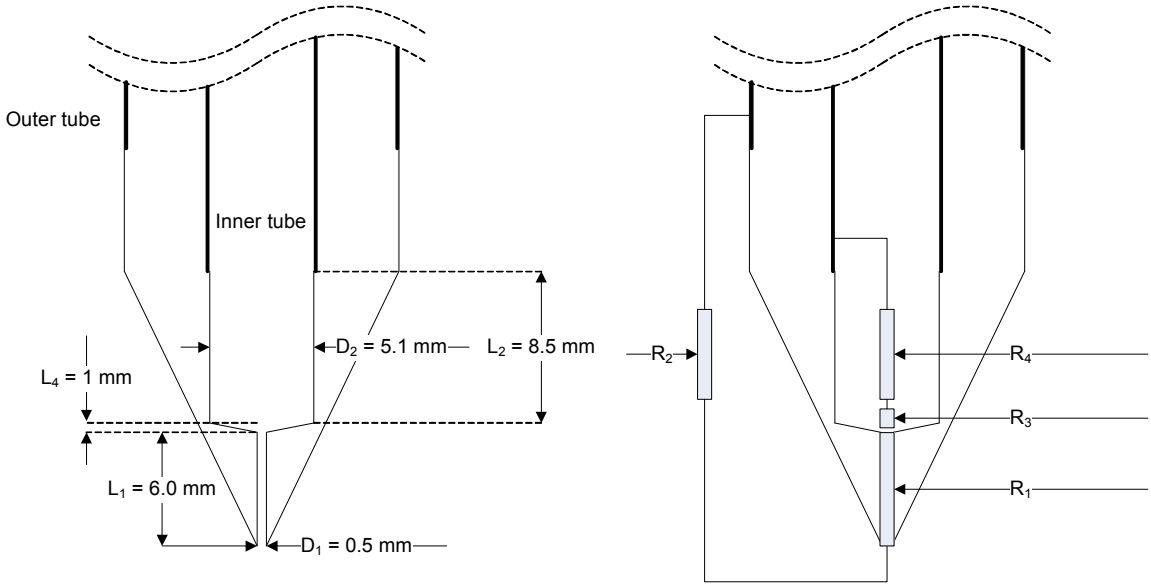

Figure B.1. Lower section of the probe, with the right figure showing its resistance analogy.

In figure B.1, resistance R_1 is for the nozzle section, R_2 is between the nozzle and outer steel piping, R_3 is for the conical section caused by the drill when manufacturing the probe. Lastly, R_4 is the resistance from the conical section to the inner steel piping. For the purpose of analysis, a thermal resistance is defined [28] as

$$R \equiv \frac{\Delta T}{q} \tag{B.1}$$

Moreover, heat transfer rate relates to shape factor as

$$q_{cond} = Sk\Delta T \tag{B.2}$$

and for a two dimensional system, the resistance of such a system's conductance can be expressed as

$$R_{cond} = \frac{1}{Sk} \tag{B.3}$$

where S is the shape factor [28].

Using this approach, the three probe resistances can be estimated to their relative order of magnitude. Firstly, the resistance of the nozzle entrance can be readily found as

$$R_1 \sim \frac{L_1}{k_1 A} = \frac{4L_1}{k_1 \pi D_1^2}$$

The same result, but with a different scaling, is found for the fourth resistance, the one after the conical shape:

$$R_4 \sim \frac{L_4}{k_4 A} = \frac{4L_4}{k_4 \pi D_4^2}$$

The second resistance can be found by considering a disk on a semi-infinite medium. The disk represents the area of the nozzle entrance, and the semi-infinite medium represents the fluid surrounding the probe and the nylon separating the rod from the nozzle. The shape factor for such a situation is two dimensional [28]. Inserting that into equation (B.3) returns

$$R_2 \sim \frac{1}{2 \times \left(2 D_3 k_3\right)}$$

To find the third resistance for the conical part of the probe, Fourier's law of conductivity, equation (B.4), has to be integrated over the cone's area.

$$q_x = -kA\frac{dT}{dx} \qquad \text{(B.4)}$$

where $A = -\frac{\pi}{4} D_2^2 = \frac{\pi}{4}\left(ax\right)^2$

If the fluid flow through the nozzle is considered constant, q_x is constant. Moreover, if the conductivity *k* is considered constant, equation (B.4) can be integrated as

$$\frac{4q_x}{\pi a^2 x^2} dx = -kdT$$

$$\frac{4q_x}{\pi a^2}\left(\frac{1}{x_1}-\frac{1}{x_2}\right)=-k\left(T_2-T_1\right)$$

$$T_2=T_1-\frac{4q_x}{\pi a^2 k}\left(\frac{1}{x_1}-\frac{1}{x_2}\right)$$

$$q_2=\frac{\pi a^2 k_2\left(T_1-T_2\right)}{4\left(\frac{1}{x_1}-\frac{1}{x_2}\right)} \qquad \text{(B.5)}$$

If applying equations (B.2) and (B.3) to (B.5), the temperature dependence is removed and the resistance can be expressed as

$$R_3 \sim \frac{4\left(\frac{1}{x_1}-\frac{1}{x_2}\right)}{\pi a^2 k_2}$$

where a is the slope of the cone. In order to find the numerical value of R_3, the slope gradient for the cone has to be calculated as

$$a=\frac{dy}{dx}=\frac{\Delta y}{\Delta x}\approx\frac{\left(6.53-2\times 0.7\right)/2}{1}=2.57$$

Furthermore, L = 0.006 and D_1 = D_3 = 0.0005. Consequently, inserting the measurements for the probe returns the following resistances:

$$R_1 \sim \frac{30558}{k_1}$$

$$R_2 \sim \frac{500}{k_2}$$

$$R_3 \sim \frac{4\left(\frac{1}{0.006}-\frac{1}{0.008}\right)}{1.63^2 \pi k_3} \approx \frac{8}{k_3}$$

$$R_4 \sim \frac{411}{k_4}$$

As the measurements are all done within the same area of stratification, it is reasonable to assume that $k_1 \approx k_2 \approx k_3 \approx k_4$ as they should be within the same order of magnitude. Thus R_1 relates to the other resistances as

$$R_1 \approx O(2) \times R_2$$
$$R_1 \approx O(3) \times R_3$$
$$R_1 \approx O(2) \times R_4$$

Ideally, R_1 should at least three order of magnitudes greater than the other resistances. Hence, the results above indicate that modifying the probe to reduce R_2-R_4 would yield more accurate readings.

B.1.3 Modification of R_4

In order to reduce the result's dependency on R_4, the probe was firstly modified by reducing the distance from the nozzle to the inner tube. This was achieved by inserting a copper wire. It was soldered to the top of the probe and the other end went down close to the nozzle. This end had the shape of a coil and it was pressed flat, increasing the surface and thus contact area.

With this modification, the resistances R_4 and R_3 are effectively reduced to a new resistance, R_5, and it is reasonable to assume that R_5 is in the same order of magnitude as R_3.

$$R_1 \approx O(3) \times R_5$$

The second modification was to reduce the distance from the nozzle to the outer tube. This modification was achieved by mounting a copper wire onto the outer tube, thus reducing resistance R_2 to a minimum. Both modifications are pictured in figure B.2.

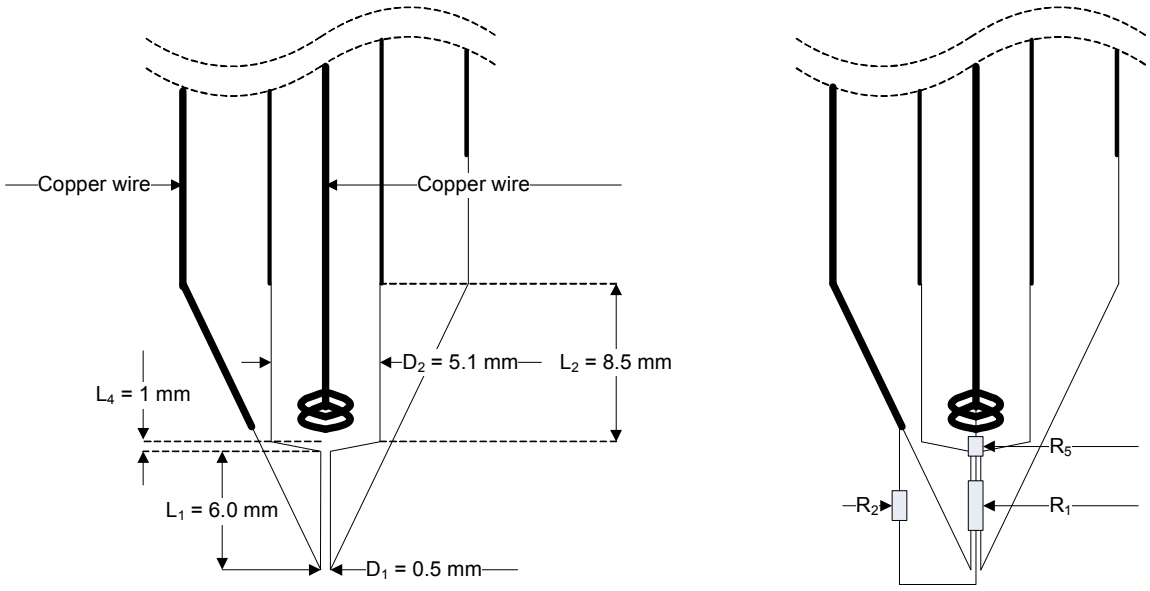

Figure B.2. Modified probe highlighting the modifications and the resulting resistances. This modification increased both sampling range and accuracy.

With this modification, the probe section could now be modeled as a vertical cylinder in a semi-infinite medium [28] where

$$S = \frac{2\pi L}{\ln\left(4L/D\right)} = \frac{2\pi \times 0.006}{\ln\left(\frac{4\times 0.006}{0.0005}\right)} = 0.009738$$

Consequently,

$$R_2 \approx \frac{100}{k}$$

And R_2 is reduced to approximately one quarter of its original size having the relationship $R_1 \approx 300 \times R_2$.

The outside copper wire does not only reduce resistance R_2, it renders measurements closer to the top of the water scale model possible. Moreover, it provides a mean to control the condition of the inner copper wire as the wires are exposed to the same environment, hence problems related to corrosion can be observed.

To sum up, this modification reduced the irrelevant resistances influence on the measurements and increased the range of the probe.

B.1.4 Probe calibration

Calibration of the probe was done using a DMA 35N density meter, manufactured by Anton Paar. The probe was inserted into a cylindrical cup filled with fluid. By using a syringe, water of constant salt concentration was injected to the cup and mixed. The returned voltage was then read from LabVIEW, and at the same time the Anton Paar was used to sample liquid right next to the nozzle. Several samples were taken for each concentration to certify that the density was uniform. This procedure is illustrated in figure B.3.

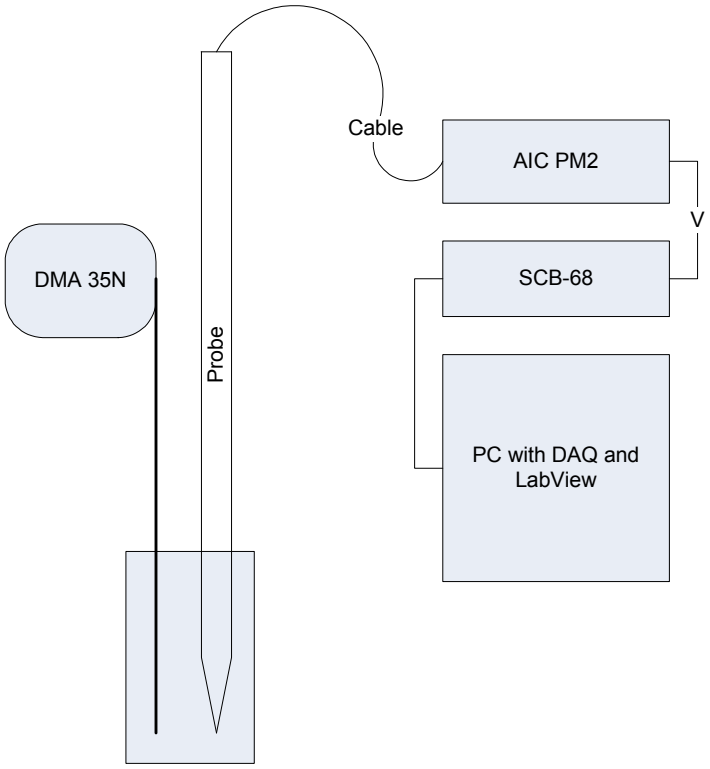

Figure B.3. Calibration procedure for the conductivity probe, using a Anton Paar DMA 35N as a reference to the readings from the conductivity meter in LabVIEW.

By plotting the samples into a graph, a relationship between density and voltage readings was developed as seen in figure B.4.

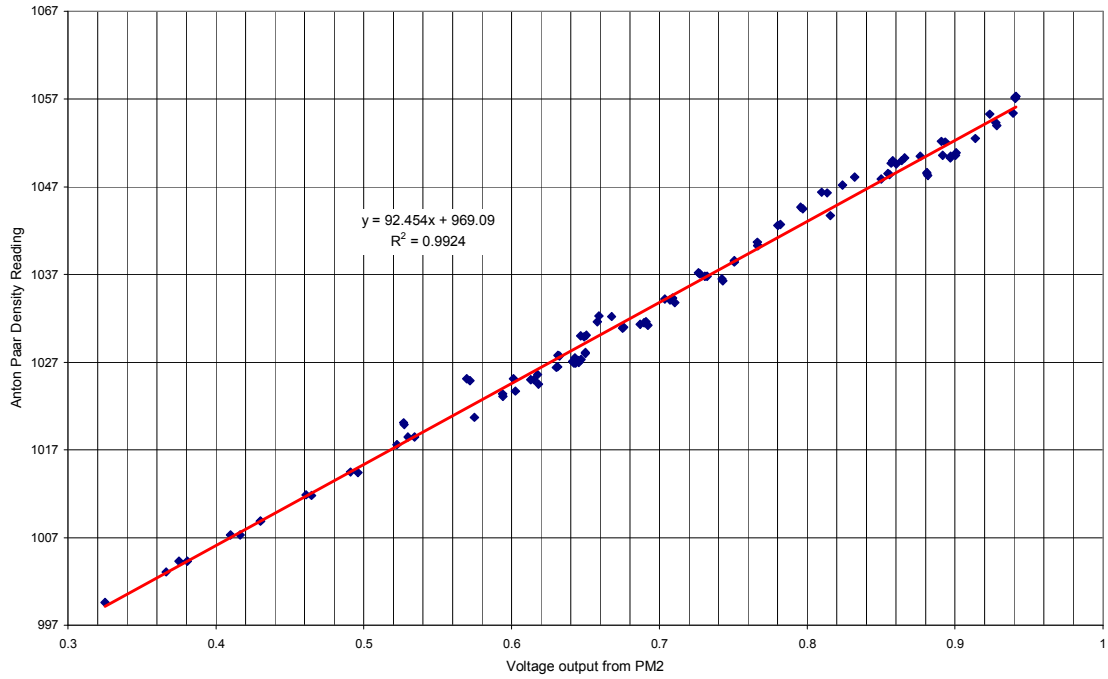

Figure B.4. Calibration curve for the conductivity probe with the line of best fit having $R^2 = 0.9924$.

The line of linear best fit was calculated to

$$\rho_{water} = 92.454 \times V_{PM2} + 969.09 \qquad \text{(B.6)}$$

where ρ is the density of the fluid and V is the voltage reading from the PM2. During this calibration it was discovered that the PM2 experiences saturation gain at approximately 1070 kg/m^3, and because of this the equipment capable of measuring conductivity in salt water within the density range of 998 to 1065 kg/m^3. However, the most important result of this calibration was that there was a linear relationship between the voltage readings and the actual density. Of this reason, linearity was assumed for calibrating the probe to density and thus fewer samples were needed. Normally, the probe would be calibrated before each experiment.

B.1.5 The time constant

The velocity of fluid thought the nozzle can be expressed as

$$v = \frac{Q}{A} \tag{B.7}$$

where Q is the volume flow through the cross sectional area A of the nozzle, $A = \frac{\pi}{4} d^2$.

Moreover, Q is calculated as $Q = \frac{\forall}{t}$ where $\forall$ is the total volume measured over time *t*.

The velocity can then be expressed as

$$v = \frac{4\forall}{\pi d^2 t} \tag{B.8}$$

The volume flow was measured by siphoning water through the probe with a height difference of 1.5 meters and using a stop watch. As the diameter of the nozzle is 5 mm, the average velocity from 12 readings was measured to 0.92 m/s. Moreover, the length of the nozzle section is 6 mm, and assuming piston flow this gives a time constant of

$$\tau \approx \frac{0.006m}{0.92\frac{m}{s}} \approx 0.007s$$

An average time for one traverse with the conductivity probe was four minutes, resulting in an average velocity of 0.002 m/s. Moreover, the PM2 conductivity meter was limited to one reading every other second, thus one traverse produced approximately 120 readings from the PM2.

As the time constant is significantly smaller than the time scale of the readings, it can be neglected when assuming that the sampled fluid is representative for the conductivity at the corresponding height.

B.2 Similarity considerations

Using experimental techniques to test theoretical predictions and analysis would be a highly resource demanding task if it was not for the analogy between buoyancy effects in air and in water. Using air in experiments for buoyancy flow involving heat would require huge enclosures where the heat transfer at the boundaries has to be known. By the use of non-dimensional characteristics of the flow, it is possible to compare the experimental results of a water scale model to a full size scenario. A water scale model can be made considerably smaller than an air model due to the differences in viscosity and density.

The Grashof number is a non-dimensional representation of the relationship between buoyancy forces and viscous forces acting on a fluid element:

$$Gr_L = \frac{g\beta\left(T_s - T_\infty\right)L^3}{\nu^2} \tag{B.9}$$

The effects of forced convection can be neglected if $\frac{Gr_L}{\mathrm{Re}_L^2} \geq 1$ [28]. In other words, it is acceptable to neglect viscous effects for high Grashof numbers.

The transition from a laminar free convection flow to a turbulent flow is traditionally classified by the Rayleigh number, the product of the Grashof and Prandtl number. For a vertical plate, the critical Rayleigh number is given by equation (B.10).

$$Ra_{z,c} = Gr_{x,c}\,\mathrm{Pr} = \frac{g\beta\left(T_s - T_\infty\right)z_c^3}{\nu\alpha} \approx 10^9 \tag{B.10}$$

Hence values of $Ra_z > 10^9$ are assumed to be turbulent. The transition to turbulence increases heat transfer significantly [28]. In the model developed by Cooper et al. [1], the Rayleigh number is set to be above critical for the entire vertically distributed source of buoyancy.

Moreover, for convective heat transfer, the Rayleigh number can be modified by use of the Nusselt number and the convective heat transfer equation for the case of a constant heat flux boundary condition [15].

$$Nu_H = \frac{hH}{\kappa}$$

$$q'' = h\left(T_s - T_\infty\right)$$

where q'' is the heat flux per unit area and h is the convective heat transfer coefficient. This gives the modified Rayleigh number

$$Ra_z^* = \frac{g\beta q'' H^4}{\nu\kappa\alpha} \tag{B.11}$$

This modification allows the Rayleigh number to be rewritten in terms of salt concentration [15]:

$$Ra_{salt}^* = \frac{g\xi G'' H^4}{\rho\nu C_{ps} D_{AB}^2} \tag{B.12}$$

where ξ is the expansion coefficient of salt, G'' is the salt flux per unit area, C_{ps} is the specific salt concentration at constant pressure and D_{AB} is the binary diffusion coefficient of the salt solution. The concentration of salt can then be compared to heat transfer. A feasibility study was presented by Hough [15], showing that the Rayleigh numbers for the water scale model were nine orders of magnitude larger than the critical Rayleigh number.

As the brine is denser and thus heavier than fresh water, these types of experiments have buoyancy forces acting downwards, in contrast to the theoretical calculations which usually define buoyancy forces as acting upwards in consideration to ventilation using air [10].

B.3 Other experimental techniques

There are three commonly used methods for modelling plume behaviour in ventilation: water scale models using heating elements, water scale models using salt water or gas modelling systems using heating elements [3]. Li et al. [34] used fine hydrogen bubbles to model smoke flow, using electrolysis to make the bubbles.

Bouzinaoui et al. [30] did large scale measurements to investigate displacement ventilation. A heat source was mounted in the middle of the ventilated space, and they performed measurements by using thermocouples mounted onto a probe capable of traversing in three dimensions. However, water scale models have an advantage to this method when it comes to compactness and ease of instalment. Moreover, heat flux can be measured as salt concentration, removing the need of insulation or boundary control. Additionally, experiments involving multiple layers can be performed by using solutions of sugar and salt [33].

Appendix C Experimental Results

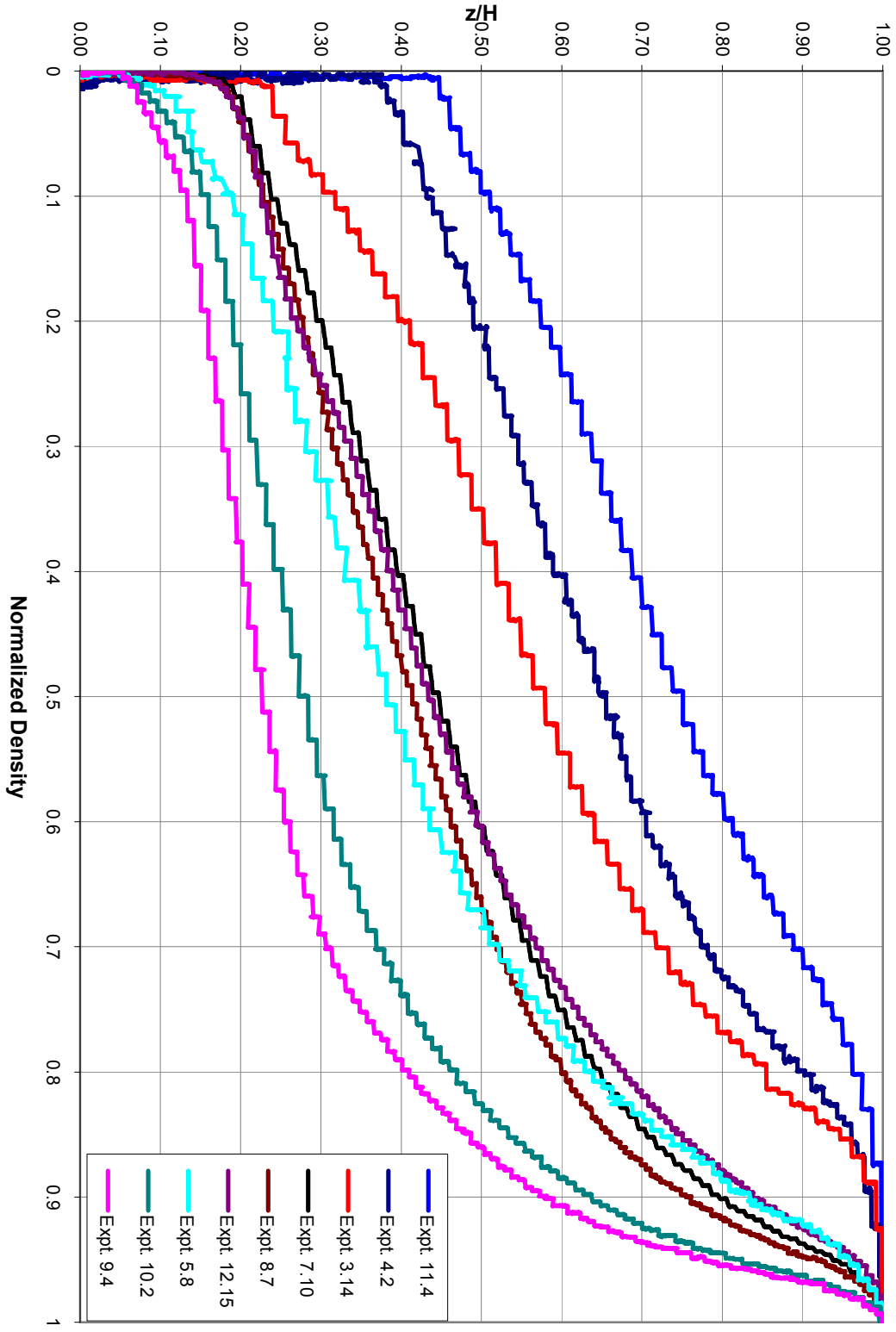

Figure C.1. The normalized stratification profile of mechanically ventilated experiment 8 at steady-state. The red lines indicate the sections of linear stratification and the height from 0.0-0.18 is a uniform area of fresh water up until the first front.

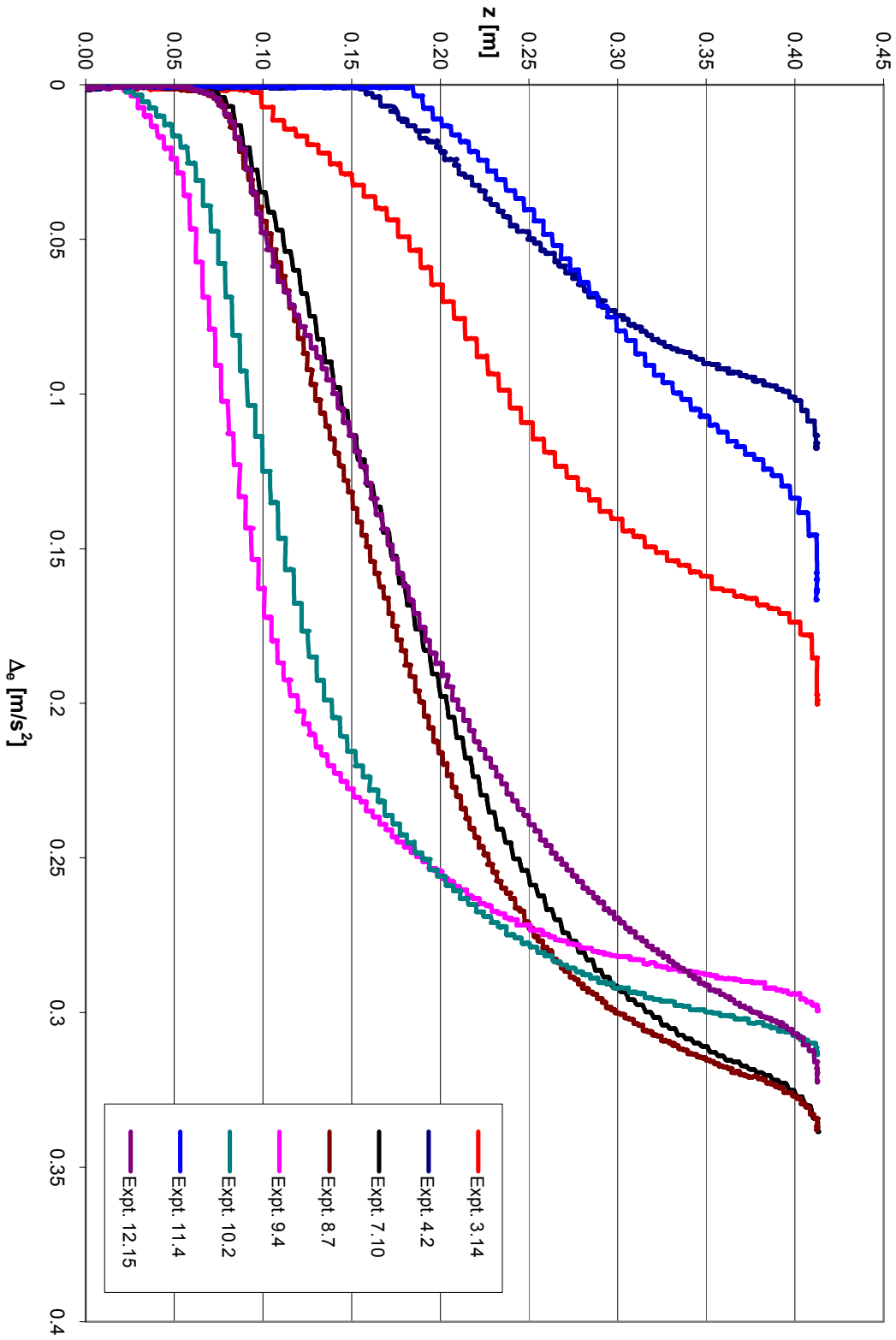

Figure C.2. The stratification profiles for the mechanically ventilated experiments at steady-state. For comparison reasons, the values of the ambient buoyancy have been calculated using 998.8 kg/m^3 as reference density instead of the ordinary minimum density of that respective experiment.

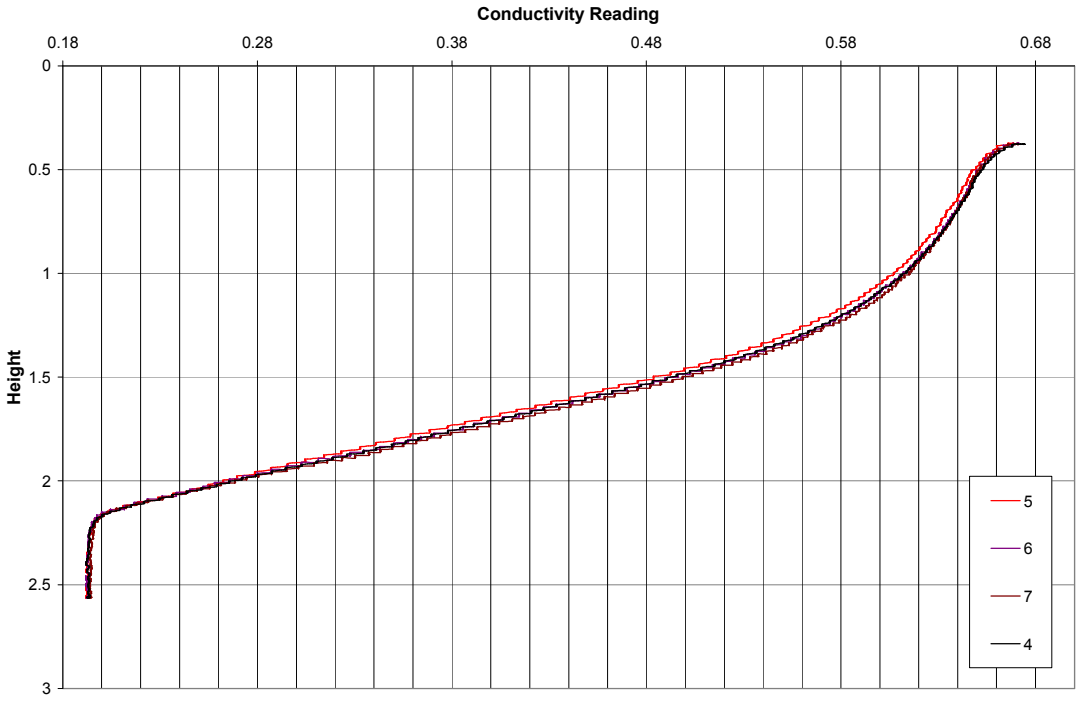

Figure C.3. Mechanically ventilated steady-state experiment 8. Maximum error at any point was found to be within 1 % using error bars. The results are plotted as direct readings from LabVIEW and are not calibrated to density or height.

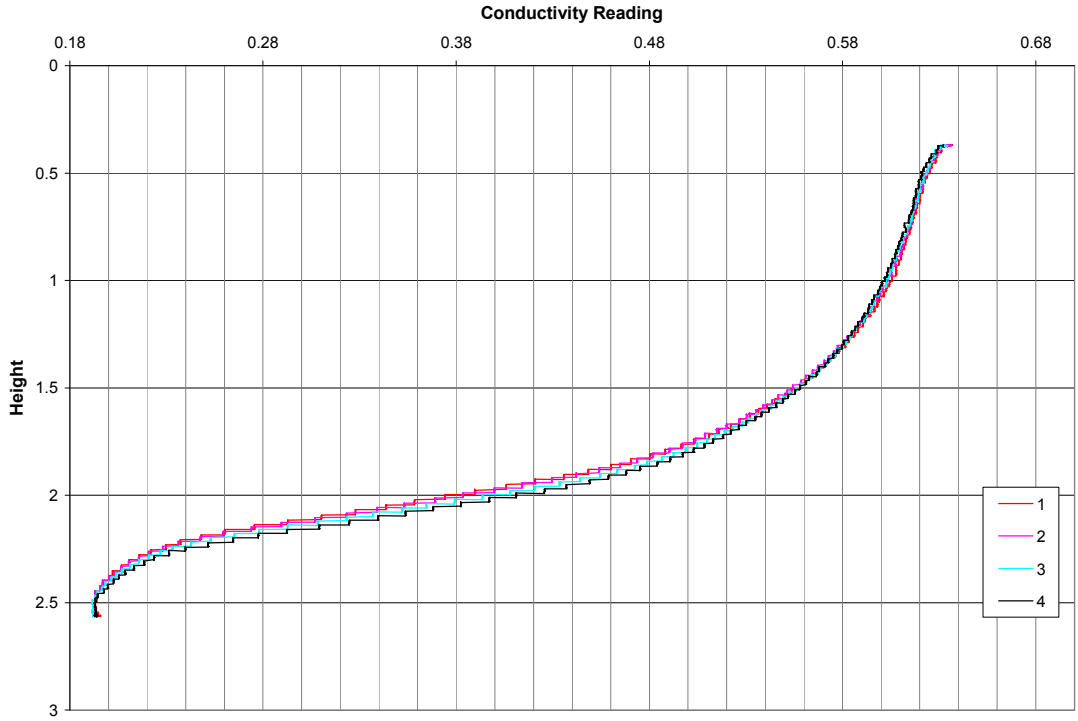

Figure C.4. Mechanically ventilated steady-state experiment 10. Maximum error at any point was found to be within 1 % using error bars. The results are plotted as direct readings from LabVIEW and are not calibrated to density or height.

Appendix D Best-fit Parameters

The parameters of the best fit lines for the net downwards flow for the linearly stratified environment experiments, where polynomial fits were used, as according to equation (D-1).

$$y(x) = a_0 + a_1 x_1 + a_2 x_2^2 \ldots + a_n x_n^n \qquad \text{(D.1)}$$

The parameters that were used are presented in table D.1.

Expt.	3	5	6	8	9
R^2	0.981	0.994	0.996	0.998	0.990
a_0	0.01394	-0.39648	0.00293	0.8949	-1.97041
a_1	0.04461	32.35436	0.98071	-43.1325	97.50952
a_2	15.54643	-874.223	-28.343	1002.643	-1940.46
a_3	-414.985	12519.81	537.9199	-12989.4	21120.38
a_4	4961.174	-105900	-5611.85	103151.3	-138125
a_5	-32480.5	555736.2	34507.02	-521167	559357.6
a_6	124374.1	-1826328	-129368	1679262	-1383344
a_7	-278648	3651758	291941.7	-3337248	1952339
a_8	339198.9	-4057993	-365472	3723211	-1310276
a_9	-173741	1920691	195122.6	-1782121	213614.6

Table D.1. Best fit parameters for the polynomials that describe the net outwards volume flux for the linearly stratified environment experiments.

Appendix E Numerical Results

E.1 Illustration of Gaussian intrusion

The equations for the Gaussian distribution are plotted in figure 4.16 to illustrate the effect of the equations (4.7) and (4.8) on the plume equations. Note that the figure is meant to illustrate its behavior on the equations only.

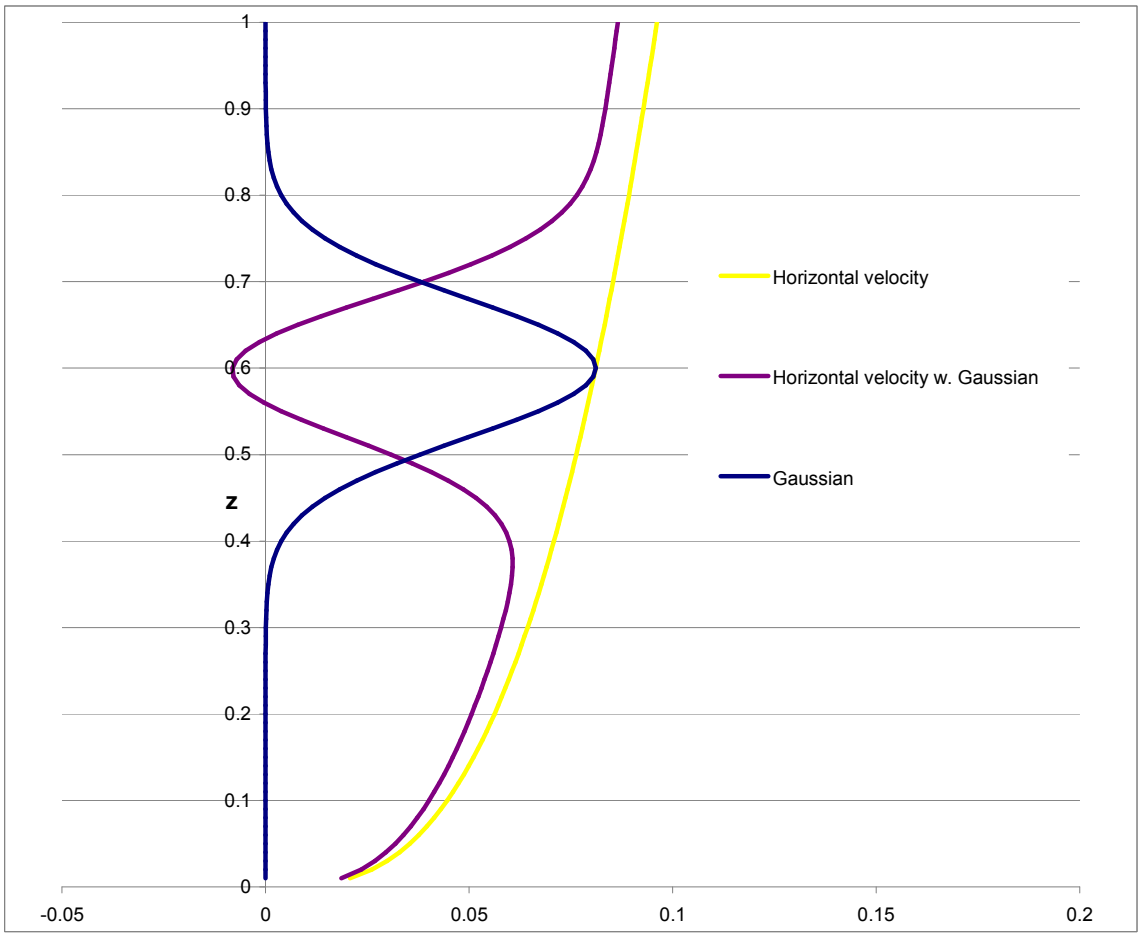

Figure E.1. An illustrative example for describing a simplified intrusion using the equations developed in this work. The intrusion is at the point of neutral buoyancy, z = 0.6.

E.2 Non-dimensional results

A relationship between the dimensionless ventilation rate, q_{vent}, and a^* can be found by using the same technique as in §5.3.1. The results are shown in the figure below. All results

are for steady-state, which was determined by the steady-state position of the first front and a constant volume flux through the vent.

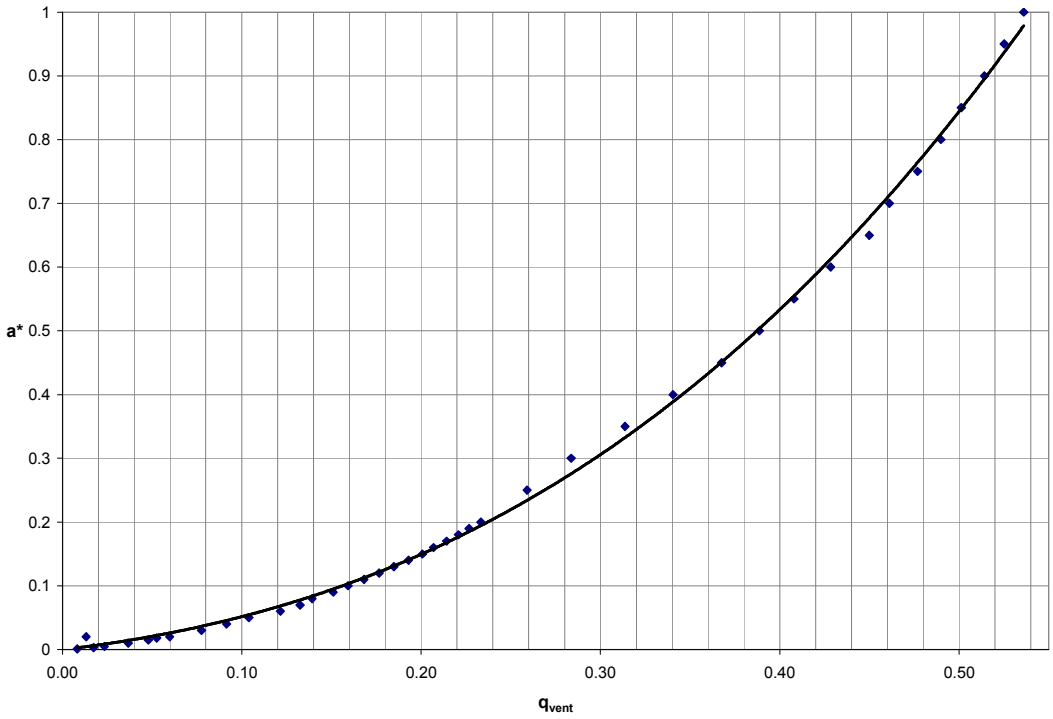

Figure E.2. Steady-state relationship between dimensionless vent area and dimensionless volume flux through the vent. The connecting line is a polynomial best fit.

The trend for the relationship in figure E-2 can be accurately expressed by the polynomial best fit:

$$a^* = 2.06656 q_{vent}^3 + 1.68964 q_{vent}^2 + 0.326621 q_{vent} \qquad \text{(E.1)}$$

Moreover, the relationship between the non-dimensional volume flux and the first front was found in similar fashion, and is plotted in the figure below.

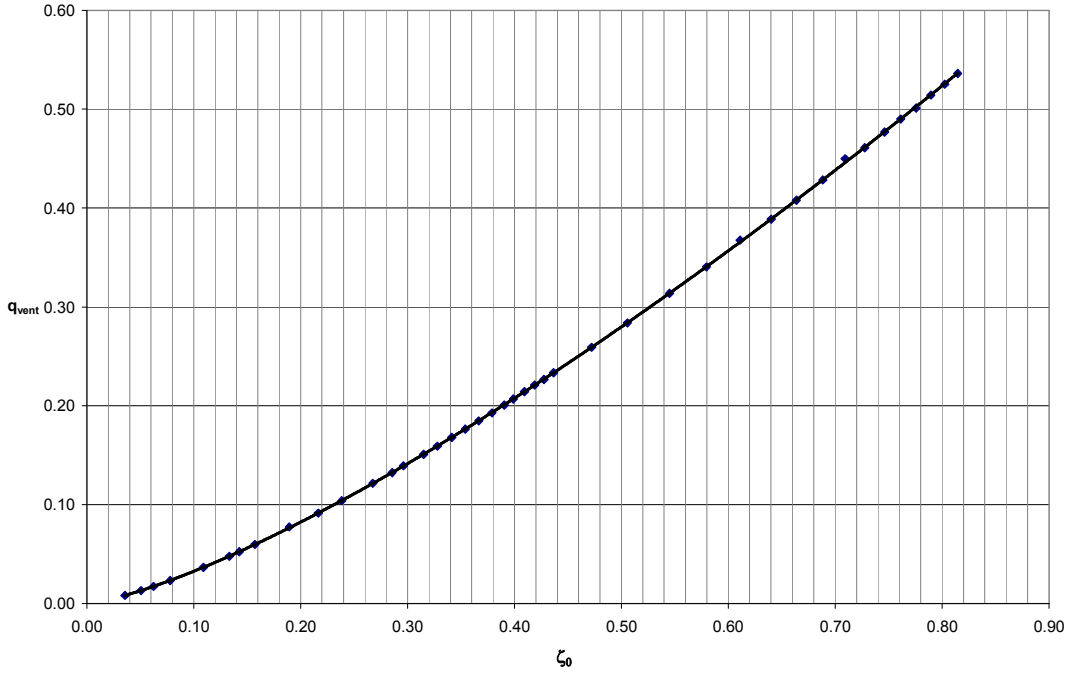

Figure E.3. Relationship at steady-state between the dimensionless volume flux through the vent and the position of the first front. The connecting line is a geometrical best fit.

The best fit line of the relationship in figure E.3 between the non-dimensional volume flux through the vent and the position of the first front is

$$q_{vent} = 0.7050894 \times \zeta_0^{1.333353} \qquad \text{(E.2)}$$

E.3 Example calculation

The non-dimensional results for the ambient buoyancy are given as δ, but can be made dimensional by using the equation for ambient buoyancy from §2.3.4, rewritten as:

$$\Delta_e = \frac{\delta}{\alpha^{2/3} H^{1/3} F_0^{-2/3}} \qquad \text{(E.3)}$$

This can be further modified by using the ideal gas equation [5]:

$$\Delta_e = g\frac{\Delta\rho}{\rho} = g\frac{\Delta T}{T} \qquad \text{(E.4)}$$

Moreover, for a flow driven by a heat source, the buoyancy flux can be expressed as $F_0 = \frac{g\beta q}{\rho c_p}$ where $\beta = \frac{1}{T}$ continuing the assumption of an ideal gas. The buoyancy source per unit length of source can be simplified for a heat flux at room temperature for air to [5]

$$F_0 = 0.0281 \times q \left[\frac{m^3}{s^3} \right].$$

where q is in kilo watts. The temperature can then be found as

$$T = T_{ref} + T \frac{\Delta_e}{g} \tag{E.5}$$

Or, as the full expression:

$$T = T_{ref} + T \frac{1}{g} \frac{\delta}{\alpha^{2/3} H^{1/3} \left(0.0281 \times q\right)^{-2/3}} \tag{E.6}$$

Equation (E.6) can then be used to convert the non-dimensional stratification profiles from the numerical solutions of *Distran* to dimensional temperature profiles driven by a convective heat flux.

E.4 Dimensional results

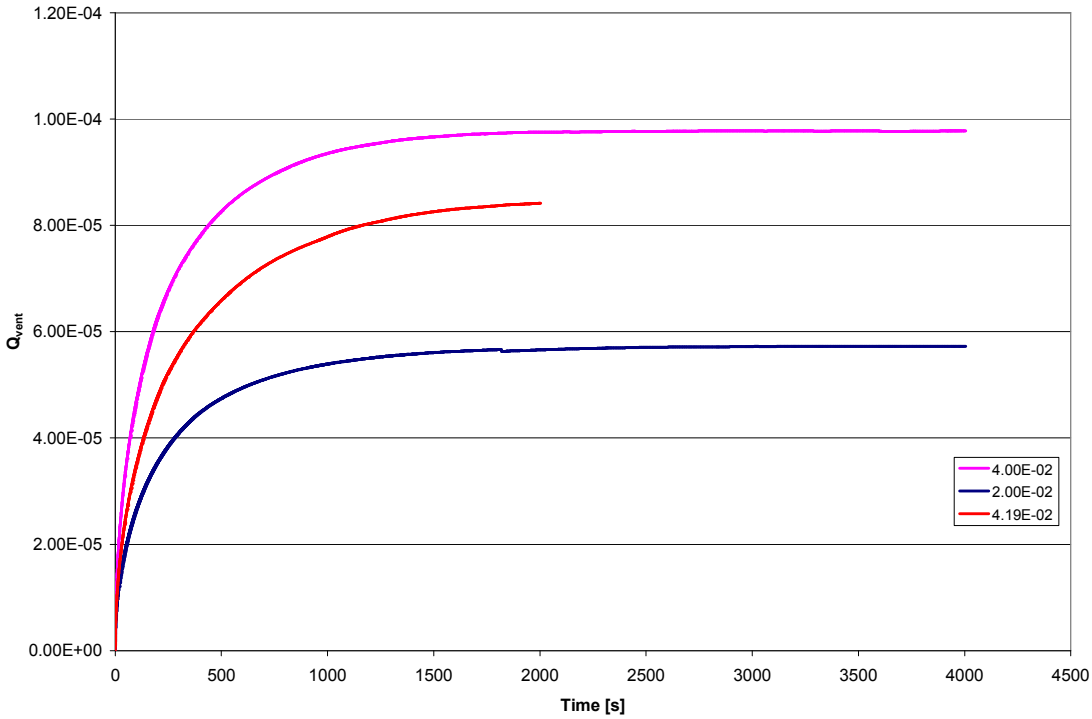

Figure E.4 The development of steady-state for the ventilation flow rate, Q_{vent} [m^2/s] through the ventilated filling box using the dimensional version of Distran using the parameters of experiment 12. The different curves indicate the effects of varying the membrane constant. Full steady-state is achieved at approximately 2500 s, which is within the same order of magnitude as the approximately 4000 s required for experiment 12.

Appendix F Conversion Table for Salt Water

Figure F.1 displays the relationship between density and salt contents of water for two different temperatures. These two temperatures represent the range experienced during the experimental procedures.

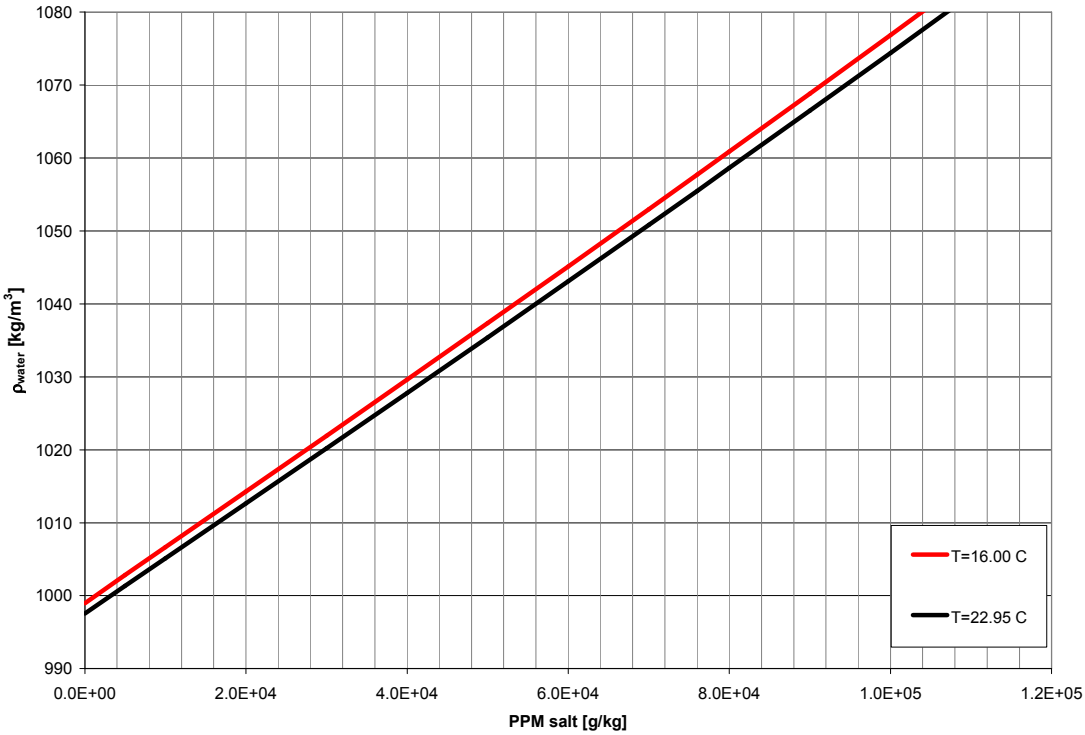

Figure F.1. Salinity – density conversion table using equation (G.1) for .temperatures of 16 °C and 22.95 °C, representing the lower and upper band of temperatures that was experienced during experiments, respectively.

Water temperature as a function of temperature and salinity in figure F-1 was calculated using equation (F.1) from Handbook of Hydrology [35]:

$$\rho_s = \rho + AS + BS^{\frac{3}{2}} + CS^2 \qquad \text{(F.1)}$$

where S is the salinity in g/kg and

$$A = 8.24493\times10^{-1} - 4.0899\times10^{-3}T + 7.6438\times10^{-5}T^2 - 8.2467\times10^{-7}T^3 + 5.3675\times10^{-9}T^4$$
$$B = -5.724\times10^{-3} + 1.0227\times10^{-4}T - 1.6546\times10^{-6}T^2$$
$$C = 4.8314\times10^{-4}$$